

SYNTHESIS AND CHARACTERIZATION OF 2,3-  
DIFUNCTIONALIZED THIENO[3,4-*b*]PYRAZINE-BASED  
TERTHIENYLS: STRUCTURE-FUNCTION RELATIONSHIPS  
AND SIDE CHAIN TUNABILITY

A Dissertation  
Submitted to the Graduate Faculty  
of the  
North Dakota State University  
of Agriculture and Applied Science

By

Ryan Lee Schwiderski

In Partial Fulfillment of the Requirements  
for the Degree of  
DOCTOR OF PHILOSOPHY

Major Department:  
Chemistry and Biochemistry

April 2014

Fargo, North Dakota

North Dakota State University  
Graduate School

---

**Title**

Synthesis and Characterization of 2,3-Difunctionalized  
Thieno[3,4-*b*]pyrazine-Based Terthienyls: Structure-Function  
Relationships and Side Chain Tunability

---

**By**

Ryan Lee Schwiderski

---

The Supervisory Committee certifies that this *disquisition* complies with  
North Dakota State University's regulations and meets the accepted  
standards for the degree of

**DOCTOR OF PHILOSOPHY**

SUPERVISORY COMMITTEE:

Seth C. Rasmussen

---

Chair

Gregory R. Cook

---

Pinjing Zhao

---

Victoria J. Gelling

---

Approved:

5/1/2014

---

Date

Gregory R. Cook

---

Department Chair

## ABSTRACT

The ability to tune the physical, electronic, and optical properties of polymer precursors has garnered a great deal of interest in the conjugated organic materials field. The Rasmussen group has previously demonstrated the ability to produce tunable, low band gap materials through the generation of new families of functionalized thieno[3,4-*b*]pyrazines (TPs). The scope of conventional TPs has been limited to either 2,3-dialkyl or diaryl analogues due to the standard synthetic approach of 3,4-diaminothiophene condensation with available stable  $\alpha$ -diones. As a consequence, this limited the ability to effectively tune the electronic and optical properties of the TP unit. In an effort to expand the application and versatility of this new approach to tunable, low band gap materials, analogous families of TP-based terthienyls have been prepared as new polymer precursors. The synthetic route utilizes the well-known 3',4'-diamino-2,2':5',2''-terthiophene precursor for the production of 2,3-bis(trifluoromethanesulfonyl)-5,7-(2-thienyl)-thieno[3,4-*b*]pyrazine as a reactive intermediate. Simple substitution with a variety of nucleophiles thus allows the possibility to tune the properties of the oligomeric unit via the addition of electron-withdrawing or electron-donating groups at the 2- and 3-positions of the central TP unit. Incorporation of these new TPs into the terthienyl framework reduces the chemical reactivity of the central fused-ring unit and more easily allows for the application of these precursors to the desired polymeric materials.

## ACKNOWLEDGEMENTS

I would like to thank my advisor, Professor Seth Rasmussen, for his guidance over the last five and a half years. His office was always open to discuss my results and he always took the initiative to help me to grow as a student and become a diligent researcher. I would also like to thank the rest of my graduate committee for helping me throughout my graduate career. A big thanks is also in order to all of the current and former Rasmussen group members, especially Casey McCausland, Cole Larsen and Rylan Wolfe, for all of their support and willingness to tolerate my debauchery.

I would also like to give special thanks to Dr. Sean Evenson and his wife Greta for being great friends. They provided me with much needed emotional support, fed me on a regular basis, took the initiative to include me in “family time” and were all around amazing people throughout my time in Fargo. I could not have finished graduate school without their kindness and support.

A very special thanks goes out to my mom, brothers and sister, as well as the rest of my family, for being extremely supportive as I pursued my doctorate degree. An extra special thanks goes out to my dad because he’s been truly inspirational for me. He has shown me that being positive is the best way to approach life and being respectful is the only way to treat people. He was there at a moment’s notice if I ever needed anything and he has provided me with everything I needed. His presence in my life has given me all of the motivation and skills I needed to see the pursuit of my Ph.D. through to completion.

So many people have helped me through this process for which I am truly grateful, thank you all.

## TABLE OF CONTENTS

ABSTRACT .....	iii
ACKNOWLEDGEMENTS .....	iv
LIST OF TABLES .....	x
LIST OF FIGURES.....	xi
LIST OF SCHEMES .....	xiii
LIST OF APPENDIX TABLES .....	xv
LIST OF APPENDIX FIGURES.....	xvii
LIST OF ABBREVIATIONS AND ACRONYMS .....	xviii
CHAPTER 1. INTRODUCTION.....	1
1.1. Conjugated Polymers .....	1
1.2. Band Gap.....	5
1.3. Band Gap and Energy Level Engineering.....	11
1.4. Energy Level Engineering in Thieno[3,4- <i>b</i> ]pyrazines .....	19
1.5. Research Goals .....	26
1.6. References .....	29
CHAPTER 2. SYNTHESIS AND CHARACTERIZATION OF THIENO[3,4- <i>b</i> ]PYRAZINE-BASED TERTHIENYLS: TUNABLE PRECURSORS FOR LOW BAND GAP CONJUGATED MATERIALS .....	38
2.1. Introduction .....	38
2.2. Results and Discussion.....	41
Synthesis.....	41
X-ray Crystallography.....	49
UV-Vis Spectroscopy.....	55
Electrochemistry.....	58

2.3. Conclusion.....	63
2.4. Experimental Methods .....	64
General .....	64
Materials.....	65
3',4'-Dinitro-2,2':5',2''-terthiophene ( <b>2</b> ) .....	65
3',4'-Diamino-2,2':5',2''-terthiophene ( <b>3</b> ).....	65
5,7-Bis(2-thienyl)thieno[3,4- <i>b</i> ]pyrazine-2,3(1H,4H)-dione ( <b>10</b> ).....	66
2,3-Dibromo-5,7-bis(2-thienyl)thieno[3,4- <i>b</i> ]pyrazine ( <b>5</b> ) .....	67
2,3-bis(trifluoromethanesulfonato)-5,7-Bis(2-thienyl)thieno[3,4- <i>b</i> ]pyrazine ( <b>6</b> ) .....	67
2,3-Bis( <i>N,N</i> -diethylamino)-5,7-bis(2-thienyl)thieno[3,4- <i>b</i> ]pyrazine ( <b>13</b> ) .....	68
2,3-Dihexyloxy-5,7-bis(2-thienyl)thieno[3,4- <i>b</i> ]pyrazine ( <b>14</b> ).....	68
2,3-Bis(phenylethynyl)-5,7-bis(2-thienyl)thieno[3,4- <i>b</i> ]pyrazine ( <b>15</b> ) .....	69
2,3-Bis(bromomethyl)-5,7-bis(2-thienyl)thieno[3,4- <i>b</i> ]pyrazine ( <b>7</b> ) .....	70
General synthesis of 2,3-dialkoxymethyl-5,7-bis(2-thienyl)thieno[3,4- <i>b</i> ]pyrazine.....	70
2,3-Bis(ethoxymethyl)-5,7-bis(2-thienyl)thieno[3,4- <i>b</i> ]pyrazine ( <b>16a</b> ) .....	71
2,3-Bis(hexyloxymethyl)-5,7-bis(2-thienyl)thieno[3,4- <i>b</i> ]pyrazine ( <b>16b</b> ).....	71
2,3-Bis( <i>N,N</i> -diethylaminomethyl)-5,7-bis(2-thienyl)thieno[3,4- <i>b</i> ]pyrazine ( <b>17</b> ) .....	71
2.5. Instrumentation.....	72
UV-vis Spectroscopy.....	72

Electrochemistry.....	72
2.6. References .....	73
CHAPTER 3. SIDE CHAIN TUNING OF FRONTIER ORBITALS IN POLYMERS OF THIENO[3,4- <i>b</i> ]PYRAZINE-BASED TERTHIENYLS .....	79
3.1. Introduction .....	79
3.2. Results and Discussion.....	82
Electrochemical and optical properties of TP-based terthienyls .....	82
Electropolymerization and electrochemistry of poly(5,7-bis(2- thienyl)thieno[3,4- <i>b</i> ]pyrazine)s .....	84
Optical properties of poly(5,7-bis(2-thienyl)thieno[3,4- <i>b</i> ]pyrazine)s .....	91
Copolymers of 5,7-bis(2-thienyl)thieno[3,4- <i>b</i> ]pyrazine and Fluorene.....	95
3.3. Conclusion.....	97
3.4. Experimental .....	98
General .....	98
Materials.....	99
2,3-Dihexyloxy-5,7-bis(5-trimethylstannyl-2-thienyl)thieno[3,4- <i>b</i> ]pyrazine ( <b>10</b> ) .....	99
Poly[2,3-dihexyloxy-5,7-bis(2-thienyl)thieno[3,4- <i>b</i> ]pyrazine- <i>co</i> - 9,9-dioctyl-9H-fluorene] ( <b>4i</b> ).....	100
Electropolymerizations.....	100
3.5. Instrumentation.....	101
Electropolymerization study .....	101
TP-terthienyl- <i>co</i> -fluorene polymer study.....	101
3.6. References .....	102

CHAPTER 4. EXTENDED FUSED-RING THIENO[3,4- <i>b</i> ]PYRAZINES WITH SOLUBILIZING CHAINS .....	106
4.1. Introduction .....	106
4.2. Results and Discussion.....	112
Synthesis.....	112
4.3. Conclusions .....	124
4.4. Experimental .....	125
General .....	125
Materials.....	125
1,2-Dibromoacenaphthylene ( <b>16</b> ).....	126
1,2-Dihydroxy-1,2-dioctylacenaphthene ( <b>20a</b> ) .....	126
1,2-Dihydroxy-1,2-diphenylacenaphthene ( <b>20c</b> ) .....	127
1,2-Dihydroxy-1,2-bis(4-octylphenyl)acenaphthene ( <b>20d</b> ) .....	128
General procedure for the reductive dehydration.....	129
1,2-Dioctylacenaphthylene ( <b>17a</b> ).....	129
1,2-Bis(2-ethylhexyl)acenaphthylene ( <b>17b</b> ).....	129
1,2-Diphenylacenaphthylene ( <b>17c</b> ) .....	129
1,2-Bis(4-octylphenyl)acenaphthylene ( <b>17d</b> ).....	130
Dibenzo[ <i>j,l</i> ]fluoranthene ( <b>23</b> ).....	130
1-Bromo-4-octylbenzene.....	130
3-Octyl-8,10-bis(2-thienyl)acenaphtho[1,2- <i>b</i> ]thieno[3,4- <i>e</i> ]pyrazine ( <b>24</b> ) .....	131
4.5. Instrumentation.....	132
UV-vis Spectroscopy.....	132
Electrochemistry.....	132



4.6. References .....	132
CHAPTER 5. SUMMARY .....	135
5.1. Conclusion.....	135
5.2. Future Directions.....	138
APPENDIX. CRYSTALLOGRAPHIC INFORMATION .....	140
A.1. 5,7-bis(2-thienyl)thieno[3,4- <i>b</i> ]pyrazine-2,3-(1H,4H)-dione (Chapter 2, <b>10</b> ).....	140
A.2. 2,3-bis(bromomethyl)-5,7-bis(2-thienyl)thieno[3,4- <i>b</i> ]pyrazine (Chapter 2, <b>7</b> ).....	146
A.3. 2,3-dihexyloxy-5,7-bis(2-thienyl)thieno[3,4- <i>b</i> ]pyrazine (Chapter 2, <b>14</b> ).....	153
A.4. Acenaphtho[1,2- <i>b</i> ]thieno[3,4- <i>e</i> ]pyrazine (Chapter 4, <b>3a</b> ).....	160
A.5. 1,2-dibromoacenaphthylene (Chapter 4, <b>16</b> ).....	166
A.6. Dibenzo[ <i>j,l</i> ]fluoranthene (Chapter 4, <b>23</b> ).....	171

## LIST OF TABLES

<u>Table</u>	<u>Page</u>
1.1. Electrochemical data for a series of TP-like compounds .....	24
2.1. Experimental bond lengths of 5,7-bis(2-thienyl)thieno[3,4- <i>b</i> ]pyrazine-2,3(1H,4H)-dione ( <b>10</b> ) and 2,3-difunctionalized 5,7-bis(2-thienyl)thieno[3,4- <i>b</i> ]pyrazines <b>4b</b> , <b>4e</b> , <b>7</b> and <b>14</b> .....	50
2.2. UV-visible absorption data for a series of TP-based terthienyls .....	56
2.3. Electrochemical data for a series of TP-based terthienyls .....	59
3.1. TP-based terthienyl electrochemical and optical data .....	83
3.2. Electrochemical data of poly(5,7-bis(2-thienyl)thieno[3,4- <i>b</i> ]pyrazine) films .....	87
3.3. Optical data for poly(5,7-bis(2-thienyl)thieno[3,4- <i>b</i> ]pyrazine) films .....	91
3.4. Optical and electronic data for poly(5,7-bis(2-thienyl)thieno[3,4- <i>b</i> ]-pyrazine- <i>co</i> -fluorene)s .....	97
4.1. Collected data for extended fused-ring TPs and corresponding TP-based terthienyl analogs .....	107
4.2. Collected data for extended fused-ring TPs and their corresponding terthienyl analogs .....	109

## LIST OF FIGURES

<u>Figures</u>	<u>Page</u>
1.1. Resonance structures of polyacetylene illustrating overlapping p orbitals and $\pi$ electron delocalization.....	1
1.2. Stereoisomers of polyacetylene.....	4
1.3. Band structure for different classes of materials.....	6
1.4. Energy level diagram illustrating the relationship between band gap ( $E_g$ ) and HOMO-LUMO energies.....	7
1.5. Determination of optical band gap.....	9
1.6. Determination of HOMO energy and LUMO energy levels and electronic band gap.....	10
1.7. Parameters influencing band gap in thiophene polymers: conjugation length (Con), bond length alternation ( $\delta r$ ), resonance energy (Res), substituents (Sub), torsion angle ( $\Theta$ ), and intermolecular interactions (Int).....	11
1.8. Aromatic and quinoidal resonance forms of polythiophene.....	13
1.9. Thiophene-based polymers with enhanced quinoidal character from off-chain fused-rings and their corresponding band gaps.....	14
1.10. Steric distortions due to a) neighboring chain-chain interactions, b) side chain backbone interactions, and c) neighboring $\beta$ -hydrogen interactions.....	15
1.11. Parameters influencing band gap in TP polymers: conjugation length (Con), bond length alternation ( $\delta r$ ), resonance energy (Res), substituents (Sub), torsion angle ( $\Theta$ ), and intermolecular interactions (Int).....	20
1.12. Steric interactions of fused-ring polymers and their corresponding band gaps.....	21
1.13. UV-vis spectra of TP, ITN, and quinoxaline.....	25
2.1. Thieno[3,4- <i>b</i> ]pyrazine-based terthienyls with good leaving groups.....	41
2.2. Thermal ellipsoid plot of 5,7-Bis(2-thienyl)thieno[3,4- <i>b</i> ]pyrazine-2,3(1H,4H)-dione ( <b>10</b> ) at the 50% probability level.....	51

2.3. Thermal ellipsoid plot of 2,3-Bis(bromomethyl)-5,7-bis(2-thienyl)thieno[3,4- <i>b</i> ]pyrazine ( <b>7</b> ) at the 50% probability level.....	53
2.4. Thermal ellipsoid plot of 2,3-dihexyloxy-5,7-bis(2-thienyl)thieno[3,4- <i>b</i> ]pyrazine ( <b>14</b> ) at the 50% probability level.....	54
2.5. UV-visible spectrum of TP-based terthienyl <b>4b</b> in CH <sub>3</sub> CN.....	55
2.6. Normalized visible spectra of a series of TP-based terthienyls.....	57
2.7. Cyclic voltammogram of terthienyl <b>7</b> .....	58
2.8. Hammet plot of TP-based terthienyls.....	62
3.1. Growth of polymer <b>P7</b> with potential cycling.....	85
3.2. Depiction of $\alpha$ - $\alpha$ and $\alpha$ - $\beta$ coupling in TP-based terthienyl polymers .....	86
3.3. Cyclic voltammograms for polymers <b>P4-P6</b> .....	88
3.4. Hammet plot of for polymers <b>P4-P8</b> .....	90
3.5. Thin film vis-NIR spectra for polymers <b>P4-P8</b> .....	92
3.6. Spectroelectrochemistry of polymer <b>P5</b> .....	94
3.7. Spectroelectrochemistry of polymer <b>P7</b> .....	94
3.8. Poly(5,7-bis(2-thienyl)thieno[3,4- <i>b</i> ]pyrazine- <i>co</i> -fluorene)s.....	95
4.1. Extended fused-ring thieno[3,4- <i>b</i> ]pyrazine monomers.....	106
4.2. Extended fused-ring thieno[3,4- <i>b</i> ]pyrazine oligomers.....	108
4.3. Solid-state absorbance and electrochemical band gap of homopolymeric and copolymeric acenaphtho[1,2- <i>b</i> ]thieno[3,4- <i>e</i> ]pyrazines.....	110
4.4. Thermal ellipsoid plot of 1,2-dibromoacenaphylene, <b>16</b> at the 50% probability level .....	115
4.5. Thermal ellipsoid plot of Dibenzo[ <i>j,l</i> ]fluoranthene, <b>23</b> at the 50% probability level .....	123

## LIST OF SCHEMES

<u>Schemes</u>	<u>Page</u>
1.1. Generation of reactive TP-based terthienyl intermediates for the production of tunable materials .....	27
1.2. Extended fused-ring TPs with solubilizing chains .....	28
2.1. Synthesis of conventional thieno[3,4- <i>b</i> ]pyrazine-based terthienyls via simple condensation reactions .....	39
2.2. Previous synthesis of 2,3-dibromothieno[3,4- <i>b</i> ]pyrazine .....	41
2.3. Synthesis of 5,7-bis(2-thienyl)thieno[3,4- <i>b</i> ]pyrazine-2,3(1H,4H)-dione .....	42
2.4. Proposed and alternative mechanisms for the generation of byproduct <b>12</b> .....	44
2.5. Conversion of <b>10</b> to TP-based terthienyls with good leaving groups .....	45
2.6. Proposed mechanism for the formation of terthienyl <b>6</b> .....	47
2.7. Generation of new TP-based terthienyls via simple substitution of <b>6</b> .....	47
2.8. Synthesis of new 2,3-difunctionalized TP-based terthienyls from precursor <b>7</b> .....	49
2.9. Possible tautomeric forms of pyrazine-2,3-dione.....	49
3.1. Polymeric materials via TP-based terthienyls .....	80
3.2. Synthesis of poly(2,3-dihexyloxy-5,7-bis(2,-thienyl)thieno[3,4- <i>b</i> ]pyrazine- <i>co</i> -9,9-dioctyl-9H-fluorene) .....	96
4.1. General synthesis of extended fused-ring thieno[3,4- <i>b</i> ]pyrazines .....	113
4.2. Synthesis of extended fused-ring 3-octyl-8,10-bis(2-thienyl)acenaphtho[1,2- <i>b</i> ]thieno[3,4- <i>e</i> ]pyrazine .....	113
4.3. Synthesis of 1,2-dioctylacenaphthylene via radical bromination.....	115
4.4. Synthesis of various 1,2-disubstituted acenaphthylenes .....	116
4.5. Synthesis of 1-bromo-4-octylbenzene.....	117
4.6. Reductive dehydration of a vicinal phenanthrene diols with proposed routes and intermediates.....	119

4.7. Friedel-Crafts acylation of 1,2-disubstituted acenaphthylenes .....	121
4.8. Reductive dehydration of <b>20c</b> utilizing triflic acid.....	122
5.1. Example of TP-based terthienyls that incorporate electron-withdrawing groups with solubilizing chains.....	138
5.2. Extended fused-ring TPs with solubilizing multiple chains.....	139

## LIST OF APPENDIX TABLES

<u>Table</u>	<u>Page</u>
A.1. Crystal data for diamide <b>10</b> .....	142
A.2. Atomic coordinates and equivalent isotropic displacement parameters ( $\text{\AA}^2 \times 10^3$ ) for diamide <b>10</b> .....	143
A.3. Bond lengths [ $\text{\AA}$ ] for diamide <b>10</b> .....	144
A.4. Bond angles [ $^\circ$ ] for diamide <b>10</b> .....	145
A.5. Crystal data for bromomethyl <b>7</b> .....	148
A.6. Atomic coordinates and equivalent isotropic displacement parameters ( $\text{\AA}^2 \times 10^3$ ) for bromomethyl <b>7</b> .....	149
A.7. Bond lengths [ $\text{\AA}$ ] for bromomethyl <b>7</b> .....	150
A.8. Bond angles [ $^\circ$ ] for bromomethyl <b>7</b> .....	151
A.9. Crystal data for hexyloxy <b>14</b> .....	155
A.10. Atomic coordinates and equivalent isotropic displacement parameters ( $\text{\AA}^2 \times 10^3$ ) for hexyloxy <b>14</b> .....	156
A.11. Bond lengths [ $\text{\AA}$ ] for hexyloxy <b>14</b> .....	157
A.12. Bond angles [ $^\circ$ ] for hexyloxy <b>14</b> .....	158
A.13. Crystal data for TP <b>3a</b> .....	162
A.14. Atomic coordinates and equivalent isotropic displacement parameters ( $\text{\AA}^2 \times 10^3$ ) for TP <b>3a</b> .....	163
A.15. Bond lengths [ $\text{\AA}$ ] for TP <b>3a</b> .....	164
A.16. Bond angles [ $^\circ$ ] for TP <b>3a</b> .....	165
A.17. Crystal data for <b>16</b> .....	168
A.18. Atomic coordinates and equivalent isotropic displacement parameters ( $\text{\AA}^2 \times 10^3$ ) for <b>16</b> .....	169
A.19. Bond lengths [ $\text{\AA}$ ] for <b>16</b> .....	169
A.20. Bond angles [ $^\circ$ ] for <b>16</b> .....	170

A.21. Crystal data for <b>23</b> .....	173
A.22. Atomic coordinates and equivalent isotropic displacement parameters ( $\text{\AA}^2 \times 10^3$ ) for <b>23</b> .....	174
A.23. Bond lengths [ $\text{\AA}$ ] for <b>23</b> .....	175
A.24. Bond angles [ $^\circ$ ] for <b>23</b> .....	176



## LIST OF APPENDIX FIGURES

<u>Figures</u>	<u>Page</u>
A.1. Thermal ellipsoid plot of diamide <b>10</b> at the 50% probability level .....	140
A.2. Crystal packing of diamine <b>10</b> with depth cue for clarity.....	141
A.3. Thermal ellipsoid plot of bromomethyl <b>7</b> at the 50% probability level.....	146
A.4. Crystal packing of bromomethyl <b>7</b> with depth cue for clarity .....	147
A.5. Thermal ellipsoid plot of hexyloxy <b>14</b> at the 50% probability level .....	153
A.6. Crystal packing of hexyloxy <b>14</b> with depth cue for clarity.....	154
A.7. Thermal ellipsoid plot of TP <b>3a</b> at the 50% probability level .....	160
A.8. Crystal packing of TP <b>3a</b> with depth cue for clarity .....	161
A.9. Thermal ellipsoid plot of <b>16</b> at the 50% probability level .....	166
A.10. Crystal packing of <b>16</b> with depth cue for clarity .....	167
A.11. Thermal ellipsoid plot of <b>23</b> at the 50% probability level .....	171
A.12. Crystal packing of <b>23</b> with depth cue for clarity .....	172

## LIST OF ABBREVIATIONS AND ACRONYMS

ACN .....	Acetonitrile
AcOH .....	Acetic acid
AIBN .....	Azobisisobutyronitrile
Ar.....	Aryl
Abs .....	Absorbance
BuLi.....	Butyllithium
<sup>t</sup> BuLi .....	<i>tert</i> -Butyllithium
C-C .....	Carbon-carbon bond
C-N .....	Carbon-nitrogen bond
C=N.....	Carbon-nitrogen double bond
C-O.....	Carbon-oxygen bond
C=O.....	Carbonyl bond
cm .....	Centimeters
CP .....	Conjugated polymers
CT.....	Charge-transfer
CV .....	Cyclic voltammetry
D-A.....	Donor-acceptor
DRE.....	Dewer resonance energy
Dbu .....	Dibenzylideneacetone
DCM.....	Dichloromethane
DMEDA .....	Dimethylethylenediamine
DMF .....	Dimethylformamide

Dppp .....	1,3-Bis(diphenylphosphino)propane
$\epsilon$ .....	Molar absorptivity
$E_g$ .....	Band gap
$E_g^{\text{opt}}$ .....	Optical band gap
$E_g^{\text{elec}}$ .....	Electronic band gap
$E_{\text{HOMO}}$ .....	Energy of highest occupied molecular orbital
$E_{\text{LUMO}}$ .....	Energy of lowest unoccupied molecular orbital
$E_{\text{onset}}$ .....	Electrochemical peak onset
$E_{\text{pa}}$ .....	Anodic peak potential
$E_{\text{pc}}$ .....	Cathodic peak potential
$E_{1/2}$ .....	Cathodic peak potential
EDOT .....	3,4-Ethylenedioxythiophene
EtOAc .....	Ethyl acetate
eV .....	Electron volt
$f$ .....	Oscillator strength
GC-MS .....	Gas chromatography-Mass spectrometry
HOMO .....	Highest occupied molecular orbital
HRMS .....	High resolution mass spectrometry
H-T .....	Hammett-Taft
ICT .....	Intramolecular charge transfer
IR .....	Infrared
ITO .....	Indium tin oxide
ITN .....	Isothianaphthene
LDA .....	Lithium diisopropylamide

LUMO .....	Lowest unoccupied molecular orbital
MeCN .....	Acetonitrile
MO .....	Molecular orbital
mp .....	Melting point
MS .....	Mass spectrometry
mV .....	Millivolt
nm .....	nanometers
NBS .....	<i>N</i> -bromosuccinimide
NIR .....	Near Infrared
NMR .....	Nuclear magnetic resonance
nr .....	Not reported
OFET .....	Organic field effect transistor
OLED .....	Organic light emitting diode
OPV .....	Organic photovoltaic
Ox .....	Oxidation
Ph .....	Phenyl
PITN .....	Poly(isothianaphthene)
PPP .....	Polyparaphenylene
PPy .....	Polypyrrole
PT .....	Polythiophene
pTP .....	Poly(thieno[3,4- <i>b</i> ]pyrazine)
pTT .....	Poly(thieno[3,4- <i>b</i> ]thiophene)
Red .....	Reduction
REPE .....	Resonance energy per electron

RT .....	Room temperature
s .....	second
S.....	Siemens
SCE.....	Standard calomel electrode
TBAPF <sub>6</sub> .....	Tetrabutylammonium hexafluorophosphate
TEA .....	Triethylamine
THF .....	Tetrahydrofuran
TLC .....	Thin layer Chromatography
TMEDA.....	Tetramethylethylenediamine
TP .....	Thieno[3,4- <i>b</i> ]pyrazine
UV-vis .....	Ultraviolet-visible
V .....	Volts

# CHAPTER 1. INTRODUCTION

## 1.1. Conjugated Polymers

Conjugated polymers (CPs) are materials that incorporate chains of alternating double and single bonds, or continuous overlapping p-orbitals that allow  $\pi$ -electron delocalization along the backbone of the polymer. The resonance and electron delocalization of polyacetylene, a common CP system often referenced, is illustrated below in Figure 1.1.<sup>1</sup> The conjugated nature of these types of materials allows them to conduct electrons similarly to conventional inorganic semiconductors. Oftentimes, the electronic nature of CPs is characterized by their conductivity. As described here, conductivity is a measure of a material's ability to conduct electricity, with a polymer being defined as semiconducting by having an electrical conductivity in the range of  $10^{-12}$  to  $100 \text{ S/cm}^2$ .

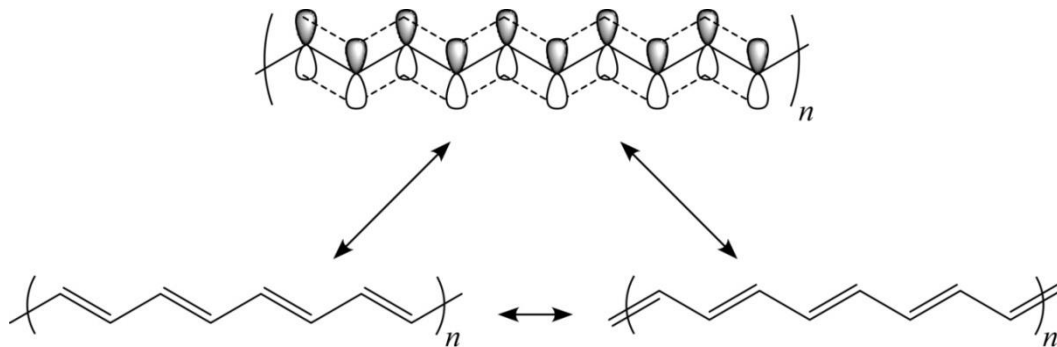


Figure 1.1. Resonance structures of polyacetylene illustrating overlapping p orbitals and  $\pi$  electron delocalization.

Conjugated polymers have garnered much attention recently because of their ability to behave as semiconductors while keeping the desirable characteristics of plastics, such as

low cost, mechanical flexibility, and solution processability.<sup>1-3</sup> Due to the organic nature of these materials, their optical and electronic properties can be tuned through synthetic manipulation, which allows researchers to tailor materials for specific electronic device applications, such as organic photovoltaics (OPVs),<sup>4-8</sup> organic light emitting diodes (OLEDs),<sup>9-17</sup> organic field-effect transistors (OFETs),<sup>16,18-25</sup> electrochromic devices,<sup>26-30</sup> and sensors.<sup>31-36</sup> The design of new organic materials for use in electronic devices is of great interest as they provide means for the production of low-cost, sustainable, and possibly even renewable materials that can reduce the environmental impact of energy production and energy use.

The first CPs exhibiting appreciable conductivity were reported in Australia in 1963 by Weiss and coworkers, where a cross-linked polypyrrole in the form of an insoluble black powder was produced from the thermolysis of 2,3,4,5-tetraiodopyrrole. Analysis of the insoluble polymer showed that the cross-linked polypyrrole exhibited conductivities between 0.005-0.1 S/cm.<sup>37</sup> Further studies of the conductive properties of these polypyrrole materials led to the discovery that iodine content affected the overall conductivity of the materials. It was shown that a decrease in iodine content correspondingly led to a decrease in conductivity. Although a conductive polypyrrole had been produced, the authors were not able to fully understand the relationship between iodine content and conductivity of the materials.<sup>38,39</sup>

A short time later in Paris, Marcel Jozefowicz, who at the time was a Ph.D. student in Rene Buvet's group, brought more attention to CPs with their work. In 1966, Jozefowicz and coworkers showed that the electronic properties of oligomeric polyanilines could be modulated based on the pH and water content of their environment, producing

materials with conductivities in the range of  $10^{-4}$  to  $10$  S/cm.<sup>40-44</sup> They followed this work by reporting in 1971 a polyaniline that exhibited an even greater range of conductivity, where the polyaniline was proton doped via the addition of sulfuric acid that affected the ionic state of the polymers, such as the internal acidic state and hydration state, and produced materials which exhibited conductivities as low as  $10^{-9}$  S/cm and as high as 30 S/cm depending on the ionic nature of the sample.<sup>45</sup> Although these materials showed promising technological applicability with fairly high conductivities, they failed to generate much interest from the scientific community.

Concurrently, Hideki Shirakawa was studying the mechanism of acetylene polymerization using Ziegler-Natta catalysts when they made a serendipitous discovery that secured a foothold for them in the field of conductive polymers. In 1967 a synthetic error in which one thousand times the amount of Ziegler-Natta catalyst was used that caused a very different result from previous trials.<sup>46</sup> This error was thought to increase the rate of the reaction several orders of magnitude, which essentially caused the polymerization of the acetylene gas as soon as contact was made on the surface of the catalyst solution producing a thin film.<sup>46</sup> The reaction produced a polyacetylene that was described as a glittering, silvery-film that appeared to look metallic.

Further analysis of the films showed that the polyacetylene was produced in two isomeric forms (Figure 1.2), both *cis*-polyacetylene and *trans*-polyacetylene, and the isomeric mixture formed was found to be temperature dependent. The thermal studies of the polymerization reaction determined that the *cis* isomer was the major product at low temperatures and the *trans* isomer was dominant at higher temperatures, with 100% *trans* product at a reaction temperature of  $150$  °C.<sup>47</sup> They also discovered that an irreversible



*cis-trans* isomerization took place at temperatures greater than 145 °C, while temperatures greater than 420 °C led to thermal decomposition.<sup>47</sup> Electrochemical measurements revealed that the two isomers had vastly different electronic properties with the *trans*-polyacetylene displaying conductivities as high as 10<sup>-4</sup> S/cm, while the *cis*-polyacetylene showed much lower conductivities of 10<sup>-10</sup> S/cm.<sup>47</sup>

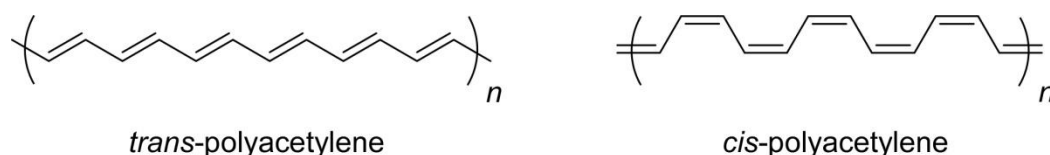


Figure 1.2. Stereoisomers of polyacetylene.

The metallic appearance to the films caught the eyes of Professor Alan G. MacDiarmid and in 1976 he invited Dr. Shirakawa to work with him in his lab at the University of Pennsylvania, where Professor Alan J. Heeger was also working. It was there where the trio made the discovery that really jump started the field of conductive polymers. Professor Heeger was collaborating with Professor MacDiarmid on electric conductivity studies of poly(sulfur-nitride) where the exposure of bromine vapor to the polymer films lead to increased conductivity.<sup>48</sup> Using the same strategy, polyacetylene films were exposed to various halogen gas vapors while measuring their corresponding conductivities. It was hypothesized that when treated with the halogen vapors, they would react with the  $\pi$  electrons from the electron-rich polymer creating positively charged carbocations.<sup>42,48</sup> The doped films exhibited increased electrical conductivity because the resulting carbocations acted as mobile charge carriers along the conjugated backbone. It

was found that the conductivity increased by four orders of magnitude when such films were exposed to vapors of bromine gas, but exposure for long periods of time resulted in decreased conductivity believed to be from over bromination of the polyacetylene film.<sup>41-45,48</sup> An increase in conductivity of seven orders of magnitude was observed when exclusively *trans*-polyacetylene was treated with iodine vapor producing films that displayed conductivities as high as 38 S/cm.<sup>49</sup>

Although conductive polymers had been studied as far back as 1963 by Weiss and coworkers, and 1966 by Jozefowicz and coworkers, their work had been largely overlooked, and in 2000, the Nobel Prize in Chemistry was awarded to Hideki Shirakawa, Alan G. MacDiarmid and Alan J. Heeger for the discovery and development of conducting polymers. Their work initiated a tremendous amount of excitement about the field of conductive polymers, which has directly led to a large and steadily growing number of publications, progression of the field into commercial applications, and a growing list of technologically interesting materials that continue to push the limits of organic electronics.

## 1.2. Band Gap

Classification of the electronic nature of materials is based on the material's band gap ( $E_g$ ) (Figure 1.3). The band gap is a solid-state property of a material that is formally defined as the energetic difference between the filled valence band and the empty conduction band, which is analogous to the energy difference between the highest occupied molecular orbital and the lowest unoccupied molecular orbital (HOMO-LUMO) for systems in the solution-state.<sup>50</sup> Metals are classified as conductors and have an  $E_g$  equal to 0 eV as electrons are able to move freely throughout the material. Semiconductors

are generally labeled as materials with an  $E_g$  between 0 to 2 eV and possess the capability of having induced conductivity because they can have electrons excited from the valence band into the conduction band leaving partially filled and unfilled bands that allow for the flow of electrons. Intuitively, as the band gap decreases it requires less energy to excite electrons from the valence band into the conduction band, resulting in materials that have better conductivities. Insulators are then thought of as any material with an  $E_g$  greater than 2 eV, where there is little to no movement of electrons between the conduction and valence bands at reasonable temperatures.

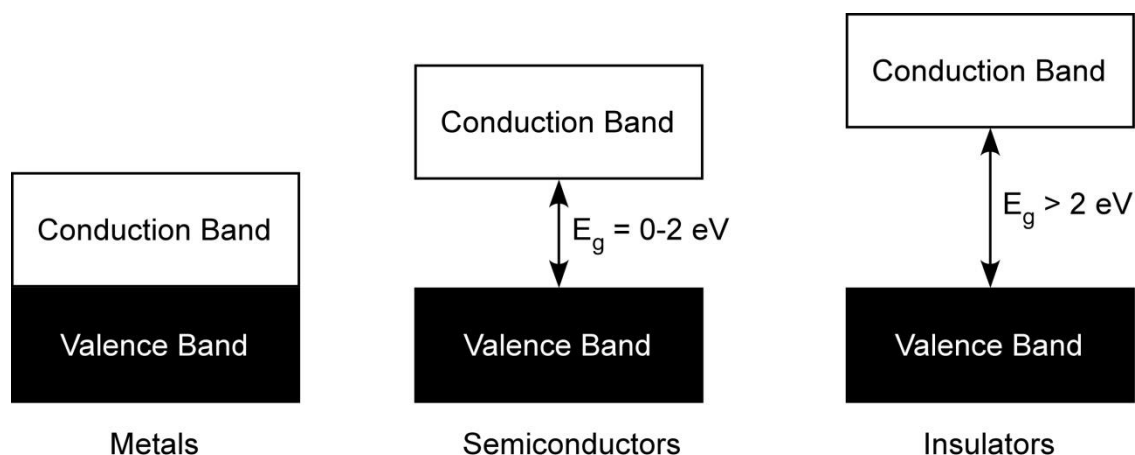


Figure 1.3. Band structure for different classes of materials.

The band structure in conjugated materials results from the combination of  $\pi$  and  $\pi^*$  molecular orbitals (MOs) that mix together that form bands attributed to the groups of filled  $\pi$  MOs and unfilled  $\pi^*$  MOs. The conjugation length of the system is determined by the number of monomer units that contribute to the overall delocalization of electrons throughout the material. As a consequence of the addition of monomers, the analogous

MOs mix with each other to create corresponding non-degenerate MOs that are now higher and lower in energy in comparison to the parent MOs. As more monomer units are added to the system, there is continued mixing of the orbitals creating networks of MOs of similar energy. This results in a large number of MOs that are so close in energy they become indistinguishable from one another. Once in the solid state and intermolecular electron delocalization introduced, the groups of MOs are described as bands (Figure 1.4). The filled lower energy band is known as the valence band and comprises a group of occupied  $\pi$  MOs that contains a delocalized network of  $\pi$ -electrons, while the empty higher energy band is known as the conduction band and contains a group of unoccupied  $\pi^*$  MOs with the energetic difference between these two bands known as the band gap.

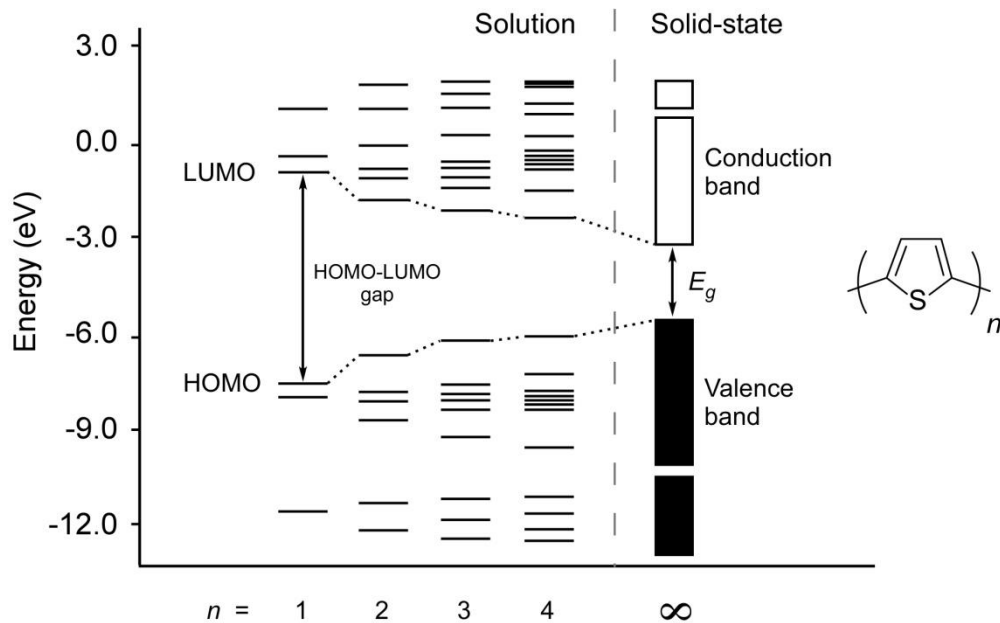


Figure 1.4. Energy level diagram illustrating the relationship between band gap ( $E_g$ ) and HOMO-LUMO energies. Adapted from Ref <sup>51</sup>

In terms of the highest occupied molecular orbital (HOMO) and the lowest unoccupied molecular orbital (LUMO), as more monomer units are added to the system, the number of MOs increases, which causes a destabilization of the HOMO energy level and a stabilization of the LUMO energy level. This causes the energetic difference between the MOs to decrease, which corresponds to a decreased HOMO-LUMO energy gap. In addition, materials in the solid-state can undergo  $\pi$ -stacking interactions, which allow for intermolecular electron delocalization to occur that extends the  $\pi$ -network of the system even further. Because of the extended conjugation in the solid-state, the band gap is typically lower than the HOMO-LUMO gap seen with the materials in solution.

The band gap is an important characteristic of conjugated organic materials, as it is a key parameter responsible for the desirable optical and electronic properties of the material and is often used to assess the value of organic semiconducting polymers. The HOMO and LUMO energy levels correspond to the  $\pi$ - and  $\pi^*$ -orbitals respectively and the HOMO-LUMO gap is referred to as a band gap when the materials are in the solid state where intermolecular delocalization is taken into account.<sup>3</sup> The  $\pi$ -system that determines the band gap of a polymer is thus responsible for the optical and electronic transitions of the material.<sup>3,9</sup> Therefore, the ability to tune the HOMO and LUMO energy levels, or band gap, of a material is of particular interest as this affords researchers the ability to design materials tailored towards specific device applications.

There are two basic methods employed in determining the band gap of a polymer. The most common approach uses the solid-state absorption spectrum of a thin film and by extrapolating the onset of the lowest energy transition in reference to the baseline, a rough estimate of the band gap can be made (Figure 1.5). The onset wavelength can then be

converted to electron volts using the conversion factor of 1240 nm/eV. The onset of the lowest energy transition corresponds to a wavelength that represents the difference in energy between the valence and conduction band edges. Since the method uses optical spectroscopy, the  $E_g$  value obtained is referred to as the optical band gap ( $E_g^{\text{opt}}$ ). This approximation of the optical band gap is a quick and efficient method for determining the  $E_g$  of materials. However, it does not give any information regarding the electronic transitions corresponding to their HOMO and LUMO energy levels. Therefore, additional analytical measurements are necessary to determine further electronic properties.

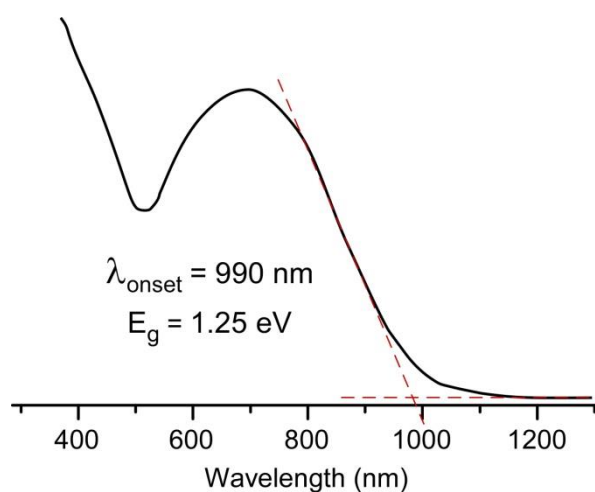


Figure 1.5. Determination of optical band gap.

Cyclic voltammetry (CV) is commonly employed to make the electrochemical measurements necessary to determine HOMO energy and LUMO energy values. This is done by extrapolating the onset of the first oxidation in reference to the baseline, which corresponds to the lowest potential required to remove an electron from the material, and is used to determine the energy of the HOMO level (Figure 1.6). Similarly, the onset of the

first reduction in reference to the baseline corresponds to the lowest potential required to add an electron into the material and determines the energy of the LUMO level. The onset potential values can then be converted to  $E_{\text{HOMO}}$  and  $E_{\text{LUMO}}$  values using the following equations.<sup>52</sup>

$$E_{\text{HOMO}} = - (E_{[\text{onset ox vs. Fc}^+/\text{Fc}]} + 5.1) \text{ eV}$$

$$E_{\text{LUMO}} = - (E_{[\text{onset red vs. Fc}^+/\text{Fc}]} + 5.1) \text{ eV}$$

Onset values are again used for CV measurements, like with spectroscopic techniques, as they correspond to the lowest potentials required to add or remove electrons and are more representative of the valence and conduction band edges. The limiting factor for this method is that both the potential of oxidation and the reduction potential must fall within the solvent window of the system. If either the HOMO or LUMO energy levels of the material being measured fall outside the solvent window, a measurement of the electrochemical band gap cannot be performed.

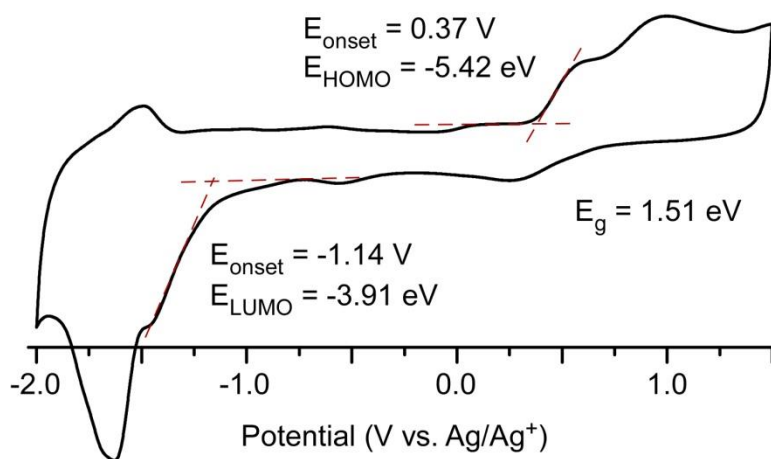


Figure 1.6. Determination of HOMO energy and LUMO energy levels and electronic band gap.

In general, it is thought that materials with decreased band gaps show an increased conductivity because of the enhanced thermal population of the conduction band that in turn generates an increased number of intrinsic charge carriers throughout the system.<sup>53</sup> As a consequence, much effort has been taken to develop methods to produce semiconductors that not only have decreased band gaps, but also exhibit high conductivities.

### 1.3. Band Gap and Energy Level Engineering

Energy level engineering of thiophene-based conjugated polymers can be accomplished through rational modification of six parameters, which include the conjugation length, bond length alternation, torsion angle, aromatic resonance energy, substituents, and intermolecular interactions experienced with the materials, and are shown below in Figure 1.7.<sup>50,54</sup> Each parameters influence on the properties of the material will be discussed as a means to understand structure-function relationships observed in these types of materials.

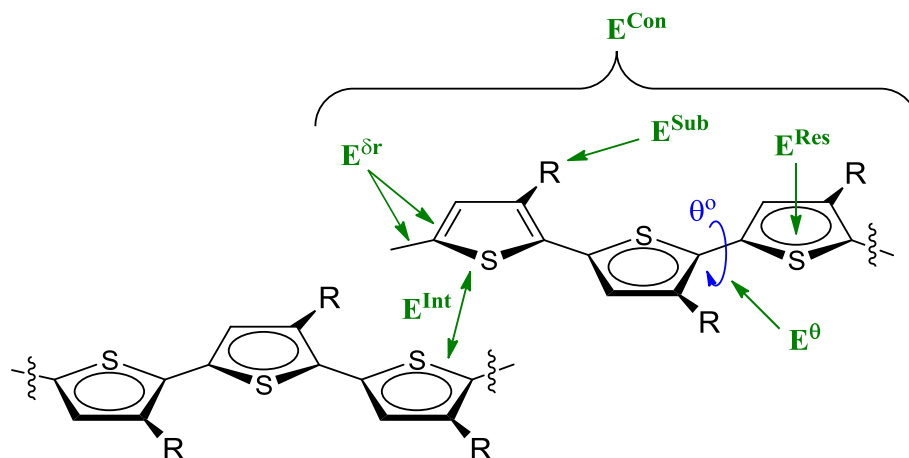


Figure 1.7. Parameters influencing band gap in thiophene polymers: conjugation length (Con), bond length alternation ( $\delta r$ ), resonance energy (Res), substituents (Sub), torsion angle ( $\Theta$ ), and intermolecular interactions (Int).



The parameter,  $E^{\text{Con}}$ , is related to the dependence of a material's band gap on the conjugation length of the polymer.<sup>50,54</sup> As discussed earlier, conjugated materials are essentially comprised of a series of overlapping p-orbitals along the polymer backbone, which gives rise to their semiconducting properties. The conjugation length of a polymer is directly related to its molecular weight and affects the properties of the material because as more polymeric units are added, an increase in orbital blending is observed due to the increased conjugation of the system, which causes a reduction of the band gap. However, this is only valid when discussing materials of low molecular weight because once the effective conjugation length of the system is reached, the effects of additional conjugation is minimal and contribute very little to the electronic properties. In the case of efficient polymerization reactions, the molecular weight of the polymer is typically determined by its solubility in the solvent in which the reaction is taking place. Therefore, it is thought that polymers of greater molecular weight, and potentially lower band gaps, can be achieved through the addition of solubilizing chains to the monomeric materials that will make these materials more soluble in common organic solvents.

The parameter,  $E^{\delta r}$ , is related to the bond length alternation, and is perhaps the most important factor in determining the band gap of a polymer when dealing with simple materials such as polyacetylene.<sup>26,55</sup> Both experimentation and theoretical calculations have shown that bond length alternation in polyacetylene, which has degenerate resonance states, plays a significant role in the size of the band gap.<sup>56</sup> The more uniform the bond lengths are between double and single bonds the lower the theoretical band gap, i.e. if each bond had an equal amount of double bond character versus alternating double and single bonds. The same concept, however, should not be applied to thiophene-based materials

because they possess non-degenerate resonance structures, which include aromatic and quinoidal forms that have vastly different optical and electronic properties, and contribute to a materials band gap to a much greater extent than simple bond length alternation. Therefore, it is more appropriate for polyaromatic conjugated materials, like polythiophene, to discuss the quinoidal character of the material (Figure 1.8).

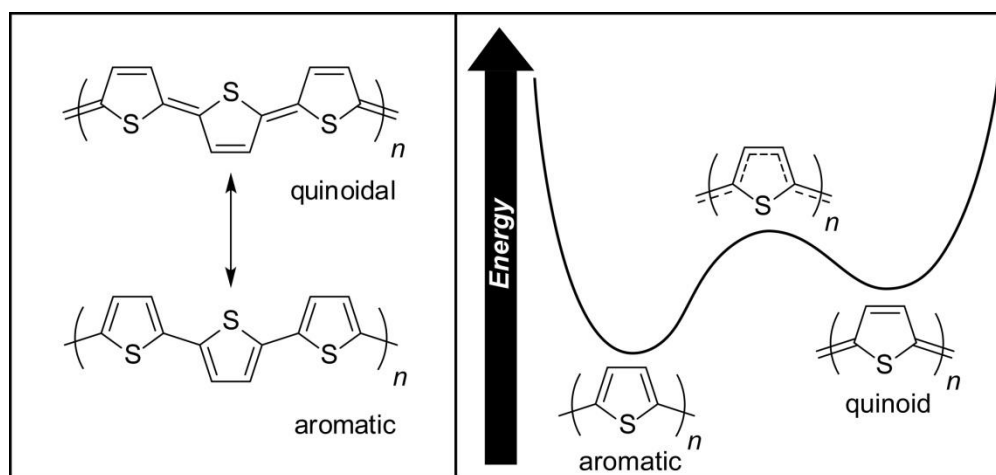


Figure 1.8. Aromatic and quinoidal resonance forms of polythiophene. Adapted from Ref <sup>57</sup>

Since these systems possess non-degenerate resonance states, aromatic versus quinoidal, the extent to which each resonance state contributes to the observed ground state will determine the band gap of the material. Brédas and coworkers conducted a theoretical study where the band gaps of some aromatic systems were calculated and in the case of polythiophene, a band gap of 2.0 eV was calculated for the aromatic form versus a band gap of 0.47 eV for the quinoidal form.<sup>56</sup> Clearly, the preferred resonance of polythiophene is the lower energy aromatic state and is representative of the true ground state of polythiophene, but the quinoidal resonance state displays a significantly lower band gap

due to the combined destabilization of the HOMO and stabilization of the LUMO energy levels. Comparative to the trends observed with bond length alternation, where reduced alternation decreases the band gap, theoretical studies have shown that increases of quinoidal contributions to the ground state correlate to decreases in band gap.<sup>56,57</sup> Therefore, a common approach to reduce the band gap of a system is through structural modifications that increase the quinoidal character of the materials. This is commonly accomplished via synthetic manipulations that incorporate the addition of fused rings to thiophene, such as the cases for poly(isothianaphthalene) (PITN), poly(thieno[3,4-*b*]pyrazine) (pTP), and poly(thieno[3,4-*b*]thiophene) (pTT) where a significant decrease in band gap is observed from the parent polythiophene ( $E_g = 2.0$  eV) to 1.0-1.2 eV for PITN, 0.7-0.9 eV for pTP, and 0.9-1.1 eV for pTT, and are shown below in Figure 1.9.<sup>53,56,57</sup>

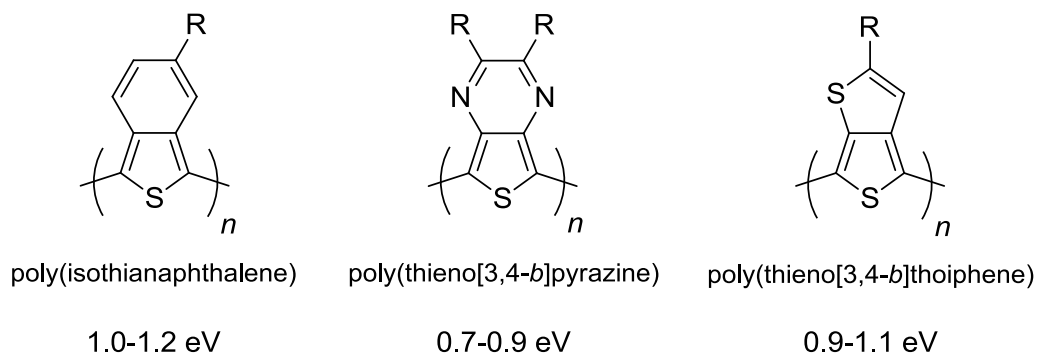


Figure 1.9. Thiophene-based polymers with enhanced quinoidal character from off-chain fused-rings and their corresponding band gaps.

The parameter,  $E^\theta$ , is related to the torsion between rings of adjacent units, which is influenced by steric interactions in the molecule.<sup>9,54,58,59</sup> The band gap of any  $\pi$ -conjugated system is directly related to the degree of p-orbital overlap between repeat units

of the polymer, with any deviations from planarity having significant detrimental effects on electron delocalization through the backbone and negatively impact the electronic properties of the material. Torsional distortions of this nature are typically encountered when neighboring side chains, side chain to backbone, or neighboring  $\beta$ -hydrogens are in close enough proximity to cause steric interactions, with representative examples shown below in Figure 1.10. Brédas and coworkers also conducted theoretical calculations that showed disruptions in  $\pi$ -orbital overlap, caused by rotations about the interannular bond of adjacent rings, of angles up to  $30^\circ$ - $40^\circ$  could be tolerated without significant effect on the electronic properties with respect to the coplanar condition.<sup>60-63</sup> Specifically, their calculations showed only  $\sim 20\%$  decrease in ionization potential for all three polymeric systems, polythiophene, polypyrrole, and polyparaphenylene, when going from the coplanar to the perpendicular conformation.<sup>62</sup> However, torsional distortions greater than  $40^\circ$  were found to have a substantial negative effect on the electronic properties.

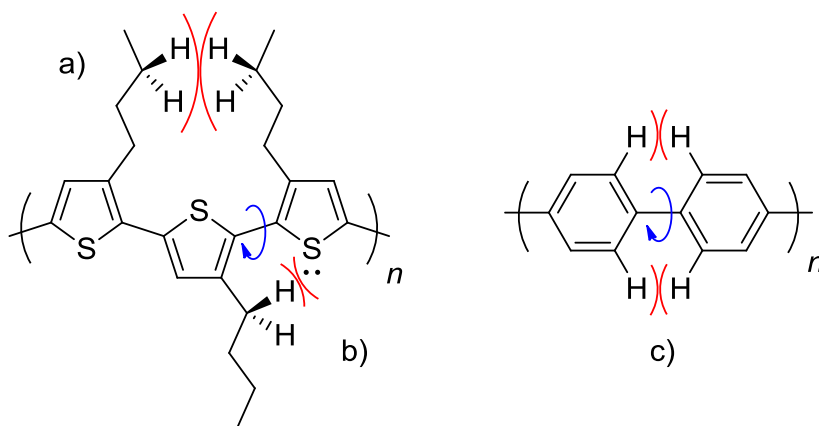


Figure 1.10. Steric distortions due to a) neighboring chain-chain interactions, b) side chain-backbone interactions, and c) neighboring  $\beta$ -hydrogen interactions.

By minimizing the torsion angle in the polymer, an enhancement of backbone planarity can be achieved, which consequently leads to materials with more desirable electronic properties. The high degree of planarity allows for better  $\pi$ -orbital overlap throughout the polymer and has the potential to produce low band gap materials.<sup>64-66</sup> Although the introduction of steric interactions caused by the addition of alkyl side chains brings about steric distortions in materials, they are necessary in order to increase the solubility of these highly planar and often insoluble polymeric materials.

The parameter,  $E^{\text{Res}}$ , is related to the aromatic resonance energy and is described by the resonance energy per electron (REPE) value.<sup>9,54</sup> The REPE value can be thought of as an indicator of the confinement potential of an aromatic system with an increase in confinement potential with an increase in aromaticity.<sup>67</sup> The confinement potential, which dictates the ability of  $\pi$ -electrons to become delocalized along the backbone of polymeric systems, has a direct effect on the band gap of materials.<sup>9,63</sup> As the confinement potential of the aromatic rings decreases,  $\pi$ -electron delocalization throughout the polymer increases, and in turn decreases the band gap.<sup>63,67</sup> A common approach that could be taken to reduce the band gap of conjugated polymers is through the addition of heteroatoms into the aromatic rings, as this decreases the aromaticity of the aryl functionalities along the polymer backbone and allows for more effective  $\pi$ -electron delocalization. A comparison of polymers polythiophene (PT) ( $E_g = 2.0$  eV), polypyrrole (PPy) ( $E_g = 3.0$  eV), and polyparaphenylene (PPP) ( $E_g = 3.4$  eV) can be made that clearly shows this trend, as both the PT and PPy have smaller band gaps than PPP.<sup>61,68</sup> There are other factors that play a role in this reduction in band gap, such as the electron affinity of the heteroatoms, but the reduction of aromaticity of thiophene and pyrrole versus benzene are significant

contributors. The difference in band gap observed between PT and PPy can be attributed to the electron affinity of sulfur (200 kJ/mol) compared to nitrogen (-7 kJ/mol) with greater electron affinities corresponding to smaller band gaps.<sup>68-70</sup>

The parameter,  $E^{\text{Int}}$ , is determined by intermolecular effects between polymer chains.<sup>54</sup> The high degree of planarity and crystalline nature of these materials allows for strong  $\pi$ - $\pi$  interactions between polymer chains in the solid-state. Consequently, the effective conjugation length of the system is extended because of the interchain electron delocalization experienced as these pack together in the solid-state, thus materials can experience a reduction of band gap. Research has shown that irregularities in molecular ordering can have a significant effect on the band gap of polymers by increasing the spatial distance between polymer chains, with an increase in band gap observed in such cases.<sup>71</sup> It is also thought that supramolecular ordering can be induced by alkyl side chain interactions in solid-state packing that could in turn lead to smaller band gaps.<sup>54</sup> Therefore, a balance between solubility and crystallinity must be maintained when the addition of solubilizing chains is employed towards the generation of low band gap materials so that the tight  $\pi$ -stacking interactions can be maintained in the solid-state while still retaining solution processability.

The parameter,  $E^{\text{Sub}}$ , is the contribution of the substituents to the HOMO and LUMO energy levels and is an important factor in describing the tunability of materials.<sup>54</sup> As discussed previously, substituents can be added to enhance the solubility of polymeric materials, but they can also be used as a tool to directly influence the HOMO and LUMO energy levels of the material. These substitutions can have varied effects on the optical and electronic properties because they interact through inductive effects that depend on

their electronic nature, i.e. if they are electron withdrawing or electron donating moieties. When dealing with traditional conjugated polymers like polythiophene-based materials, the addition of electron-donating groups such as alkoxy and amine moieties at the 3- and 4-position will push electron density into the  $\pi$ -system, effectively destabilizing the corresponding orbitals and making it easier to remove an electron from the HOMO energy level.<sup>55,72</sup> In turn, electron-withdrawing groups, such as cyano or trifluoromethyl substituents, will pull electron density out of the  $\pi$ -system causing a stabilization of the LUMO energy level, which decreases the reduction potential (makes it more positive), making it easier to push an electron into the LUMO energy level.<sup>54,69,70</sup>

All of the parameters discussed above not only influence the band gap of a material, but have an effect on each other and the rest of the chemical, mechanical, and physical properties as well.<sup>54</sup> An example of this is the influence of substituents on the torsion about the interannular bond between aromatic ring units. A common approach to increase the solubility of these highly planar systems is through the addition of aliphatic chains that not only inductively influence the electronics of the system ( $E^{\text{sub}}$ ), but also effect the supramolecular arrangement of the materials in the solid-state by making them less crystalline ( $E^{\text{int}}$ ), the torsion angle between adjacent units is increased due to steric interactions ( $E^{\ominus}$ ), and the conjugation length of the polymers can be effect because of the enhanced solubility ( $E^{\text{Con}}$ ). Therefore, the simple control of a single parameter is nearly impossible and conscious effort must be taken to fully understand the effects of the synthetic manipulations of conjugated polymers.

#### 1.4. Energy Level Engineering in Thieno[3,4-*b*]pyrazines

Thieno[3,4-*b*]pyrazines have garnered quite a lot of interest for use in conjugated polymers as they have proven very successful in producing a wide variety of low band gap materials, which are defined as materials with a band gap below 1.5 eV.<sup>53,56,57</sup> They exhibit a great deal of synthetic flexibility that allows them to be versatile building blocks in the designing of materials for specific device applications. In terms of energy level engineering, they share some qualities with traditional polythiophene materials, but also exhibit unique characteristics that set them apart. Most notably, is the ability to asymmetrically manipulate the frontier orbitals of TP-based materials to tune their optical and electronic properties.

As done previously for polythiophenes, the structure-function relationships of poly(thieno[3,4-*b*]pyrazine)s (pTPs) will be discussed based on the six parameters that contribute to a materials band gap, which will again include the conjugation length of the system, bond length alternation, interannular bond torsion angles, aromatic resonance energy, substituent contributions, and intermolecular interactions experienced with the materials as shown below in Figure 1.11.

The concept of conjugation length, labeled by  $E^{\text{Con}}$  in the Figure 1.11, is the same as previously described for the polythiophene systems. As discussed earlier, conjugated polymers are essentially comprised of a series of overlapping p-orbitals along the polymer backbone and the extent of that conjugation is described as its conjugation length. It is common in TP-based materials that an increase in conjugation length leads to a decreased HOMO-LUMO gap, or band gap. This phenomenon was demonstrated by Rasmussen and decreased reduction potential ( $-2.03 \text{ V} \rightarrow -1.83 \text{ V} \rightarrow -1.64 \text{ V}$ ) were observed when the



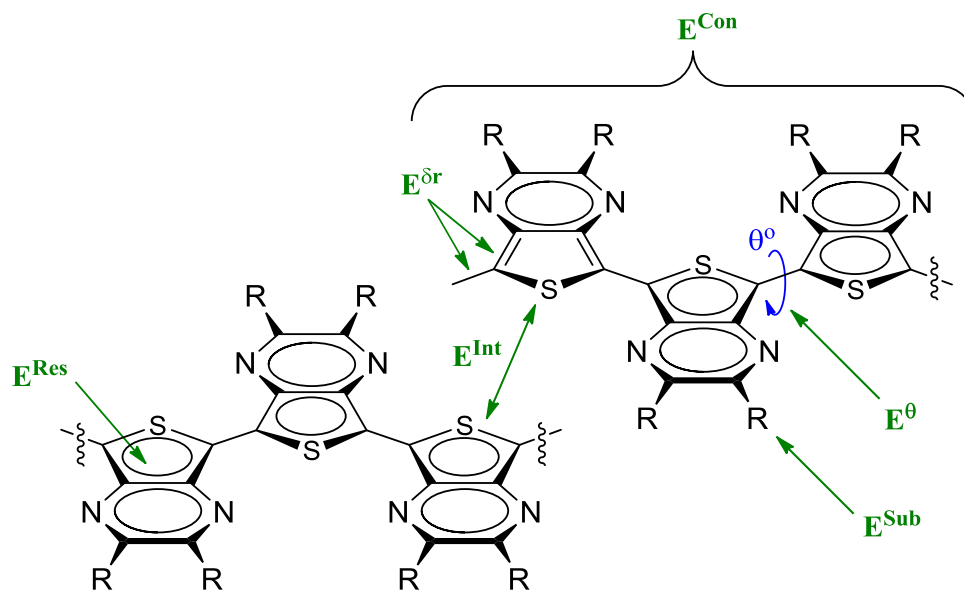


Figure 1.11. Parameters influencing band gap in TP polymers: conjugation length (Con), bond length alternation ( $\delta r$ ), resonance energy (Res), substituents (Sub), torsion angle ( $\Theta$ ), and intermolecular interactions (Int).

conjugation length of the 2,3-dihexylthieno[3,4-*b*]pyrazine system was extended from a monomer up to dimers and trimers, respectively.<sup>73</sup> Also, homopolymeric TPs that were produced electrochemically, which were insoluble and of higher molecular weight, were routinely found to have lower band gaps ( $E_g = 0.6\text{-}0.7$  eV) than pTPs that were generated via chemical oxidation methods and exhibited increased solubility in common organic solvents ( $E_g \sim 0.7\text{-}1.0$  eV), which as a consequence were now solution processable.<sup>53</sup> Therefore, it is thought that TP polymers that exhibit low band gaps, while maintaining solution processability, can be achieved through the addition of solubilizing chains.

One of the most important characteristics in conjugated polymers is for materials to adopt very planar conformations, as this allows for the production of low band gap materials. For the parameter,  $E^\theta$ , which is related to the torsion between rings of adjacent

units, TPs provide materials with greatly reduced steric interactions between adjacent units in comparison to structurally similar materials. The nitrogen in the pyrazine ring allow for a cleft, or void, between beta units in the polymer chain as well as minimize the interaction with the sulfur of the adjacent units (Figure 1.12). When comparing PITNs, which have hydrogens on the fused benzene rings that encroach on one another, as well as the sulfur atom of the adjacent unit that cause torsional strain and lead to materials with decreased planarity.<sup>53</sup> This decrease in backbone planarity causes materials to exhibit higher band gap values, which for PITN are between 1.0 eV and 1.2 eV while the more planar systems of pTPs exhibit lower band gaps between 0.7 eV and 0.9 eV.<sup>78,79</sup> This trend is echoed in the even more sterically challenged polyquinoxaline materials, which exhibit a great deal of torsional strain between adjacent units that causes these materials to be even less planar and consequently have larger band gap values ( $E_g = 2.6$  eV).<sup>76</sup> The minimized steric interactions of TP contribute to the lower band gaps observed with these materials but because it is impossible to manipulate one aspect of conjugated polymers without affecting another, there are other factors that need to be taken into account.

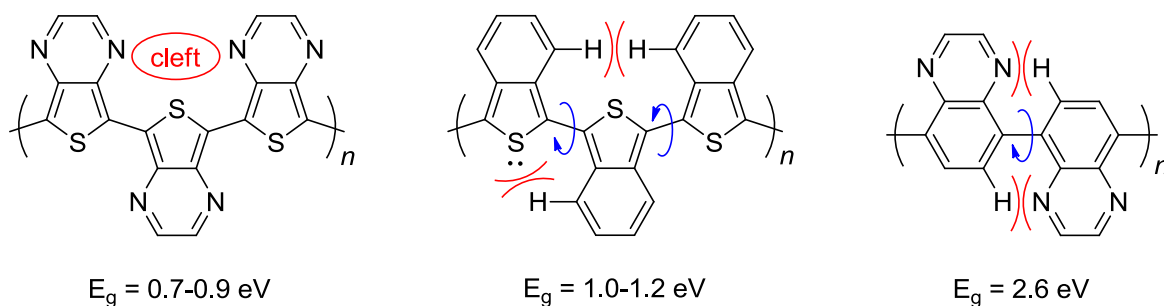


Figure 1.12. Steric interactions of fused-ring polymers and their corresponding band gaps.

Like in the case for polythiophenes, pTPs have non-degenerate resonance states where the polymers can adopt either aromatic or quinoid resonance forms. So the parameter of bond length alternation,  $E^{\delta r}$ , plays a far less important role than the quinoidal character of the polymer. As previously mentioned, it is commonly observed that increased quinoidal character in the ground state of the polymers, leads to decreased band gaps of the materials and a common approach to increasing the quinoidal character is through the addition of fused-rings.<sup>56,57</sup> Therefore, systems that incorporate fused-rings typically produce materials that have lower band gaps than single component systems in comparison to polythiophene, which was demonstrated with PITN ( $E_g \sim 1.0$  eV), pTP ( $E_g \sim 0.7$  eV) and pTT ( $E_g \sim 0.9$  eV), for similar thiophene-based materials, as previously shown in Figure 1.9.<sup>53</sup> However, since the extent of quinoidal character of TP and the materials that are being compared cannot be determined, we can assume the degree of quinoidal character among these are roughly equivalent and that other factors contribute a great deal more to the differences observed in their optical and electronic properties.

The parameter,  $E^{\text{Res}}$ , which describes the relative aromaticity of an aromatic system, is very important in describing the properties of fused-ring materials. This can affect the polymers in a couple of ways, one of which deals with the electron-confinement, within the monomeric units. Aromatic rings with greater electron-confinements will limit electron delocalization along the polymer backbone, which will in turn cause increases in band gap. The other aspect of aromaticity that is more relevant to TP-like systems is dependent on the aromatic nature of the off-chain ring fusion, the quinoidal character of the backbone can be enhanced. The Dewar approach of estimating aromaticity, defined as the Dewar resonance energy (DRE), is considered to be the most successful and provides

clear explanations to the observed properties of the three different materials discussed here.<sup>74</sup> According to the DRE values, benzene > pyrazine >> thiophene (14.0 KJ/mol > 12.0 KJ/mol >> 4.5 KJ/mol), which indicates that the benzene and pyrazine of these fused-ring systems prefer to be in their aromatic resonance state.<sup>74,75</sup> So, for thiophene-based polymers, such as PITN and pTP, the off-chain ring fusion leads to a substantial increase in the quinoidal character in the ground state of these materials, which as a consequence leads to lower band gaps, while the polyquinoxaline would not see this kind of enhancement as the benzene backbone would prefer the aromatic resonance state. This trend is also echoed in the band gap values measured for these materials that are shown above in Figure 1.12.

Another aspect of these materials that needs to be taken into account is the electronic nature of the rings that make up the fused-ring systems. TPs have been shown to possess an advantageous characteristic that is not observed in most other thiophene-based materials and arises from the differences in electron richness between the thiophene and pyrazine rings. Aromatic rings are said to be electron rich if they readily give up electrons in oxidative electrochemical processes and electron deficient if they readily accept electrons in reductive electrochemical processes. Thiophenes are described as electron rich systems as they oxidize at lower potentials than benzene (2.06 V vs. 2.48 V), while the potential at which pyrazine is formally oxidized is too great to be measured using common organic solvents (Table 1.1).<sup>76-78</sup> However, the electrochemical reduction of pyrazine has been measured to be at a more positive potential in comparison to benzene (-2.08 V vs. -2.62 V), which would suggest that pyrazine is more electron deficient than both benzene and thiophene.<sup>76,77</sup>

Table 1.1. Electrochemical data for a series of TP-like compounds.

Compound	Oxidation	Reduction	
	$E_p^a$ , V	$E_{1/2}^a$ , V	Ref.
thiophene	2.06	<i>nr</i>	78
benzene	2.48	-2.62	76,77
pyrazine	<i>nr</i>	-2.08	77
benzo[ <i>c</i> ]thiophene	0.60	<i>nr</i>	78
quinoxaline	<i>nr</i>	-1.62	77
thieno[3,4- <i>b</i> ]pyrazine	1.03	-2.33	79

<sup>a</sup>All potentials vs. SCE. *nr* = not reported.

The difference in electron richness of the rings becomes important with TPs because the difference is large enough that these monomers now exhibit an intramolecular charge transfer (ICT) within the molecule that is not observed in either the ITN or quinoxaline monomers, and is shown below in Figure 1.13.<sup>80</sup> This low energy charge transfer absorption of TPs (350 nm) is red-shifted approximately 25 nm from ITN (~325 nm) and quinoxaline (~323 nm) and allows for the production of materials with decreased band gaps, as a material's lowest energy absorption describes the energetic magnitude of the band gap .

The intermolecular effects,  $E^{Int}$ , that deal with the interspatial separation between polymer chains in the solid state can be affected greatly in systems with off-chain fused-rings. The extended conjugation of these monomers can allow for a much greater degree of  $\pi$ - $\pi$  overlap between polymer chains in the solid state, which would lead to increased  $\pi$ -stacking and decreased band gaps. Even though there is no evidence to support this, based on observations of oligomeric systems that show TP-based terthienyls more readily undergo  $\pi$ -stacked configurations in crystal packing than the corresponding terthiophenes,

it can be confidently assumed that the polymers of such materials would exhibit the same types of behaviors.

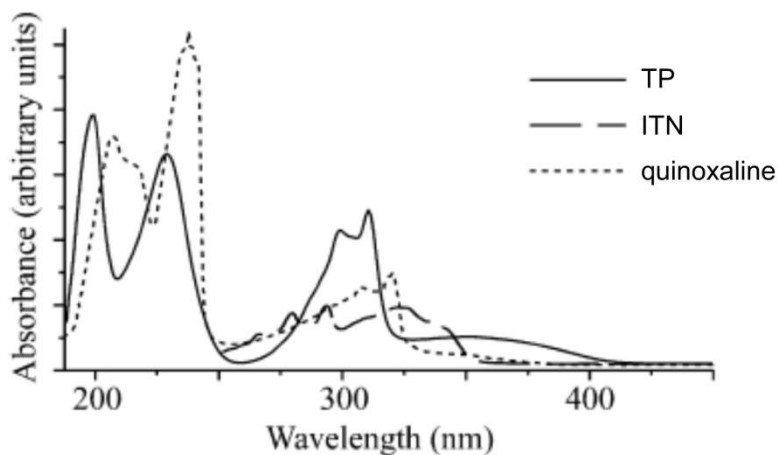


Figure 1.13. UV-vis spectra of TP, ITN, and quinoxaline.<sup>80</sup>

The parameter,  $E^{\text{Sub}}$  that describes the contribution of the substituents to the HOMO and LUMO energy levels of the material, is perhaps the most important contribution to the tunability of TP-based materials.<sup>54</sup> As discussed previously, substituents can be added to as a tool to directly influence the HOMO and LUMO energy levels of the material. However, in TP-based materials the HOMO and LUMO energy levels are distributed asymmetrically on the molecule, with the HOMO located primarily on the thiophene while the LUMO is predominantly located on the pyrazine.<sup>80</sup> Therefore, substitutions on the pyrazine ring in TPs can essentially allow for the asymmetric manipulation of the HOMO and LUMO energy levels in which the effect can be varied based on the electronic nature of the substituents.<sup>81</sup> Because the substituents interact

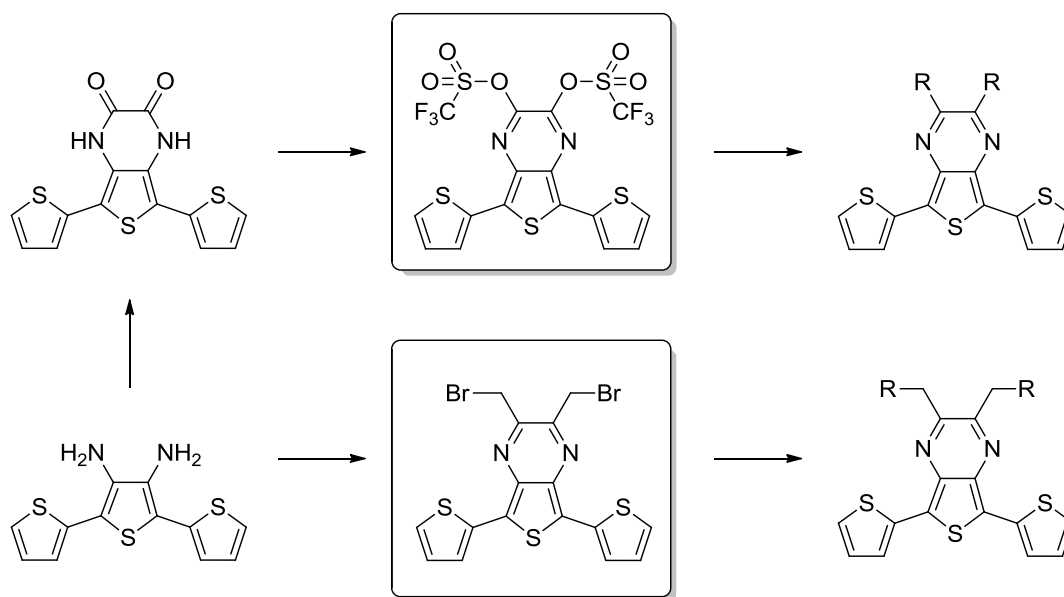
through inductive effects, electron-donating and electron-withdrawing groups will either stabilize or destabilize the LUMO energy level to a greater extent than the HOMO level.

Contrary to the trends for polythiophenes, it was found that the addition of electron-withdrawing groups to the 2- and 3-positions of TPs reduced HOMO-LUMO energies that led to reduced band gaps in the corresponding polymers, while electron-donating groups increased HOMO-LUMO energies that produced materials with increased band gaps.<sup>81</sup> By changing the electronic nature of the substituents, it was found that TP monomers could have their  $\lambda_{\text{max}}$  values tuned over a range of approximately 100 nm (0.92 eV) by going from the electron-donating alkoxy groups, which exhibited a  $\lambda_{\text{max}}$  of 315 nm that is blue shifted from the naked TP ( $\lambda_{\text{max}} = 350$  nm), to the electron-withdrawing cyano groups, which exhibited a red shifted  $\lambda_{\text{max}}$  of 410 nm.<sup>81,82</sup> These trends also carried over into the corresponding polymers where the dialkoxy substituted pTP exhibited a band gap of approximately 1.2 eV, which is significantly larger than that of the analogous dialkyl pTPs ( $E_{\text{g}} \sim 0.7$  eV), while the dicyano pTP derivative exhibited a decreased band gap of  $\sim 0.5$  eV.<sup>81</sup> So, TP-based materials have demonstrated the ability to be quite versatile building blocks for conjugated polymers that allow the opportunity for one to design materials for specific applications.

## 1.5. Research Goals

The generation of organic semiconducting materials with tunable optical and electronic properties is of great interest with much attention being focused on the TP building block in recent years. The scope of conventional TPs has been limited to either 2,3-dialkyl or diaryl analogues due to the standard synthetic approach of a condensation

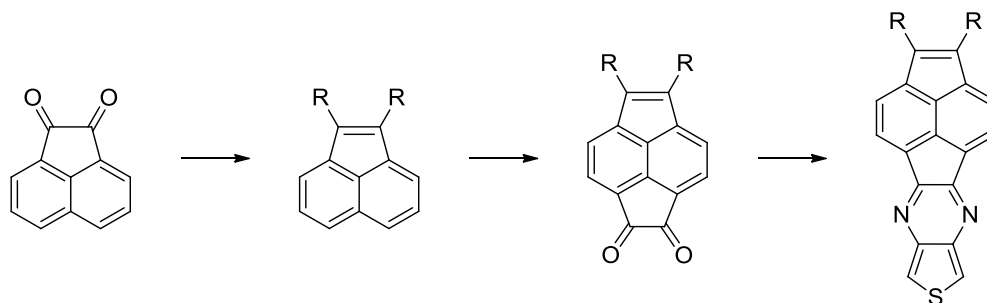
reaction between 3,4-diaminothiophene and available stable  $\alpha$ -diones. As a consequence, this limited the ability to effectively tune the electronic and optical properties of the TP unit. The Rasmussen group has previously demonstrated the ability to produce tunable, low band gap materials through the generation of new families of functionalized TPs.<sup>82,83</sup> However, these materials are hindered by lack of solubility because they are highly planar systems that exhibit a great deal of  $\pi$ - $\pi$  interactions, and stability due to the reactive nature of TPs that are susceptible to oxidative polymerization. Therefore, the application of these methods to TP-based terthienyl systems was sought as the addition of thiophenes at the 5,7-positions not only imparts increased solubility, but also lends a great deal of stability to these materials by occupying reactive sites of the TP as well (Scheme 1.1).



Scheme 1.1. Generation of reactive TP-based terthienyl intermediates for the production of tunable materials.



Another aspect of the presented research was the development of extended fused-ring TPs with increased solubility. Previous work has shown that extended fused-ring TPs have the ability to produce polymers with very low band gaps, with acenaphtho[1,2-*b*]thieno[5,4-*e*]pyrazines demonstrating  $E_g$  values close to 0.5 eV.<sup>83</sup> Work was done to add multiple solubilizing chains on the fused acenaphthylene ring so that materials could be produced that were both soluble in common organic solvents and demonstrated very low band gaps (Scheme 1.2).



Scheme 1.2. Extended fused-ring TPs with solubilizing chains.

The overall goal of this research project was aimed at understanding the structure-function relationship of the TP-based terthienyl system and how the electronic nature of functionalities attached at the 2- and 3-positions would affect their corresponding optical and electronic properties of the material. Such insights would allow for the understanding of the advantageous property of TP-based materials to have their HOMO and LUMO energy levels selectively tuned based on the electronic nature of the substituents used for functionalization.

## 1.6. References

1. Nguyen, T. P.; Destruel, P. In *Handbook of Luminescence, Display Materials, and Devices*; Nalwa, H. S., Rohwer, L. S., Eds.; American Scientific Publishers: Stevenson Ranch, CA, 2003; Vol. 1, p 5.
2. Epstein, A. J.; Wang, Y. Z. In *Semiconducting Polymers: Applications, Properties, and Synthesis*, 735th ed.; Hsieh, B. R., Wei, Y., Eds.; American Chemical Society: Washington, DC, 1999; pp 119-133.
3. Skotheim, T. A., Reynolds, J. R., Eds. *Handbook of Conducting Polymers*, 3rd ed.; CRC Press: Boca Raton, FL, 2007.
4. Granström, M.; Harrison, M. G.; Friend, R. H. In *Handbook of Oligo- and Polythiophene*; Fichou, D., Ed.; Wiley-VCH: Weinheim, 1999; pp 405-458.
5. Mozer, A. J.; Sariciftci, N. S. In *Handbook of Conducting Polymers: Processing and Applications*, 3rd ed.; Skotheim, T. A., Reynolds, R., Eds.; CRC Press: Boca Raton, FL, 2007; pp 10-1-10-37.
6. Brabec, C. J.; Sariciftci, N. S. In *Semiconducting Polymers: Chemistry, Physics, and Engineering*; Hadziioannou, G., van Hutten, P. F., Eds.; Wiley-VCH: Weinheim, 2000; pp 515-560.
7. Barbarella, G.; Melucci, M. In *Handbook of Thiophene-Based Materials: Applications in Organic Electronics and Photonics*; Perepichka, I. F., Perepichka, D. F., Eds.; Wiley: West Sussex, U. K., 2009; Vol. 1, pp 255-292.
8. Gevorgyan, S. A.; Krebs, F. C. In *Handbook of Thiophene-Based Materials*; Perepichka, I. F., Perepichka, D. F., Eds.; Wiley: West Sussex, U. K., 2009; Vol. 1, pp 673-694.

9. Cui, T.; Liu, Y. In *Organic Electronics and Photonics: Electronic Materials and Devices*; Nalwa, H. S., Ed.; American Scientific Publishers: Stevenson Ranch, 2008; Vol. 1, pp 263-303.
10. Friend, R. H.; Greenham, N. C. In *Handbook of Conducting Polymers*, 2nd ed.; Skotheim, T. A., Elsenbaumer, R. L., Reynolds, J. R., Eds.; Marcel Dekker, Inc.: New York, 1998; pp 823-846.
11. Christian-Pandya, H.; Vaidyanathan, S.; Galvin, M. In *Handbook of Conducting Polymers*, 3rd ed.; Skotheim, T. A., Reynolds, J. R., Eds.; CRC Press: Boca Raton, FL, 2007; Chapter 5.
12. Grimsdale, A. C.; Chan, K. L.; Martin, R. E.; Jokisz, P. G.; Holmes, A. B. *Chem. Rev.* **2009**, *109*, 897-1091.
13. Epstein, A. J.; Wang, Y. Z. In *Semiconducting Polymers: Applications, Properties, and Synthesis*, 735th ed.; Hsieh, B. R., Wei, Y., Eds.; American Chemical Society: Washington, DC, 1999; pp 119-133.
14. Chen, S.-A.; Chang, E.-C. In *Semiconducting Polymers: Applications, Properties, and Synthesis*, 735th ed.; Hsieh, B. R., Wei, Y., Eds.; American Chemical Society: Washington, DC, 1999; pp 163-173.
15. Murray, M. M.; Holmes, A. B. In *Semiconducting Polymers: Chemistry, Physics, and Engineering*; Hadziioannou, G., van Hutten, P. F., Eds.; Wiley-VCH: Weinheim, 2000; pp 1-35.

16. Campbell, I. H.; Smith, D. L. In *Semiconducting Polymers: Chemistry, Physics, and Engineering*; Hadziioannou, G., van Hutten, P. F., Eds.; Wiley-VCH: Weinheim, 2000; pp 333-364.
17. Scott, J. C.; Malliaras, G. G. In *Semiconducting Polymers: Chemistry, Physics, and Engineering*; Hadziioannou, G., van Hutten, P. F., Eds.; Wiley-VCH: Weinheim, 2000; pp 411-462.
18. Katz, H. E.; Dodabalapur, A.; Bao, Z. In *Handbook of Oligo- and Polythiophenes*; Fichou, D., Ed.; Wiley-VCH: Weinheim, 1999; pp 459-490.
19. Tessler, N.; Veres, J.; Globerman, O.; Rappaport, N.; Preezant, Y.; Roichman, Y.; Solomesch, O.; Tal, S.; Gershman, E.; Adler, M.; Zolotarev, V.; Gorelik, V.; Eichen, Y. In *Handbook of Conducting Polymers: Processing and Applications*, 3rd ed.; Skotheim, T. A., Reynolds, J. R., Eds.; CRC Press: Boca Raton, FL, 2007; pp 7-1-7-42.
20. Bao, Z. In *Semiconducting Polymers: Applications, Properties, and Synthesis*, 735th ed.; Hsieh, B. R., Wei, Y., Eds.; American Chemical Society: Washington, DC, 1999; pp 244-257.
21. Horowitz, G. In *Semiconducting Polymers: Chemistry, Physics, and Engineering*; Hadziioannou, G., van Hutten, P. F., Eds.; Wiley-VCH: Weinheim, 2000; pp 463-514.
22. Otsubo, T.; Takimiya, K. In *Handbook of Thiophene-Based Materials: Applications in Organic Electronics and Photonics*; Perepichka, I. F., Perepichka, D. F., Eds.; Wiley: West Sussex, U. K., 2009; Vol. 1, pp 321-340.

23. Hotta, S. In *Handbook of Thiophene-Based Materials*; Perepichka, I. F., Perepichka, D. F., Eds.; Wiley: West Sussex, U. K., 2009; Vol. 1, pp 477-496.
24. Facchetti, A. In *Handbook of Thiophene-Based Materials*; Perepichka, I. F., Perepichka, D. F., Eds.; Wiley: West Sussex, U. K., 2009; Vol. 1, pp 595-646.
25. McCulloch, I.; Heeney, M. In *Handbook Thiophene-Based Materials*; Perepichka, I. F., Perepichka, D. F., Eds.; Wiley: West Sussex, U. K., 2009; Vol. 1, pp 647-672.
26. Thomas, C. A.; Reynolds, R. In *Semiconducting Polymers: Applications, Properties, and Synthesis*, 735th ed.; Hsieh, B. R., Wei, Y., Eds.; American Chemical Society: Washington, DC, 1999; pp 367-373.
27. Meng, X. S.; Desjardins, P.; Wang, Z. Y. In *Semiconducting Polymers: Applications, Properties, Synthesis*, 735th ed.; Hsieh, B. R., Wei, Y., Eds.; American Chemical Society: Washington, DC, 1999; pp 61-75.
28. Invernale, M. A.; Acik, M.; Sotzing, G. A. In *Handbook of Thiophene-Based Materials: Applications in Organic Electronics and Photonics*; Perepichka, I. F., Perepichka, D. F., Eds.; Wiley: West Sussex, U. K., 2009; Vol. 1, pp 757-782.
29. Beaujuge, P. M.; Reynolds, R. *Chem. Rev.* **2010**, *110*, 268-320.
30. Beaujuge, P. M.; Amb, C. M.; Reynolds, J. R. *Acc. Chem. Res.* **2010**, *43*, 1396-1407.
31. Guiseppi-Elie, A.; Wallace, G. G.; Matsue, T. In *Handbook of Conducting Polymers*, 2nd ed.; Skotheim, T. A., Elsenbaumer, R. L., Reynolds, J. R., Eds.; Marcel Dekker, Inc.: New York, 1998; pp 963-992.
32. Kossmehl, G.; Engelmann, G. In *Handbook of Oligo- and Polythiophenes*; Fichou, D., Ed.; Wiley-VCH: Weinheim, 1999; pp 491-524.

33. Guiseppi-Elie, A.; Brahim, S.; Wilson, A. M. In *Handbook of Conducting Polymers: Processing and Applications*, 3rd ed.; Skotheim, T. A., Reynolds, J. R., Eds.; CRC Press: Boca Raton, FL, 2007; pp 12-1-12-45.
34. Nilsson, P.; Inganäs, O. In *Handbook of Conducting Polymers: Processing and Applications*, 3rd ed.; Skotheim, T. A., Reynolds, J. R., Eds.; CRC Press: Boca Raton, FL, 2007; pp 13-1-13-24.
35. MacDiarmid, A. G.; Huang, F.; Feng, J. In *Semiconducting Polymers: Applications, Properties, and Synthesis*, 735th ed.; Hsieh, B. R., Wei, Y., Eds.; American Chemical Society: Washington, DC, 1999; pp 184-215.
36. Ho, H.-A.; Leclerc, M. In *Handbook of Thiophene-Based Materials: Applications in Organic Electronics and Photonics*; Perepichka, I. F., Perepichka, D. F., Eds.; Wiley: West Sussex, U. K., 2009; Vol. 1, pp 813-832.
37. McNeill, R.; Siudak, R.; Wardlaw, J. H.; Weiss, D. E. *Aust. J. Chem.* **1963**, *16*, 1056-1075.
38. Bolto, B. A.; Weiss, D. E. *Aust. J. Chem.* **1963**, *16*, 1076-1089.
39. Bolto, B. A.; McNeill, R.; Weiss, D. E. *Aust. J. Chem.* **1963**, *16*, 1090-1103.
40. Jozefowicz, M.; Yu, L.-T. *Rev. Gen. Electr.* **1966**, *75*, 1008.
41. Yu, L.-T.; Jozefowicz, M. *Rev. Gen. Electr.* **1966**, *75*, 1014.
42. Jozefowicz, M.; Yu, L.-T.; Belorgey, G.; Buvet, R. *J. Polym. Sci. Pol. Sym.* **1967**, *16*, 2943.

43. Elschner, A.; Kirchmeyer, S.; Lovenich, W.; Merker, U.; Reuter, K. In *PEDOT: Principles and Applications of an Intrinsically Conductive Polymer*; CRC Press: Boca Raton, FL 2011.
44. De Surville, R.; Jozefowicz, M.; Yu, L. T.; Perichon, J.; Buvet, R. *Electrochim. Acta.* **1968**, *13*, 1451-1458.
45. Doriomedoff, M.; Hautiere-Cristofini, F.; De Surville, R.; Jozefowicz, M.; Yu, L. T.; Buvet, R. *J. Chim. Phys. Phys.-Chim. Biol.* **1971**, *68*, 1055-1069.
46. The Official Web Site of the Nobel Prize.  
[http://www.nobelprize.org/nobel\\_prizes/chemistry/laureates/2000/shirakawa-bio.html](http://www.nobelprize.org/nobel_prizes/chemistry/laureates/2000/shirakawa-bio.html)  
(accessed April 18,2014).
47. Shirakawa, H. *Angew. Chem. Int. Ed.* **2001**, *40*, 2574-2580.
48. Heeger, A. J. *Angew. Chem. Int. Ed.* **2001**, *40*, 2591-2611.
49. Shirakawa, H.; Louis, E. J.; MacDiarmid, A. G.; Chiang, C. K.; Heeger, A. J. *Chem. Commun.* **1977**, 578-580.
50. Roncali, J. *Chem. Rev.* **1997**, *97*, 173-205.
51. van Mullekom, H. A. M.; Vekemans, J. A. J. M.; Havinga, E. E.; Meijer, E. W. *Mater. Sci. Eng., R*, **2001**, *32*, 1.
52. Cardona, C. M.; Li, W.; Kaifer, A. E.; Stockdale, D.; Bazan, G. C. *Adv. Mater.* **2011**, *23*, 2367-2371.
53. Rasmussen, S. C.; Schwiderski, L.; Mulholland, M. E. *Chem. Commun.* **2011**, *47*, 11394-11410.

54. Kroon, R.; Lenes, M.; Hummelen, J. C.; Blom, P. W. M.; De Boer, B. *Polym. Rev.* **2008**, *48*, 531.
55. Rasmussen, S. C.; Ogawa, K.; Rothstein, S. D. In *Handbook of Organic Electronics and Photonics: Electronic Materials and Devices*; Nalwa, H. S., Ed.; American Scientific Publishers: Stevenson Ranch, CA, 2008; Vol. 1, pp 1-50.
56. Rasmussen, S. C. In *Encyclopedia of Polymeric Nanomaterials*; Kobayashi, S., Mullen, K., Eds.; Springer-Verlag: Berlin, Germany, 2015; Chapter 57.
57. Pomerantz, M. In *Handbook of Conducting Polymers*, 2nd ed.; Skotheim, T. A., Elsenbaumer, R. L., Reynolds, J. R., Eds.; Marcel Dekker Inc.: New York, 1998; pp 277-310.
58. Daoust, G.; Leclerc, M. *Macromolecules* **1991**, *24*, 455-459.
59. Leclerc, M.; Daoust, G. *Synth. Met.* **1991**, *41*, 529-530.
60. Brédas, J. L. *J. Chem. Phys.* **1985**, *82*, 3808-3811.
61. Dkhissi, A.; Louwet, F.; Groenendaal, L.; Beljonne, D.; Lazzaroni, R.; Brédas, J. L. *Chem. Phys. Lett.* **2002**, *359*, 466-472.
62. Brédas, J. L.; Street, G. B.; Thémans, B.; André, J. M. *J. Chem. Phys.* **1985**, *83*, 1323-1329.
63. Rasmussen, S. C.; Straw, B. D.; Hutchison, J. E. In *Semiconducting Polymers: Applications, Properties, and Synthesis*, 735th ed.; Hsieh, B. R., Wei, Y., Eds.; American Chemical Society: Washington, DC, 1999; pp 347-366.
64. McCullough, R. D.; Lowe, R. D. *J. Chem. Soc., Chem. Commun.* **1992**, 70-72.
65. Chen, T. A.; Rieke, R. D. *J. Am. Chem. Soc.* **1992**, *114*, 10087-10088.



66. Loewe, R. S.; Khersonsky, S. M.; McCullough, R. D. *Adv. Mater.* **1999**, *11*, 250-253.
67. Hernandez, V.; Castiglioni, C.; Del Zoppo, M.; Zerbi, G. *Phys. Chem. B.* **1994**, *50*, 9815-9823.
68. Kertesz, M.; Yang, S.; Tian, Y. In *Handbook of Thiophene-Based Materials: Applications in Organic Electronics and Photonics*; Perepichka, I. F., Perepichka, D. F., Eds.; Wiley: West Sussex, 2009; Vol. 1, Chapter 7.
69. Wu, X.; Rieke, D. *J. Org. Chem.* **1995**, *60*, 6658-6659.
70. Wu, X.; Chen, T. A.; Rieke, R. D. *Macromolecules* **1996**, *9*, 7671-7677.
71. Kondo, T.; Ishii, A.; Manabe, H.; Munekata, H. *Appl. Phys. Lett.* **2001**, *78*, 1352-1354.
72. Roncali, J. *Chem. Rev.* **1992**, *92*, 711-738.
73. Wen, L.; Heth, C. L.; Rasmussen, S. C. *Phys. Chem. Chem. Phys.*, **2014**, *16*, 7231.
74. Katritzky, A. R.; Pozharskii, A. F. In *Handbook of Heterocyclic Chemistry*, 2nd ed.; Elsevier Science: Kidlington, Oxford, UK, 2000; pp 44-45.
75. Katritzky, A. R.; Pozharskii, A. F. In *Handbook of Heterocyclic Chemistry*, 2nd ed.; Elsevier Science: Kidlington, Oxford, UK, 2000; p 80.
76. Merkel, P. B.; Luo, P.; Dinnocenzo, J. P.; Farid, S. *J. Org. Chem.* **2009**, *74*, 5163-5173.
77. Mancilha, F. S.; DaSilveira Neto, B. A.; Lopes, A. S.; Moreira, P. F.; Quina, F. H.; Gonclaves, R. S.; Dupont, J. *Eur. J. Org. Chem.* **2006**, 4924-4933.
78. Kobayashi, M.; Colaneri, N.; Boysel, M.; Wudl, F.; Heeger, A. J. *J. Chem. Phys.* **1985**, *82*, 5717-5723.

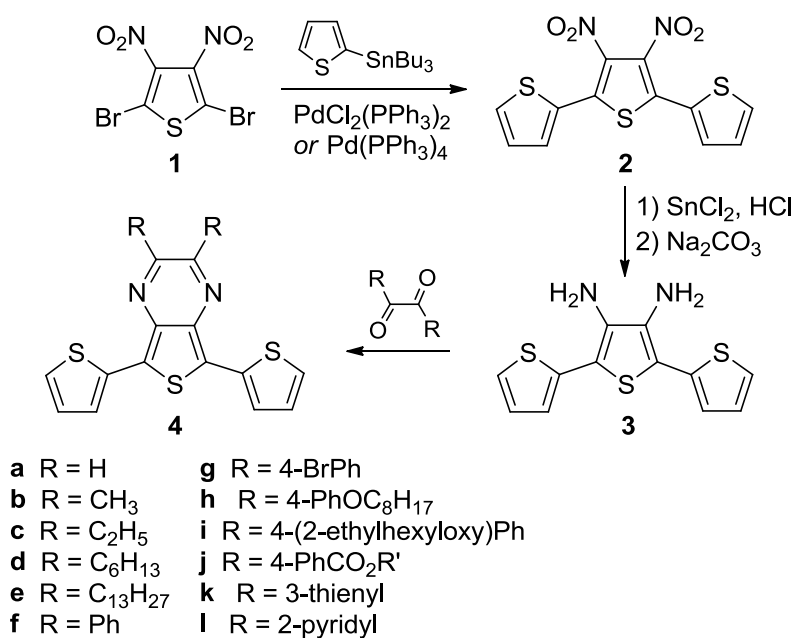
79. Kenning, D. D.; Mitchell, K. A.; Calhoun, T. R.; Funfar, M. R.; Sattler, D. J.; Rasmussen, S. C. *J. Org. Chem.* **2002**, *67*, 9073.
80. Rasmussen, S. C.; Sattler, D. J.; Mitchell, K. A.; Maxwell, J. J. *Lumin.* **2004**, *109*, 111-119.
81. Wen, L.; Nietfeld, J. P.; Amb, C. M.; Rasmussen, S. C. *Synth. Met.* **2009**, *159*, 2299-2301.
82. Wen, L.; Nietfeld, J. P.; Amb, C. M.; Rasmussen, S. C., *J. Org. Chem.* **2008**, *73*, 8529-8536.
83. Nietfeld, J. P.; Schwiderski, R. L.; Gonnella, T. P.; Rasmussen, S. C. *J. Org. Chem.*, **2011**, *76*, 6383-6388.

# CHAPTER 2. SYNTHESIS AND CHARACTERIZATION OF THIENO[3,4-*b*]PYRAZINE-BASED TERTHIENYLS: TUNABLE PRECURSORS FOR LOW BAND GAP CONJUGATED MATERIALS

## 2.1. Introduction

Thieno[3,4-*b*]pyrazine (TP) is a fused-ring, thiophene-based unit that has become a relatively popular building block for the production of low band gap ( $E_g < 1.5$  eV) and reduced band gap ( $E_g = 1.5$ -2.0 eV) conjugated organic materials.<sup>1-4</sup> Band gap is a critical parameter that is responsible for many of the technologically useful properties of conjugated polymers. Control of a material's band gap is very desirable as this affords researchers the ability to tune the optical and electronic properties of the material, ultimately allowing the generation of materials tailored to specific device applications. TPs have been shown to be one of the more successful approaches towards this goal as they allow for convenient synthetic manipulation for band gap tuning.<sup>2</sup> The TP unit itself has been used frequently as a monomer in the production of a number of polymeric materials.<sup>2-4</sup> However, the somewhat reactive nature of TPs oftentimes causes materials scientists to find these monomeric units difficult to work with.<sup>2-4</sup> Consequently, many favor the application of TPs in the form of terthienyl analogs in which the reactive  $\alpha$ -positions of the TP are substituted with 2-thienyl groups, such as in 5,7-bis(2-thienyl)thieno[3,4-*b*]pyrazine (**4a**) (Scheme 2.1).<sup>5-8</sup> Comparatively, TP-based terthienyls undergo oxidation at much lower potentials than the simple TP monomers, but the

increased size and conjugation length of the oligomeric terthienyls results in decreased reactivity, thus lowering the chances of losing material through unwanted oxidative coupling processes or decomposition.



Scheme 2.1. Synthesis of conventional thieno[3,4-*b*]pyrazine-based terthienyls via simple condensation reactions.<sup>9</sup>

Examples of TP-based terthienyls were initially reported by Yamashita and co-workers in 1994 and have since become quite common precursors to TP-based polymeric materials.<sup>5,6</sup> These TP-based terthienyls are prepared using methods analogous to the common monomeric TPs. To make the terthienyl analogs, the bromine functionalities of the common precursor 2,5-dibromo-3,4-dinitrothiophene (**1**) are utilized in a Stille coupling reaction with 2-(tributylstannyl)thiophene to generate the 3',4'-dinitro-2,2':5',2''-terthiophene (**2**).<sup>10</sup> Then the reduction of **2** with either SnCl<sub>2</sub> or tin metal/HCl will generate

the diamine salt and, upon neutralization with base, the diamine **3** is produced. This then allows for typical condensation reactions with various  $\alpha$ -diones to generate the corresponding TP-based terthienyls. Methods such as these have been used to produce a wide variety of unfunctionalized-, dialkyl-, diaryl-, and heteroaryl-TP-based terthienyls of which **4a-1** in Scheme 2.1 are representative examples.<sup>5-8,11-38</sup>

The tunability of both the monomeric TPs and their terthienyl analogs is limited by the stability of the  $\alpha$ -dione employed during their synthesis, as depicted in Scheme 2.1. This limits the amount of tuning possible for these fused-ring units because the functional groups are limited to either alkyl or aryl substituents, as determined by the available diones. Therefore, a rather narrow range of optical and electronic variance has been achieved with these types of systems, which ultimately hinders the production of low band gap materials. As a means to overcome this constraint, the Rasumussen group recently reported new synthetic methods for the production of monomeric TPs that allows for the introduction of both strongly electron-donating and electron-withdrawing side chains.<sup>39</sup> Herein this dissertation, work is presented that expands on this new synthetic approach to introduce reactive leaving groups to TP-based terthienyls through the synthesis of two new 2,3-difunctionalized TP-based terthienyls, in the form of 2,3-ditriflate- and 2,3-bis(bromomethyl)-5,7-bis(2-thienyl)thieno[3,4-*b*]pyrazines as precursors to a variety of new analogues (Figure 2.1). The synthetic versatility of the precursor terthienyls **5-7** has been demonstrated with the production of new TP-terthienyls containing electron-donating and electron-withdrawing groups.<sup>9,40</sup> The characterization of these materials provides further insights into the extent of which the optical and electronic properties of these systems can be tuned through modulating the electron-donating or electron-withdrawing

character of the TP functional groups. The bulk of the work reported in this chapter has been published as a paper in the *Journal of Organic Chemistry*.<sup>9</sup>

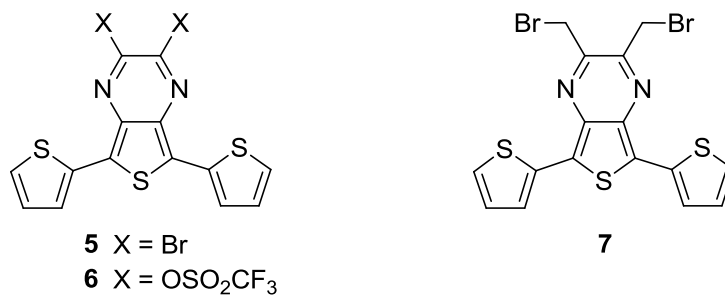
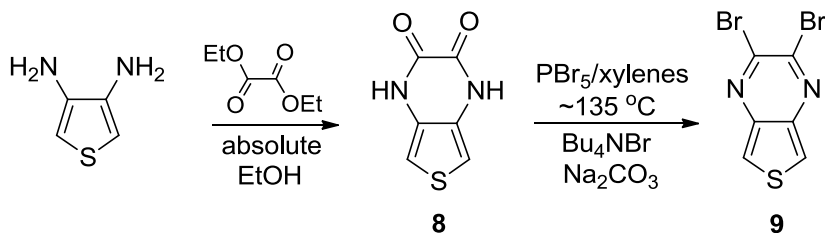


Figure 2.1. Thieno[3,4-*b*]pyrazine-based terthienyls with good leaving groups.<sup>9</sup>

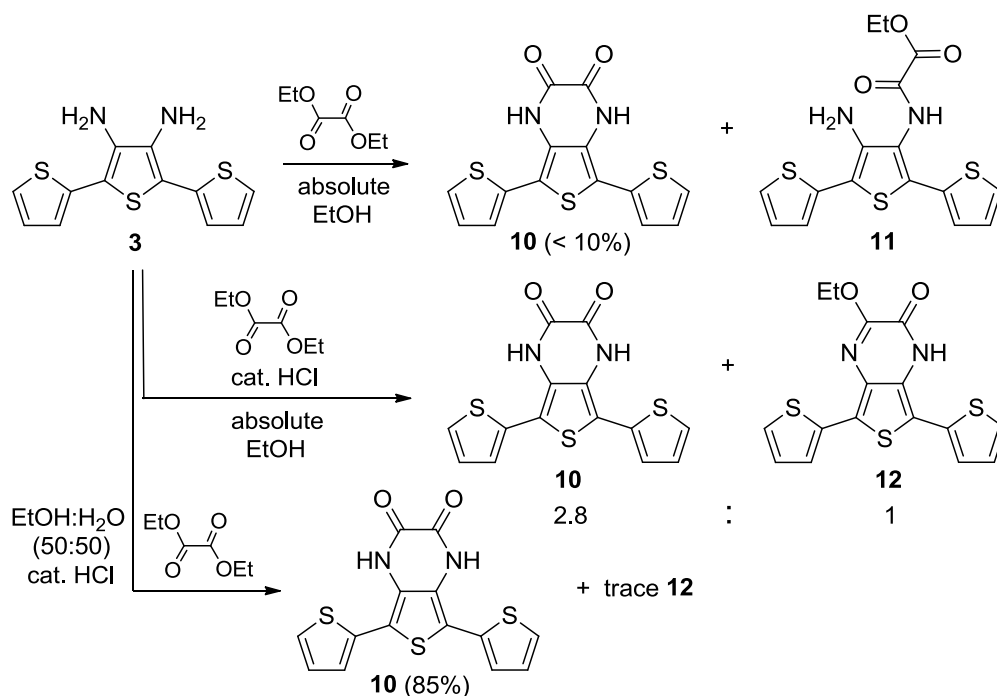
## 2.2. Results and Discussion

**Synthesis.** A synthetic approach to produce 2,3-dibromothieno[3,4-*b*]pyrazine (**9**), the monomeric TP analogue of terthienyl **5**, was previously established via the bromination of the intermediate thieno[3,4-*b*]pyrazine-2,3(1*H*,4*H*)-dione (**8**) and is illustrated in Scheme 2.2.<sup>39</sup> Using this same synthetic methodology as a starting point, the approach was applied to the generation of terthienyl **5**.



Scheme 2.2. Previous synthesis of 2,3-dibromothieno[3,4-*b*]pyrazine.<sup>9</sup>

The condensation of diamine **3** with diethyl oxalate using the conditions that were successful for the monomeric TP analogue resulted in very low yields (<10%) of the desired product **10** (Scheme 2.3). The majority of the material isolated consisted of the non-cyclized product **11** as a result of only one condensation reaction taking place. The reaction seemed to progress much better with the addition of a catalytic amount of HCl resulting in significantly higher yields, but also presented the problem of generating a mixture of the desired product **10** as well as byproduct **12**.



Scheme 2.3. Synthesis of 5,7-bis(2-thienyl)thieno[3,4-*b*]pyrazine-2,3(1*H*,4*H*)-dione.<sup>9</sup>

Diamide **10** could be selectively extracted from the mixture by aqueous KOH, as the desired product was soluble in aqueous basic solutions, while the byproduct was not. However, this resulted in a significant reduction of yield as the ratio of the two species in

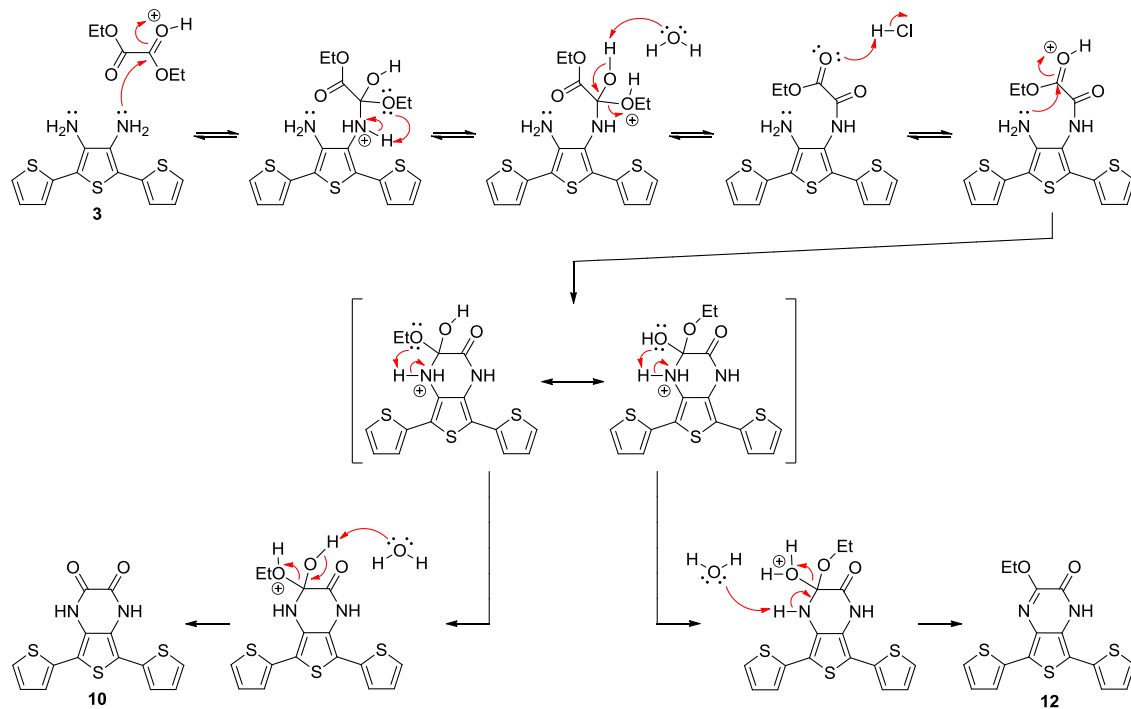
the mixture was approximately 2.8:1, as shown in Scheme 2.3. Attempts were made to shift this ratio by treatment of the mixture with aqueous HCl at reflux temperatures, but this ultimately had no effect on the amount of byproduct in the mixture. Finally, changing the solvent conditions of the reaction to a 50:50 water-ethanol mixture significantly increased the formation of **10** with only trace amounts of the byproduct **12** now observed. These modified conditions allowed for the successful production of the desired product **10** in isolated yields of 85%. Its structure was also confirmed by X-ray crystallography.

As a means to discover the reasoning for the formation of the byproduct **12** in these reactions, a pure sample of **10** was heated at reflux in absolute ethanol containing a catalytic amount of HCl over a period of 24 h. Under the described conditions, approximately 53% of the original sample of **10** was converted to **12**. This experiment confirmed that **12** was being produced via the nucleophilic attack of ethanol on **10**, rather than directly from the condensation of diethyl oxalate and diamine **3** as illustrated below in Scheme 2.4. The enhanced ethanol solubility of **10** in comparison to the monomeric analogue **8** and the presence of catalytic amounts of HCl are believed to have been responsible for the difference in reactivity ultimately producing the undesirable byproduct. This problem was circumvented by moving to a more polar solvent mixture that reduced the solubility of **10** so the product would crash out of solution upon formation, therefore inhibiting the side reaction with ethanol. An ethanol-water mixture was found to be suitable as it still allowed for the efficient production of diamide **10** as well as eliminating the production of the unwanted byproduct **12**.

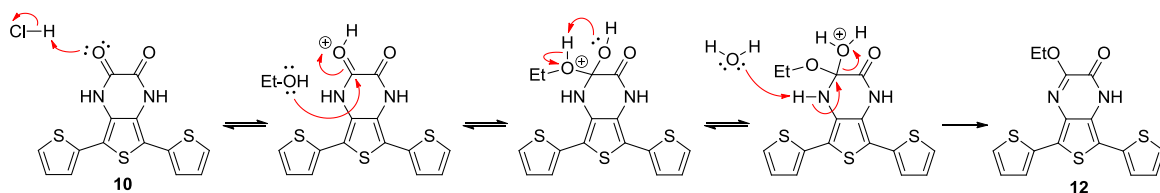
Now that the production of **10** had been accomplished, focus was turned to its conversion to the corresponding 2,3-dibromo-5,7-bis(2-thienyl)thieno[3,4-*b*]pyrazine (**5**)



\* Alternative mechanism for the generation of byproduct **12**



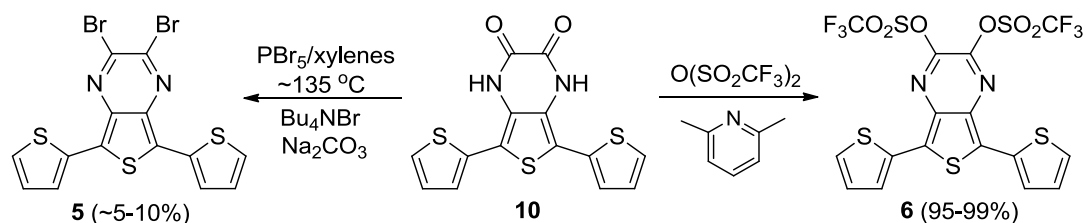
\* Proposed mechanism for the generation of byproduct **12**



Scheme 2.4. Proposed and alternative mechanisms for the generation of byproduct **12**.

via the conditions that were previously established for the conversion of the monomeric TP analogue **8** to the 2,3-dibromo analogue **9** (Scheme 2.2).<sup>39</sup> However, it was again determined that the conditions that were successful for monomeric TPs did not translate well to the corresponding terthienyl analogues. Attempts to convert **10** to **5** resulted in very low yields, which were routinely less than 10%, and produced significant amounts of

black insoluble material that is indicative of oxidative polymerization, as shown below in Scheme 2.5. The conditions used in the bromination reaction depicted in Scheme 2.2 were previously optimized to reduce decomposition of TP-based materials via oxidative coupling and polymerization processes, but the processes could not be completely eliminated in the presence of the oxidative conditions of the  $\text{PBr}_5$  mixtures.<sup>39</sup> Decomposition via oxidative processes became a much more significant problem with terthienyls **5** and **10** as these species undergo oxidation at potentials close to 1.0 V (~0.80-0.90 V) lower than their corresponding monomeric analogs, which severely hindered the successful production of the desired dibromo product **5** under these conditions.<sup>2</sup>



Scheme 2.5. Conversion of **10** to TP-based terthienyls with good leaving groups.<sup>9</sup>

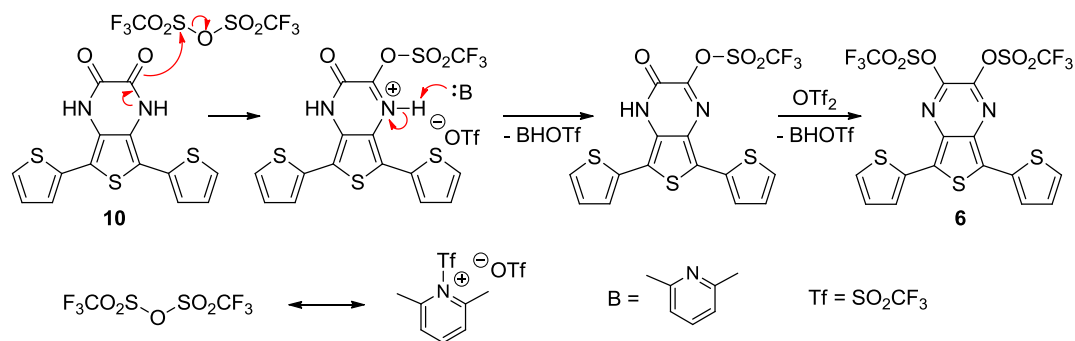
An alternate method for the generation of TP-based terthienyls containing good leaving groups was sought because of the difficulties encountered with the production of dibromo **5**. Activation of amides with triflic anhydride to generate triflatoiminium triflate salts had been reported by many groups, so effort was made to apply similar conditions to diamide **10** in an attempt to produce the ditriflate analogue **6**, as shown in Scheme 2.5.<sup>41-44</sup> Typical conditions for these types of reactions commonly utilized various pyridine bases to neutralize the triflic acid generated in the process, with the application of less bulky

pyridines shown to undergo substitution reactions with the triflatoimine product to generate the pyridinium species.<sup>43,44</sup> Therefore, a less nucleophilic and cost-effective base, 2,6-lutidine, was used in order to avoid these kinds of secondary reactions with the pyridine base. Subsequently, the treatment of **10** with 2.2 equivalents of triflic anhydride and 2.6 equivalents of 2,6-lutidine allowed for the successful production of the desired ditriflato species **6** as a reactive, yet stable, purple solid in near quantitative yields.

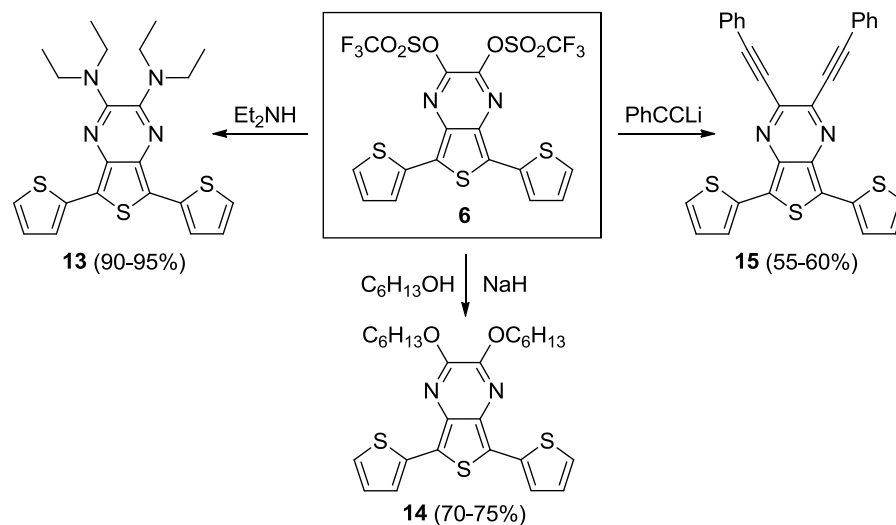
A proposed mechanism for the transformation of diamide **10** to ditriflato **6** is shown in Scheme 2.6 and is based on previously reported mechanistic studies of similar amide activation reactions.<sup>43</sup> It is thought that under the basic conditions of the reaction the nucleophilic amide carbonyl oxygen will attack a sulfonyl group of the triflic anhydride and displace the triflate base, which would then form a salt with the pyridinium acid after hydrogen abstraction. Also, it is possible that the 2,6-lutidine will react with the triflic anhydride first to generate 2,6-dimethyl-*N*-(trifluoromethylsulfonyl)pyridinium triflate, which would be analogous to previously reported methods utilizing pyridine.<sup>43</sup> However, it was thought that the reduced nucleophilicity of the 2,6-lutidine would limit this process or possibly eliminate it all together. If the pyridinium intermediate was produced, the proposed mechanism would be essentially the same with the only deviation lying in the exact identity of the electrophile in the initial step.

Once the successful generation of ditriflato **6** had been accomplished, effort was made towards the application of **6** to the production of new difunctionalized TP-based terthienyls, with three such examples shown in Scheme 2.7. The three new TP-based terthienyls include the diethylamino species **13**, dihexyloxy species **14**, and the phenylethynyl analogue **15**. All of these new TP-based terthienyls were produced in

moderate to good yields by simple nucleophilic aromatic substitution of the triflate groups of **6**. However, the applications of electron-withdrawing moieties, such as acyl, nitro, and nitrile functionalities, in substitution reactions as well as catalytic transformations were all unsuccessful in producing the corresponding TP-based terthienyls. Ditriflate **6** was found to be unstable in polar solvents, such as acetonitrile (ACN), dimethylformamide (DMF), and dimethylsulfoxide (DMSO) and led to the generation of complex mixtures of products.



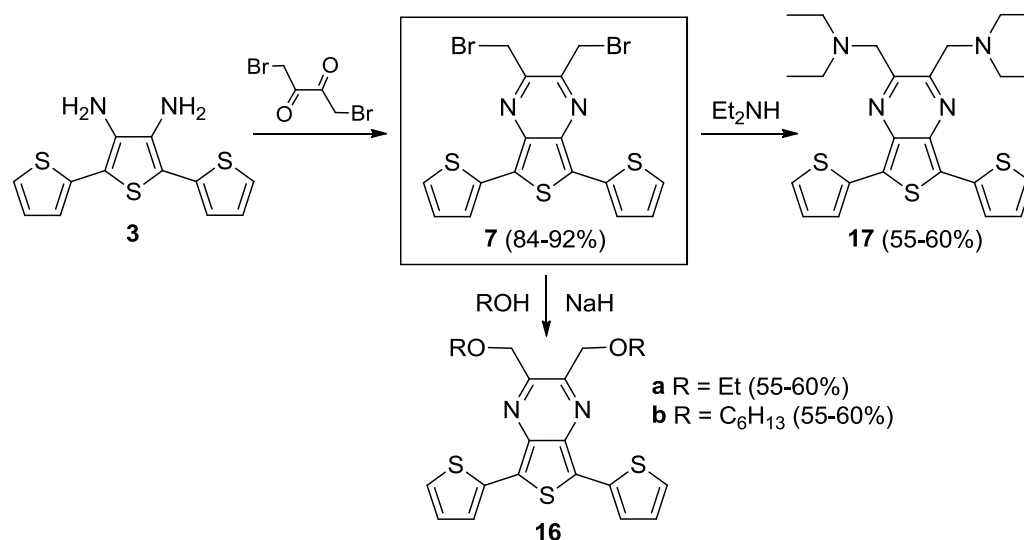
Scheme 2.6. Proposed mechanism for the formation of terthienyl **6**.<sup>9</sup>



Scheme 2.7. Generation of new TP-based terthienyls via simple substitution of **6**.<sup>9</sup>

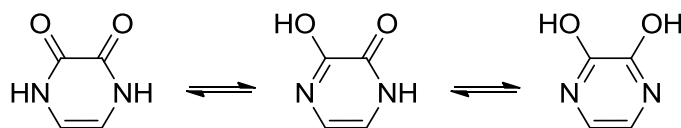
Lastly, to further expand the variety of functionality possible in TP-based terthienyls, the bis(bromomethyl) analogue **7** (Scheme 2.8) was produced via the room temperature condensation of diaminoterthiophene **3** with the commercially available 1,4-dibromo-2,3-butanedione. As in the case of **6** above, ether (**16a,b**) or amine (**17**) functionalities are then produced via simple substitution reactions. However, these substitutions have a propensity to generate byproducts based upon **16a**, **16b**, and **17** undergoing side reactions that are structurally similar to their parent compounds, which are especially noticeable when strong nucleophiles are used. It is possible that the methylene spacer could behave similarly to traditional benzylic protons, which exhibit enhanced reactivity towards processes that involve oxidation, free-radical halogenation, and hydrogenolysis.<sup>45</sup> This enhanced reactivity could explain the generation of many byproducts that have similar spectral characteristics compared to the desired products.

As in the case for the ditriflate **6**, significant effort was also applied towards the generation of electron-withdrawing moieties from **7** to further enhance the scope of TP-based terthienyls. Such attempts included the incorporation of acyl, nitro, and nitrile functionalities, but again, these efforts only produced complex mixtures of products whose identities could not be established. It is thought that the electron-deficient nature of the pyrazine ring makes the 2- and 3-positions weak nucleophiles that will not readily undergo simple substitution reactions as well as some catalytic transformations. Therefore, methods utilizing various transition metal catalysts with an appropriate corresponding ligand will likely be needed for the successful incorporation of electron-withdrawing substituents on the TP-based terthienyl building block.



Scheme 2.8. Synthesis of new 2,3-difunctionalized TP-based terthienyls from precursor **7**.<sup>9</sup>

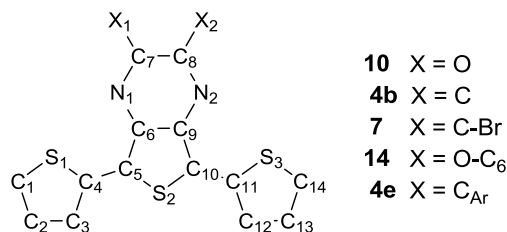
**X-ray Crystallography.** X-ray quality crystals of the precursor diamide **10** were grown from the slow evaporation of methanol solutions and selected bond angles are given below in Table 2.1. There are multiple tautomeric forms that the cyclic diamide ring of pyrazine-2,3(1*H*,4*H*)-dione ring of **10** can adopt and are represented in Scheme 2.9. The equilibrium of typical amides favors the amide tautomer almost exclusively over the iminol, with a  $K = 10^8$ , regardless of the nature of any functional group bound to the carbonyl.<sup>46,47</sup>



Scheme 2.9. Possible tautomeric forms of pyrazine-2,3-dione.<sup>9</sup>

If one of the tautomeric forms of the amide would favor an aromatic system one could reasonably expect that the aromatic state would dominate. One such system does seem to follow this line of reasoning, as is the case for the cyclic system of 4-hydroxypyrimide, in which the iminol form represents an aromatic system. In fact, this does seem to hold true in the gas phase, where the equilibrium for 4-hydroxypyrimide to exist in the aromatic iminol form has been reported to be near unity.<sup>48</sup> However, the authors also suggest that the oxo, or amide, form is again thought to predominate in either solution or the crystalline state.<sup>48</sup>

Table 2.1. Experimental bond lengths of 5,7-bis(2-thienyl)thieno[3,4-*b*]pyrazine-2,3(1*H*,4*H*)-dione (**10**) and 2,3-difunctionalized 5,7-bis(2-thienyl)thieno[3,4-*b*]pyrazines **4b**, **4e**, **7** and **14**.<sup>9</sup>



Bond	<b>10</b>	<b>4b<sup>a</sup></b>	<b>7</b>	<b>14</b>	<b>4e<sup>b</sup></b>
S(1)-C(4)	1.699(3)	1.719(5)	1.695(3)	1.727(2)	1.712(7)
C(1)-C(2)	1.360(4)	1.340(1)	1.343(4)	1.359(2)	1.320(1)
C(3)-C(4)	1.414(4)	1.424(7)	1.371(7)	1.422(2)	1.390(1)
C(2)-C(3)	1.443(3)	1.417(8)	1.488(8)	1.428(2)	1.410(1)
C(4)-C(5)	1.456(3)	1.442(7)	1.438(3)	1.445(2)	1.450(1)
S(2)-C(5)	1.727(3)	1.719(5)	1.733(2)	1.735(2)	1.713(6)
C(5)-C(6)	1.376(2)	1.406(7)	1.394(3)	1.380(2)	1.399(9)
C(6)-C(9)	1.420(4)	1.418(6)	1.426(3)	1.419(2)	1.427(9)
N(1)-C(6)	1.394(3)	1.381(6)	1.370(3)	1.382(2)	1.371(7)
N(1)-C(7)	1.355(2)	1.298(7)	1.311(3)	1.291(2)	1.313(9)
C(7)-C(8)	1.537(4)	1.469(7)	1.458(3)	1.469(2)	1.470(1)
C(7)-X(1)	1.222(3)	1.495(8)	1.489(3)	1.341(2)	1.489(7)

<sup>a</sup>Ref. 5a. <sup>b</sup>Ref. 16a.

The combination of a cyclic system capable of an aromatic form and two different amide groups that are both able to undergo tautomerism for diamide **10** could further favor the iminol form. However, this does not seem to be the case as the structure of **10** appears to consist exclusively of the dione tautomer in its crystalline solid-state, with the structure shown in Figure 2.2. The C–O bond lengths shown in this case are 1.222 and 1.226 Å, which are both slightly shorter than the C=O bond lengths of 1.23 Å that are typically observed in carbonyl systems.<sup>49</sup> While the C–N bond lengths, 1.355 and 1.351 Å respectively, exhibit some shortening when compared to the pure C–N single bond, which typically has a bond length of 1.47 Å, they are still longer than that reported for formamide (1.32 Å).<sup>49</sup> Using this x-ray crystallographic data, it can be reasonably assumed that the dione structure presented in Schemes 2.3 through 2.5 is indeed an accurate representation of the crystalline structure of diamide **10**.

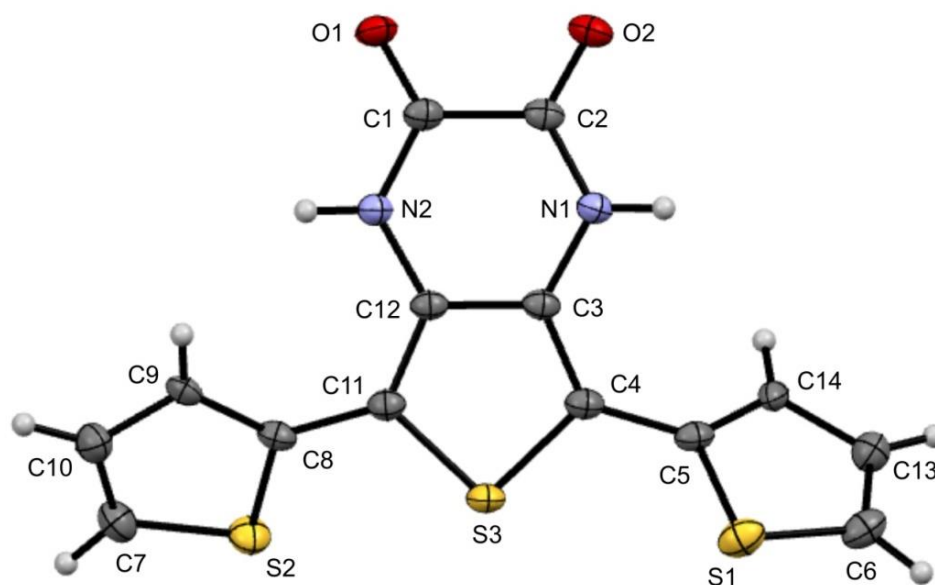


Figure 2.2. Thermal ellipsoid plot of 5,7-Bis(2-thienyl)thieno[3,4-*b*]pyrazine-2,3(1*H*,4*H*)-dione (**10**) at the 50% probability level.



The X-ray quality crystals of the TP-based terthienyls **7** and **14**, with structures shown in Figures 2.3 and 2.4, were also obtained and selected bond lengths are given in Table 2.1. Previously reported data from the analogues **4b** and **4e** are included so comparisons can be made between the presented data and literature values.<sup>5,25</sup> The bond lengths and angles of all four TP-based terthienyls are in fairly good agreement and in all of the reported cases the terthienyl backbones adopted a predominately s-trans configuration, which is analogous to  $\alpha$ -terthiophenes.<sup>50</sup> Previously reported TP-based terthienyls exhibited non-planar conjugated backbones with the external thiophenes rotated approximately 10° to 25° out-of-plane in regards to the central TP unit.<sup>5,25</sup> However, both terthienyls **7** and **14** showed near-planar geometries, which is also consistent with the structure of  $\alpha$ -terthiophene. Terthienyl **14** exhibits torsion angles of 7.9° and 8.9°, which is similar to that of  $\alpha$ -terthiophene that has torsion angles of 6° to 9°, while **7** exhibits a very near planar backbone with torsion angles of only 0.7° and 1.2° respectively.<sup>50</sup>

Previously reported monomeric TPs were shown to exhibit some bond fixation within the fused pyrazine ring and similar results were obtained for all three TP-based terthienyls shown here.<sup>1,39</sup> In the case of the parent pyrazine heterocycle, the delocalized structure results in four equivalent C-N bonds, however, the fused pyrazine ring of TPs exhibits elongation of the thiophene-N bonds and shortening of the exterior C-N bonds of the pyrazine ring, for example N(1)-C(7). As shown in Table 2.1, the exterior C-N bond lengths have an average length of 1.30 Å and are nearly equivalent to that of localized C=N bonds, which are typically 1.28 Å.<sup>51</sup> Comparison of the TP of **14** with the analogous bonds of **10** further illustrates the structural distinction between the diamide form of **10** and the dialkoxyaromatic pyrazine ring of **14**. As one would expect, the N(1)-C(7) bond of **14**

exhibits significant shortening in comparison to diamide **10**, which has bond lengths of 1.291 Å and 1.355 Å respectively. Additionally, the alkoxy C–O bond of **14** exhibits notable elongation relative to the C=O bond of **10** (1.341 vs. 1.222 Å), which supports previous conclusions about the true nature of the pyrazine rings in these TP-based terthienyl systems.

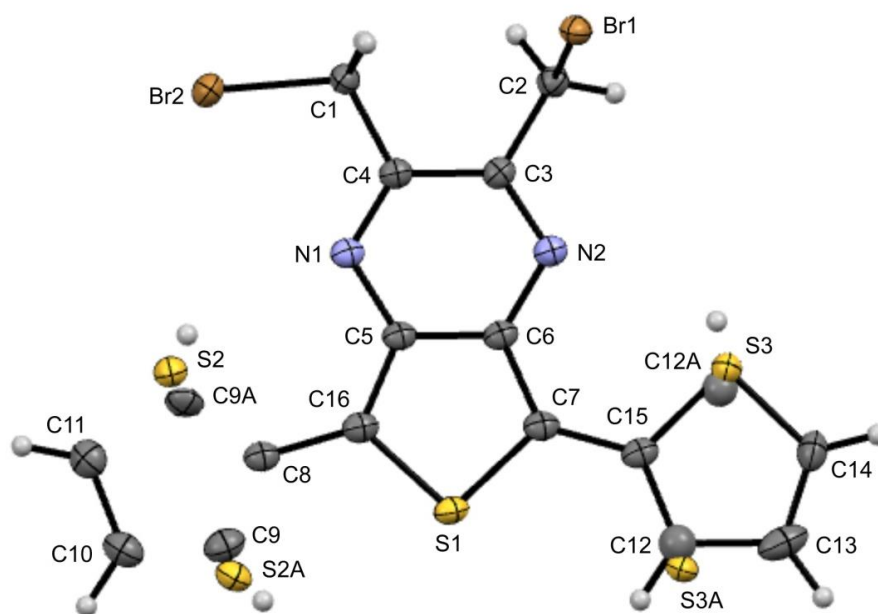


Figure 2.3. Thermal ellipsoid plot of 2,3-Bis(bromomethyl)-5,7-bis(2-thienyl)thieno[3,4-*b*]pyrazine (**7**) at the 50% probability level.

Some mixing of the S1/C3 and S3/C12 positions of the external thiophenes of the TP-based terthienyls due to the positional disorder resulting from a portion of the thiophenes that are rotated 180° around the interannular bond is expected. The example where this is most prominent is in the structure of **7**, which exhibits positional disorder in both external rings that result in approximately 17.32% mixing of the S1/C3 positions and

31.53% mixing of the S3/C12 positions. Similarly, terthienyl **14** exhibits disorder in the external thiophenes, but only does so for one of the rings, in which a mixing of approximately 7.43% for the S3/C12 positions is observed. Other noticeable deviations include shortened external  $\alpha$ - $\beta$ -C-C bonds where C(1)-C(2) bond lengths are between 1.32 Å and 1.36 Å in comparison to the parent thiophene, which is 1.370 Å.<sup>52</sup> The crystallographic data presented here for both the positional disorder of the external thiophenes and the shortening of external  $\alpha$ - $\beta$ -C-C bonds is consistent with previously reported results for other oligothiophenes,<sup>53-56</sup> as well as the previous TP-based terthienyls **4b** and **4e**.<sup>5,25</sup>

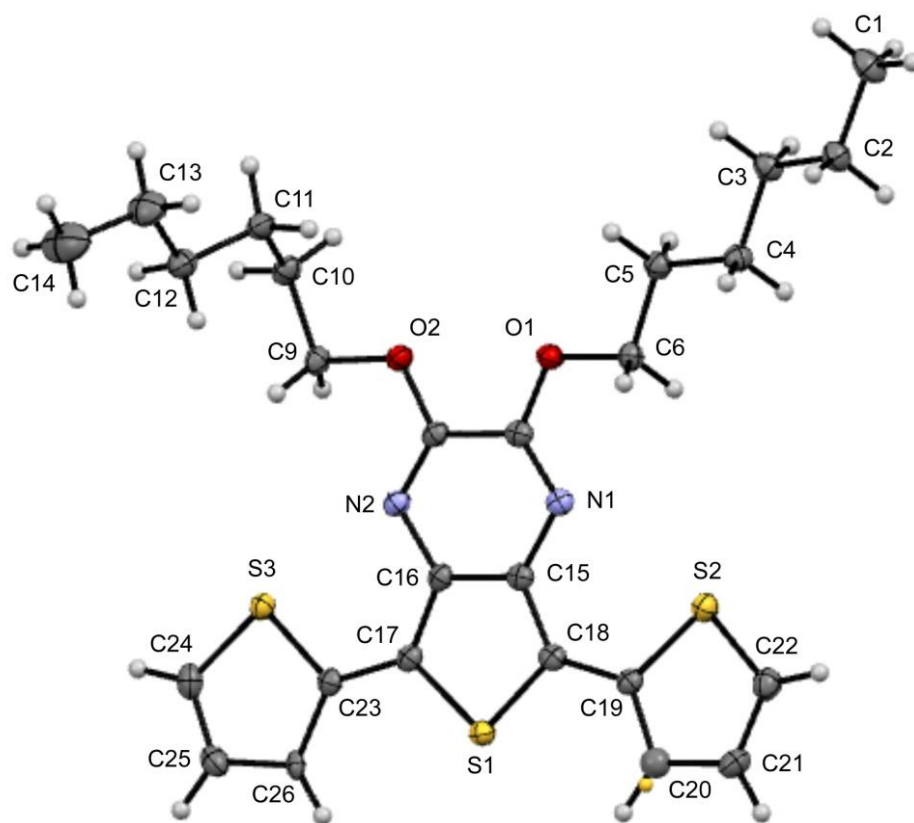


Figure 2.4. Thermal ellipsoid plot of 2,3-dihexyloxy-5,7-bis(2-thienyl)thieno[3,4-*b*]pyrazine (**14**) at the 50% probability level.

**UV-vis Spectroscopy.** The spectral data of a number of TP-based terthienyls are given in Table 2.2 with a representative UV-vis spectrum of **4b** shown in Figure 2.5. The absorption properties of TP-based terthienyls are characterized by a broad, low energy transition, which is formally assigned as an intramolecular charge transfer (ICT) band and higher energy transitions that are formally assigned as  $\pi \rightarrow \pi^*$  transitions. This assignment of the transitions is consistent with previous photophysical studies, which have shown that the lowest energy absorption of monomeric TPs is a broad ICT band resulting from a transition between a HOMO that is predominately thiophene-localized and a LUMO that has a greater contribution from pyrazine.<sup>1,39,56</sup>

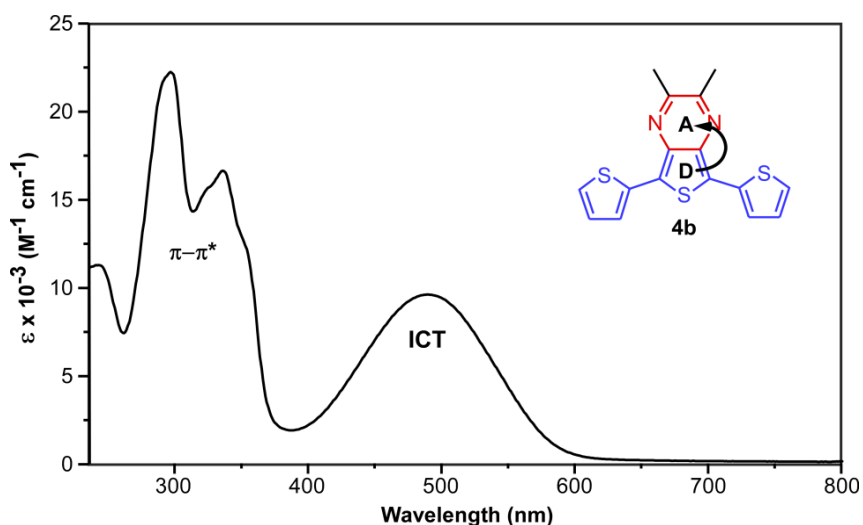


Figure 2.5. UV-visible spectrum of TP-based terthienyl **4b** in  $\text{CH}_3\text{CN}$ .<sup>9</sup>

In the case for TP-based terthienyls, the LUMO is still dominated by pyrazine contributions, but the addition of the 2-thienyl groups to the 5- and 7-positions of the TP unit in TP-based terthienyls results in a HOMO which is now delocalized across the entire

terthienyl backbone (Figure 2.5). The significant red-shift observed for dialkylITP-based terthienyls in comparison to the parent  $\alpha$ -terthiophene (492 vs. 354 nm) is a result of the ICT nature of the low energy transition and is observed in all TP-based materials.<sup>57</sup> As can be seen in Table 2.2, the extinction coefficients and oscillator strengths of these transitions are somewhat low and can be explained by the reduced "allowedness" of the transition as a result of limited spatial overlap of the orbitals involved in the ICT transition.<sup>58</sup>

Table 2.2.<sup>9</sup> UV-visible absorption data for a series of TP-based terthienyls.<sup>a</sup>

Terthienyl	$S_0 \rightarrow S_1$ (ICT)			$S_0 \rightarrow S_2$ ( $\pi \rightarrow \pi^*$ )		
	$\lambda_{\max}$ (nm)	$\epsilon$ ( $M^{-1}cm^{-1}$ )	$f$	$\lambda_{\max}$ (nm)	$\epsilon$ ( $M^{-1}cm^{-1}$ )	$f$
<b>4b</b>	492	12100	0.242	339	21000	0.268
<b>4f</b>	540	7800	0.123	338	45100	0.908
<b>5</b>	542	7400	0.134	313	35400	1.391
<b>6</b>	556	<i>b</i>	<i>b</i>	337	<i>b</i>	<i>b</i>
<b>7</b>	544	7100	0.146	312	33300	1.012
<b>13</b>	404	11800	0.225	348	12800	0.163
<b>14</b>	444	10200	0.193	328	19000	0.390
<b>15</b>	586	4400	0.065	361	58000	1.327
<b>16a</b>	511	9600	0.192	339	21400	0.349
<b>17</b>	500	9600	0.197	338	19300	0.321

<sup>a</sup> In  $CH_3CN$ . <sup>b</sup> Accurate determination not possible due to reaction with solvent.

The two stronger sets of bands that are observed in the higher-energy region of 250 nm to 350 nm can be assigned as two  $\pi \rightarrow \pi^*$  transitions, which are localized primarily along the terthienyl backbone. As one would expect, the energies of these higher-energy transitions agree well with the absorption energies that have been previously reported for  $\alpha$ -terthiophene.<sup>57</sup> For the most part, the extinction coefficients for these  $\pi \rightarrow \pi^*$  bands fall roughly between  $20\text{--}58 \times 10^3 M^{-1} cm^{-1}$ , with corresponding oscillator strengths of approximately 0.30–1.30 and ranging from moderately allowed to fully allowed

transitions. The outlier in this case is **13**, which exhibits an extinction coefficient for the  $\pi \rightarrow \pi^*$  band of about  $13 \times 10^3 \text{ M}^{-1} \text{ cm}^{-1}$ , with a corresponding oscillator strength of 0.163. The reduced allowedness observed for **13** is thought to arise from increased contributions from  $n \rightarrow \pi^*$  transitions because of the appended amine functionalities.

The overall effect of the side chains in the TP-based terthienyls is similar to that previously reported for the monomeric TP analogues, but does exhibit some significant differences.<sup>39</sup> The HOMO-LUMO energy, and thus the energy of the ICT transition, decreases as the electron-withdrawing nature of the side chain increases, as shown in both Table 2.2 and the absorption spectra in Figure 2.6.

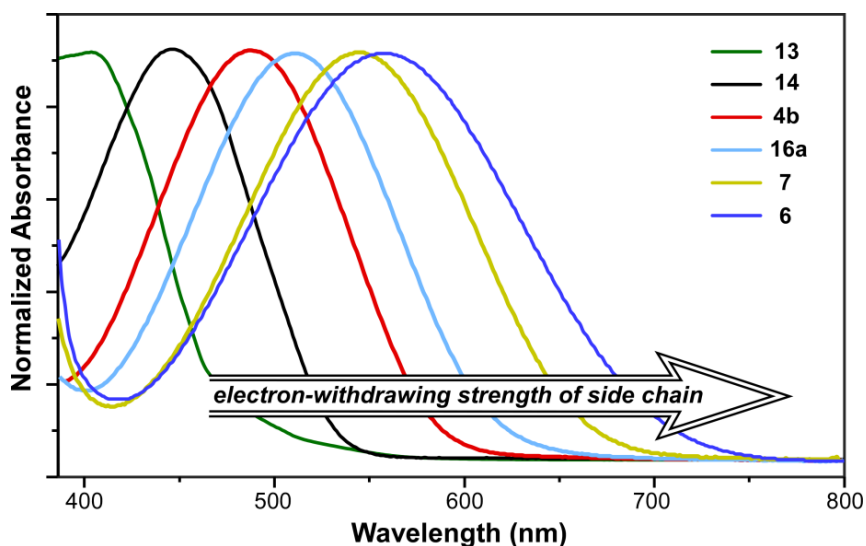


Figure 2.6. Normalized visible spectra of a series of TP-based terthienyls.<sup>9</sup>

Therefore, by simply changing the identity of the side chains of the TP-based terthienyls reported here, it is possible to shift the  $\lambda_{\text{max}}$  of the ICT transition by over 180 nm. When presented in terms of wavelength, the extent of tuning observed in the TP-based

terthienyls appears to be even greater than that previously reported for the simple monomeric TP analogues (180 nm vs. 95 nm).<sup>39</sup> However, when viewed in terms of a linear electron-volt scale, the changes in energy are actually very similar, with the TP-based terthienyls exhibiting a tunable range of 0.95 eV versus 0.92 eV for the monomeric TP analogues.<sup>39</sup>

**Electrochemistry.** The electrochemical data of the TP-based terthienyls is given in Table 2.3 with a representative cyclic voltammogram shown in Figure 2.7. The TP-based terthienyls exhibit a well-defined irreversible oxidation that can be assigned to the oxidation of the terthiophene backbone, as well as a quasireversible pyrazine-based reduction that is similarly seen in typical monomeric TPs.<sup>39,59</sup>

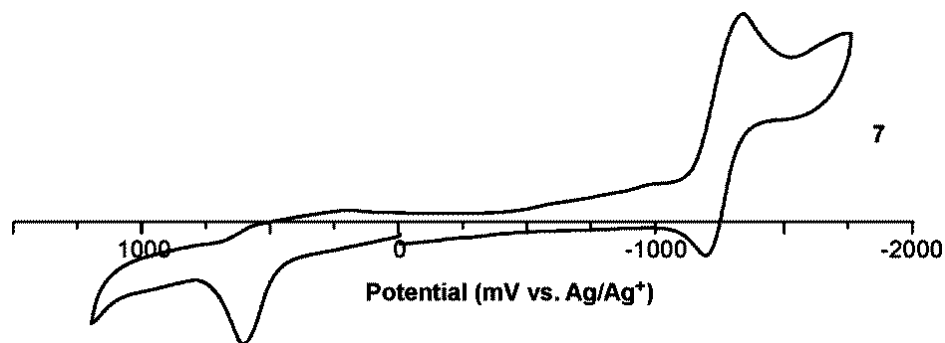


Figure 2.7. Cyclic voltammogram of terthienyl 7.<sup>9</sup>

Like the majority of thiophene species, the irreversible nature of the oxidation here is due to the formation of thiophene-based radical cations. These radical cations can then undergo rapid coupling that result in production of higher oligomeric and polymeric species, which accounts for the observed irreversibility. It should also be noted that for

terthienyls **13** (2,3-bis(*N,N*-diethylamino))- and **17** (2,3-bis(*N,N*-diethylaminomethyl))- , the alkylamino side chains are also redox active, therefore, oxidations of both the amine functionality and the thiophene are observed. In both of these cases, the initial oxidation can be attributed to the amine, as is the case for previously observed electrochemical measurements reported for 3-(*N*-alkylamino)thiophenes and the related 2,3-di(*N*-decylamino)thieno[3,4-*b*]pyrazine.<sup>39,60</sup>

Table 2.3.<sup>9</sup> Electrochemical data for a series of TP-based terthienyls<sup>a</sup>

Terthienyl	Oxidation	Reduction	
	$E_p^a$ , V	$E_{1/2}$ , V	$\Delta E$ , mV
<b>4b</b>	0.50	-1.68	100
<b>4f</b>	0.54	-1.46	60
<b>5</b>	0.70	-1.14 <sup>b</sup>	-
<b>6</b>	0.80	-0.99 <sup>b</sup>	-
<b>7</b>	0.62	-1.26	160
<b>13</b>	-0.06 <sup>c</sup> ,0.24	<i>N</i> <sub>WSW</sub>	-
<b>14</b>	0.45	-2.03	90
<b>15</b>	0.59	-0.96 <sup>b</sup>	-
<b>16a</b>	0.57	-1.48	110
<b>16b</b>	0.57	-1.48	120
<b>17</b>	0.32 <sup>c</sup> ,0.62	-1.65	90

<sup>a</sup>All potentials vs. Ag/Ag<sup>+</sup>. *n*<sub>WSW</sub> = not within solvent window.

<sup>b</sup>Irreversible, value corresponds to  $E_p^c$ . <sup>c</sup>Nitrogen-based oxidation.

With the TP-based terthienyl system, the potential of oxidation becomes more positive as the electron-withdrawing nature of the side chain is increased, indicative of a stabilization of the HOMO and is similar to the trend previously seen for the monomeric TP analogues.<sup>39</sup> All of TP-based terthienyls reported here still undergo oxidation at lower potentials than that of the parent  $\alpha$ -terthiophene (0.65 V vs. Ag/Ag<sup>+</sup>), with the exception of



terthienyls **5** and **6**, which incorporate highly electron-withdrawing functionalities that push their potential of oxidation out to 0.70 V and 0.80 V, respectively.<sup>61</sup> The effect on the reduction potentials follows the opposing trend, as should be expected, with electron-withdrawing groups decreasing the corresponding reduction potentials to as low as -0.99 V. Similarly, functionalities that are electron-donating groups decrease the potential of oxidation, as well as increase the reduction potential. In some cases, TP-based terthienyls with strongly donating groups, such as dialkylamino, the extent that the reduction potential is shifted is such that it is no longer within the measureable solvent window of CH<sub>3</sub>CN.

Terthienyl **15**, which exhibits extended conjugation through the phenylethynyl functionalities, behaved significantly different than the rest of the terthienyls with an additional sharp irreversible oxidation that was observed at -60 mV after cycling through the reduction that occurs at approximately -1 V. While the exact nature of this additional redox process is currently unknown, it is believed that this may be the result of a redox-initiated 1,5-cyclization of the enediyne structure. Similar cyclization of enediynes via both oxidation and reduction process have been previously reported and a separate study of the electrochemical, photochemical, and thermal cyclization of **15** should be undertaken.<sup>62,63,64</sup>

Despite the fact that the side chain effect on the reduction potentials of the TP-based terthienyls is essentially the same as that previously seen with the monomeric TPs, the effect on the potential of oxidation is significantly diminished in the corresponding terthienyl analogues. For example, changing the functional groups of monomeric TPs from the hexyloxy to methylbromo results in nearly a 300 mV shift in the potential of oxidation, while in comparison a shift of only 170 mV is observed for the exact same change in the TP-based terthienyls.<sup>39</sup> This difference can be attributed to the effect of the

two additional 2-thienyl groups in the terthienyls, where the thiophenes of the terthienyl backbone contribute more significantly to the HOMO than the functional groups at the 2- and 3-positions of the central TP unit. This is illustrated by a shift in the potential of oxidation by 850 mV from monomeric TP to TP-based terthienyl and is a result of increased delocalization of the HOMO across the terthienyl backbone as well as significant destabilization of the HOMO energy.<sup>39,59</sup> Therefore, the side chain effects of the central TP unit are diluted across the entire conjugated backbone, which causes the destabilization of the HOMO by the added external thiophenes, that effectively overpowers the weaker contributions of the TP side chains.

As a means to demonstrate the magnitude of the structure-function relationships in TP-based terthienyls described here, the data was further analyzed via a Hammett plot. The variations observed in the potentials of both the oxidation and reduction of the TP-based terthienyls correlate well with the respective Hammett substituent constants ( $\sigma_p^+$  or  $\sigma_p^-$ ) and are shown in Figure 2.8. Shifts in redox potentials of comparable molecular species are dependent on a number of factors exerted on the parent molecule by the substituents, which include polar, steric, and mesomeric effects, and can be described by the Hammett-Taft equation:

$$E = \rho_{\pi}\sigma + S$$

where  $\rho_{\pi}\sigma$  describes the polar-mesomeric parameters and  $S$  takes into account the steric factors.<sup>39,60,65-68</sup> Cases where the steric interactions that are a result of the added functional groups are low or comparable (i.e.  $S$  is constant), linear relationships are found between the potential of oxidation and  $\sigma_p^+$ , as well as for the reduction potential and  $\sigma_p^-$ .

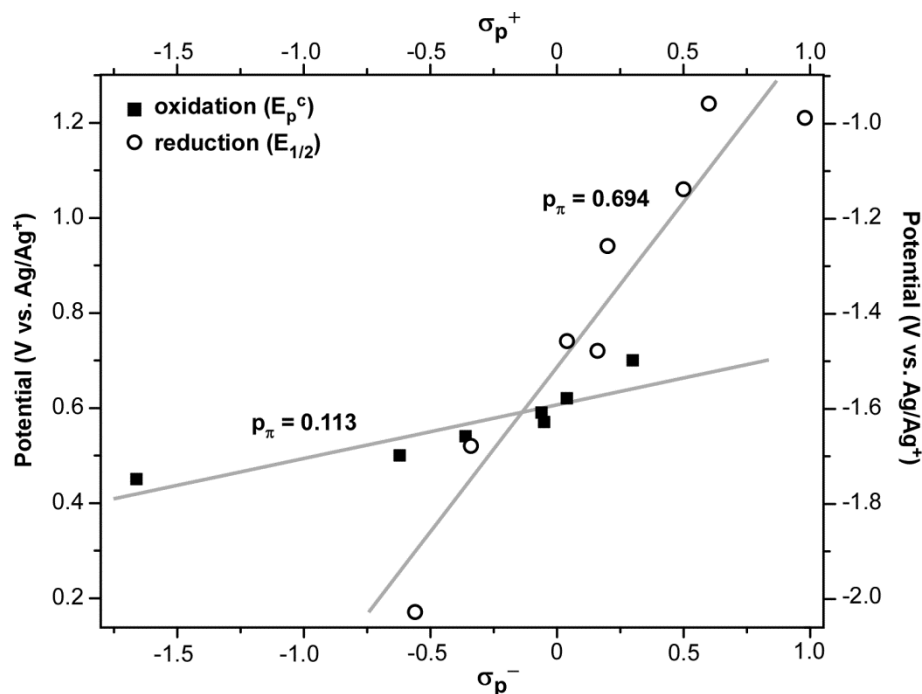


Figure 2.8. Hammett plot of TP-based terthienyls.<sup>9</sup>

Both the plots, the oxidation vs.  $\sigma_p^+$  and the reduction vs.  $\sigma_p^-$ , give linear relationships with respective R values of 0.900 and 0.953, and are shown above in Figure 2.8. The plot for the potential of oxidation gives a  $\rho_\pi$  value of 0.113, which is exactly one-third of the value previously found for the corresponding monomeric thieno[3,4-*b*]pyrazines that were shown to give a  $\rho_\pi = 0.340$ .<sup>26</sup> The one-third reduction of the  $\rho_\pi$  value for the side chain effects is perfectly consistent with the fact that only one-third of that backbone is comprised of a functionalized TP unit and the oxidation of the TP-terthienyls is now delocalized across the terthienyl backbone. The  $\rho_\pi$  value for the TP-based terthienyls was also significantly lower than that observed for typical thiophenes, which have a  $\rho_\pi = 0.80$ .<sup>65,66</sup> Lower  $\rho_\pi$  values for the analogous sets of thieno[3,4-*b*]pyrazine compounds, TP-based terthienyls and monomeric TPs, is indicative of a diminished effect

of the functional group on the potential of oxidation in these species. The diminished effect on the potential of oxidation is expected as the functional groups are spatially removed from the site of oxidation, which is localized either on the thiophene ring of the TP unit or across the terthienyl backbone.

The Hammett plot of the reduction potentials of the TP-based terthienyls gives a higher value of  $\rho_{\pi} = 0.694$  as expected, which is indicative of a greater effect of the functional group on the TP reduction. However, what was unexpected is the fact that this value is considerably larger than that previously found for the monomeric thieno[3,4-*b*]pyrazines, which was shown to have a  $\rho_{\pi} = 0.463$ .<sup>39</sup> The contributions of the side chains to the pyrazine ring should be identical between both the TP monomers and the TP-based terthienyls, therefore, the  $\rho_{\pi}$  values should be fairly consistent. Re-evaluation of the original TP data set indicated that there was one out-lying data point, which belonged to the 2,3-dicyanothieno[3,4-*b*]pyrazine monomer, that was responsible for the skewing of the determined slope.<sup>39</sup> Once this data point was removed, the newly calculated  $\rho_{\pi}$  value of 0.613 for the TP monomers now demonstrated to be in good agreement with the TP-based terthienyls studied here. The cause of the poor correlation for the 2,3-dicyanothieno[3,4-*b*]pyrazine monomer is currently unknown and the study of its electrochemistry in greater detail is recommended.<sup>39</sup>

### 2.3. Conclusion

The work presented herein describes the synthesis and characterization of new classes of TP-based terthienyls containing electron-donating and electron-withdrawing groups that have been prepared from terthienyls containing central 2,3-ditriflato- and 2,3-

bis(bromomethyl)-5,7-bis(2-thienyl)thieno[3,4-*b*]pyrazines. The ability to vary the functional groups allows for a significant degree of tuning of the electronic and optical properties of these popular conjugated building blocks, as was previously demonstrated for the thieno[3,4-*b*]pyrazine monomers.<sup>39</sup> It was shown here that the addition of the terminal thiophenes of the TP-based terthienyls reduced the effect of the functional groups on the modulation of the HOMO energies by approximately one-third when compared to that of the TP monomers. However, it was also demonstrated that the effect on the modulation of the corresponding LUMO energies was analogous to that found with the TP monomers. The tunability of these TP-based terthienyls is complementary to that of the TP monomers, with variations of the HOMO-LUMO gap energies of these materials of almost a full 1.0 eV. As such, the robust nature of TP-based materials, the tunability of these systems, and the degree to which they have been studied provides reason to believe that these materials are indeed a promising class of building blocks for the production of new low band gap materials.

## 2.4. Experimental Methods

**General.** Unless noted, all materials were reagent grade and used without further purification. Chromatographic separations were performed using standard column chromatography methods with silica gel (230-400 mesh). Dry THF and xylenes were obtained via distillation over sodium/benzophenone. All glassware was oven-dried, assembled hot, and cooled under a dry nitrogen stream before use. Transfer of liquids was carried out using standard syringe techniques and all reactions were performed under a dry nitrogen stream. Melting points were determined using a digital thermal couple with a 0.1

°C resolution. The <sup>1</sup>H NMR and <sup>13</sup>C NMR were completed on a 400 MHz spectrometer. All NMR data was referenced to the chloroform signal and peak multiplicity was reported as follows: s = singlet, d = doublet, t = triplet, q = quartet, p = pentet, dd = doublet of doublets, m = multiplet and br = broad. HRMS was performed in house.

**Materials.** 2,5-Dibromo-3,4-dinitrothiophene (**1**),<sup>47</sup> tributyl(2-thienyl)stannane,<sup>69</sup> 2,3-dimethyl-5,7-bis(2-thienyl)thieno[3,4-*b*]pyrazine (**4b**),<sup>6</sup> 2,3-diphenyl-5,7-bis(2-thienyl)thieno[3,4-*b*]pyrazine (**4f**),<sup>17</sup> and PBr<sub>5</sub><sup>70</sup> were all prepared as previously reported. Xylenes and THF were distilled from sodium/benzophenone prior to use. CH<sub>2</sub>Cl<sub>2</sub> and CH<sub>3</sub>CN were dried over CaH and distilled prior to use. DMF was dried over MgSO<sub>4</sub> prior to use. All other materials were reagent grade and used without further purification.

**3',4'-Dinitro-2,2':5',2''-terthiophene (2).** The following is a modification of previously reported methods.<sup>6</sup> Compound **1** (17.2 g, 51.8 mmol) and tributyl(2-thienyl)stannane (42.51 g, 114 mmol) were added to dry THF (250 mL), followed by the addition of PdCl<sub>2</sub>(PPh<sub>3</sub>)<sub>2</sub> (0.364 g, 1 mol %). The mixture was heated to reflux for 16 h. After cooling, the reaction mixture was concentrated under vacuum to approximately 50 mL. Hexanes were then added and the resulting orange precipitate was filtered and washed with hexanes. The solid was recrystallized in methanol and purified by silica chromatography (gradient of hexanes to 20% CH<sub>2</sub>Cl<sub>2</sub> in hexanes) to give 12.3-13.1 g (70-75%). mp 144-145 °C (lit.<sup>5b</sup>149-151 °C). <sup>1</sup>H NMR: δ 7.61 (dd, *J* = 1.2, 5.2 Hz, 2H), 7.55 (dd, *J* = 1.2, 3.6 Hz, 2H), 7.18 (dd, *J* = 3.6, 5.2 Hz, 2H); <sup>13</sup>C NMR: δ 136.2, 134.1, 131.5, 131.4, 128.6, 128.3.

**3',4'-Diamino-2,2':5',2''-terthiophene (3).** The following is a modification of previously reported methods.<sup>6</sup> Terthiophene **2** (13.5 g, 40.0 mmol) was suspended in a

mixture of ethanol (340 mL) and concentrated HCl (280 mL). Tin metal (45.6 g, 384 mmol) was then added slowly in small portions and the mixture stirred at room temperature for 72 h. The mixture was then cooled to  $-25^{\circ}\text{C}$ , filtered, and the isolated solid washed with diethyl ether. The light green diammonium salt was added to 400 mL of cold water and made basic with 1 M KOH. The basic solution was then extracted with  $\text{CH}_2\text{Cl}_2$  until no color was observed in the extract. The combined organics were dried with  $\text{MgSO}_4$ , filtered, and concentrated under vacuum. The crude product was purified by silica chromatography (gradient  $\text{CHCl}_3$  to 5% triethylamine in  $\text{CHCl}_3$ ) to give 8.4-8.9 g of a yellow-brown powder (75-80%). mp  $90-92^{\circ}\text{C}$  (lit.<sup>5b</sup>  $96.0-96.5^{\circ}\text{C}$ ).  $^1\text{H}$  NMR:  $\delta$  7.25 (dd,  $J = 1.2, 3.6$  Hz, 2H), 7.07 (m, 4H), 3.71 (s, 4H).  $^{13}\text{C}$  NMR:  $\delta$  136.2, 133.8, 128.0, 124.2, 124.1, 110.4. All NMR values agree with previously reported values.<sup>6</sup>

**5,7-Bis(2-thienyl)thieno[3,4-*b*]pyrazine-2,3(1*H*,4*H*)-dione (10).** Diamine **3** (1.39 g, 5.0 mmol) was added to 120 mL of a 1:1 ethanol:water mixture under a nitrogen atmosphere. Diethyl oxalate (5.98 mL, 44 mmol) and concentrated HCl (0.20 mL, 6.5 mmol) were then added and heated at reflux for 24 h. The mixture was then cooled to room temperature and the ethanol removed under vacuum. The remaining mixture was then cooled in a freezer, after which the resulting precipitate was collected via vacuum filtration and washed with water (300 mL). The collected solid was then dissolved in 1 M aqueous KOH (500 mL) and filtered to remove any undissolved material. The KOH solution was then made acidic and the resulting precipitate collected via vacuum filtration. The solid was washed with water (~100 mL) and then diethyl ether until dry to produce 1.33-1.41 g of a yellow powder (80-85%). mp  $216^{\circ}\text{C}$  dec.  $^1\text{H}$  NMR:  $\delta$  7.17 (m, 4H), 7.46 (dd,  $J = 2.0$ ,

4.4 Hz, 2H), 8.68 (br, 2H);  $^{13}\text{C}$  NMR (*d*-DMSO):  $\delta$  159.1, 136.4, 133.9, 133.2, 132.6, 129.3, 115.6; HRMS  $m/z$  354.9642 [ $\text{M} + \text{Na}$ ] $^+$  (calcd for  $\text{C}_{14}\text{H}_8\text{N}_2\text{NaO}_2\text{S}_3$  354.9640).

**2,3-Dibromo-5,7-bis(2-thienyl)thieno[3,4-*b*]pyrazine (5).** The reagents  $\text{PBr}_5$  (0.32 g, 0.75 mmol),  $\text{Bu}_4\text{NBr}$  (0.19 g, 0.60 mmol), and  $\text{Na}_2\text{CO}_3$  (0.06 g, 0.6 mmol) were added to 50 mL of xylenes in a 100 mL round-bottom flask equipped with a Vigreux column. To this column was fitted a condenser with an outlet submerged in 2.5 M aqueous KOH solution. The entire assembly was maintained under a gentle stream of nitrogen. The reaction mixture was then heated to reflux, which resulted in a color change from deep red to light yellow-orange. Compound **10** (0.10 g, 0.30 mmol) was then added, and the reaction was allowed to stir at reflux overnight. The reaction was quenched with a saturated aqueous  $\text{NH}_4\text{Cl}$  solution (100 mL) and extracted with  $\text{CH}_2\text{Cl}_2$  (3 x 50 mL). The combined organic layers were dried with anhydrous  $\text{MgSO}_4$ , concentrated, and purified by column chromatography (2%  $\text{CH}_2\text{Cl}_2$  in hexanes) to give ~10 mg of a purple solid (<10% yield).  $^1\text{H}$  NMR:  $\delta$  7.64 (dd,  $J = 1.1, 3.7$  Hz, 2H), 7.42 (dd,  $J = 1.1, 5.1$  Hz, 2H), 7.13 (dd,  $J = 3.7, 5.1$  Hz, 2H).

**2,3-Bis(trifluoromethanesulfonato)-5,7-bis(2-thienyl)thieno[3,4-*b*]pyrazine (6).** Dione **10** (1.10 g, 3.3 mmol) was added to a flask under a nitrogen atmosphere, which was then charged with 2,6-lutidine (0.92 g, 8.6 mmol) and dry  $\text{CH}_2\text{Cl}_2$  (150 mL) and cooled to  $-10$  °C in an ice/salt bath. Once cooled, trifluoromethanesulfonic anhydride (7.26 mL, 1.0 M in  $\text{CH}_2\text{Cl}_2$ , 7.26 mmol) was added dropwise over 1 h to limit heat evolution. The reaction was then quenched with saturated aq.  $\text{NaHCO}_3$  (200 mL) and extracted with  $\text{CH}_2\text{Cl}_2$  (3 x 100 mL). The combined organics were dried with  $\text{MgSO}_4$ , filtered, and concentrated. The crude product was purified by silica chromatography (1:1



CH<sub>2</sub>Cl<sub>2</sub>:hexanes) to give 1.87-1.95 g of a purple solid (95-99%). mp 174°C dec. <sup>1</sup>H NMR: δ 7.63 (dd, *J* = 1.2, 3.6 Hz, 2H), 7.47 (dd, *J* = 1.2, 5.2 Hz, 2H), 7.15 (dd, *J* = 3.6, 5.2 Hz, 2H); <sup>13</sup>C NMR: δ 139.8, 133.1, 132.7, 128.4, 126.7, 128.1, 127.5, 126.6, 118.7 (q, *J*<sub>C-F</sub> = 300 Hz); HRMS *m/z* 618.8601 [M + Na]<sup>+</sup> (calcd for C<sub>16</sub>H<sub>6</sub>F<sub>6</sub>N<sub>2</sub>O<sub>6</sub>S<sub>5</sub>Na 618.8626).

**2,3-Bis(*N,N*-diethylamino)-5,7-bis(2-thienyl)thieno[3,4-*b*]pyrazine (13).**

Ditriflate **6** (0.190 g, 0.32 mmol) was added to a flask and brought under a nitrogen atmosphere. Dry CH<sub>2</sub>Cl<sub>2</sub> (40 mL) was added, followed by the addition of *N,N*-diethylamine (10.0 mL, 193 mmol). The reaction was allowed to stir at room temperature overnight, after which it was quenched with saturated aq. NaHCO<sub>3</sub> (100 mL) and extracted with CH<sub>2</sub>Cl<sub>2</sub> (3 x 50 mL). The combined organics were dried with MgSO<sub>4</sub>, filtered, and concentrated. The crude product was purified by basic silica chromatography (prepared with 80:20 hexanes:CH<sub>2</sub>Cl<sub>2</sub> containing 3% triethylamine, eluted with hexanes:CH<sub>2</sub>Cl<sub>2</sub>) to give 0.13-0.14 g of a shiny red-orange solid (90-95%). mp 106-109 °C; <sup>1</sup>H NMR: δ 7.43 (dd, *J* = 1.2, 3.6 Hz, 2H), 7.27 (dd, *J* = 1.2, 5.2 Hz, 2H), 7.06 (dd, *J* = 3.6, 5.2 Hz, 2H), 3.64 (q, *J* = 7.1 Hz, 8H), 1.17 (t, *J* = 7.1 Hz, 12H); <sup>13</sup>C NMR: δ 12.9, 43.9, 118.3, 122.2, 124.8, 126.9, 135.8, 136.3, 148.6; HRMS *m/z* 443.1393 [M + H]<sup>+</sup> (calcd for C<sub>22</sub>H<sub>26</sub>N<sub>4</sub>S<sub>3</sub>H 443.1392).

**2,3-Dihexyloxy-5,7-bis(2-thienyl)thieno[3,4-*b*]pyrazine (14).** Sodium hexyloxide was prepared by the addition of NaH (0.20 g, 5.0 mmol, 60-65% in oil) to a flask under a nitrogen atmosphere. The oil was removed with hexanes washes (2 x 10 mL) and the remaining NaH brought to dryness under vacuum. The flask was then equipped with an addition funnel charged with ditriflate **6** (0.298 g, 0.5 mmol) in 50 mL of dry CH<sub>2</sub>Cl<sub>2</sub>, after which dry DMF (50 mL) was added to the reaction flask. The reaction was cooled to -

15°C in an ice/salt bath and 1-hexanol (1.0 mL, 8 mmol) was added to the DMF solution and allowed to stir for 1 h. The solution of **6** was then added dropwise while maintaining a temperature below -10 °C. Once the addition was complete, the reaction was allowed to warm to room temperature and stirred overnight. Saturated aqueous NH<sub>4</sub>Cl (100 mL) was then added and the mixture extracted with CH<sub>2</sub>Cl<sub>2</sub> (3 x 100 mL). The combined organics were dried with MgSO<sub>4</sub>, filtered, and concentrated. The crude product was purified by silica chromatography (hexanes:CH<sub>2</sub>Cl<sub>2</sub>, 95:5) to give 0.18-0.20 g of an orange solid (70-75%). mp 113-115 °C; <sup>1</sup>H NMR: δ 7.44 (dd, *J* = 1.2, 3.0 Hz, 2H), 7.30 (dd, *J* = 1.2, 4.5 Hz, 2H), 7.05 (dd, *J* = 3.0, 4.5 Hz, 2H), 4.55 (t, *J* = 7.0 Hz, 4H), 1.91 (p, *J* = 7.0 Hz, 4H), 1.49 (p, *J* = 7.0 Hz, 4H), 1.36 (m, 8H), 0.90 (t, *J* = 7.0 Hz, 6H); <sup>13</sup>C NMR: δ 150.3, 135.4, 134.1, 127.1, 125.5, 123.3, 120.5, 68.1, 31.8, 28.5, 26.0, 22.8, 14.2. All NMR values agree with previously reported values.<sup>40</sup>; HRMS *m/z* 551.1846 [M + Na]<sup>+</sup> (calcd for C<sub>28</sub>H<sub>36</sub>N<sub>2</sub>O<sub>2</sub>S<sub>3</sub>Na 551.1831).

**2,3-Bis(phenylethynyl)-5,7-bis(2-thienyl)thieno[3,4-*b*]pyrazine (15).**

Phenylacetylene (0.064 g, 0.625 mmol) was added to a flask under nitrogen and cooled to 0 °C. Once cool, butyl lithium (0.25 mL, 0.625 mmol, 2.5 M in hexanes) was added dropwise and the reaction allowed to stir for 30 min. In a separate flask, ditriflate **6** (0.149 g, 0.25 mmol) was dissolved in 50 mL THF and cooled to 0 °C in an ice bath. The lithium phenylacetylide solution was then added dropwise to the solution of **6**, after which the mixture was allowed to warm to room temperature and stirred overnight. The THF was then removed under vacuum, 100 mL saturated aq. NH<sub>4</sub>Cl added, and the mixture extracted with CH<sub>2</sub>Cl<sub>2</sub> (3 x 50 mL). The combined organics were dried with MgSO<sub>4</sub>, filtered, and concentrated. The crude product was purified by silica chromatography

(prepared with 100% hexanes, eluted with 70:30 hexanes:CH<sub>2</sub>Cl<sub>2</sub>) to give 69-75 mg of a dark blue solid (55-60%). mp 206-209 °C; <sup>1</sup>H NMR: δ 7.72 (d, *J* = 3.6 Hz, 2H), 7.68 (d, *J* = 6.5 Hz, 4H), 7.41 (m, 8H), 7.14 (dd, *J* = 3.6, 5.2 Hz, 2H); <sup>13</sup>C NMR: δ 140.0, 136.6, 132.6, 129.9, 128.7, 127.8, 127.3, 125.9, 125.8, 122.1, 96.5, 87.9; HRMS *m/z* 523.0383 [M + Na]<sup>+</sup> (calcd for C<sub>30</sub>H<sub>16</sub>N<sub>2</sub>S<sub>3</sub>Na 523.0368).

**2,3-Bis(bromomethyl)-5,7-bis(2-thienyl)thieno[3,4-*b*]pyrazine (7).** The following is a modification of previously reported methods.<sup>40</sup> Diamine **3** (1.39 g, 5.0 mmol) was added to absolute ethanol (80 mL) and gently heated with stirring until completely dissolved, after which it was allowed to cool to room temperature. In a similar manner, 1,4-dibromo-2,3-butanedione (1.89 g, 7.5 mmol) was added to absolute ethanol (40 mL), gently heated with stirring until completely dissolved, and allowed to cool to room temperature. The dione solution was then added dropwise to the solution of **3** and the mixture was allowed to stir for 6 hours, during which precipitation of the product occurred. The mixture was then cooled to -25 °C in a freezer (ca. 1 h), filtered, and washed with cold ethanol to give 2.03-2.23 g of a purple solid (84-92%); mp 160 °C dec. <sup>1</sup>H NMR: δ 7.66 (dd, *J* = 1.2, 3.6 Hz, 2H), 7.39 (dd, *J* = 1.2, 5.2 Hz, 2H), 7.11 (dd, *J* = 3.6, 5.2 Hz, 2H), 4.86 (s); <sup>13</sup>C NMR: δ 150.1, 137.5, 134.1, 127.7, 127.4, 126.3, 125.7, 31.6. NMR values agree with previously reported values.<sup>27</sup>; HRMS *m/z* 506.8290 [M + Na]<sup>+</sup> (calcd for C<sub>16</sub>H<sub>10</sub>Br<sub>2</sub>N<sub>2</sub>S<sub>3</sub>Na 506.8265).

**General synthesis of 2,3-dialkoxymethyl-5,7-bis(2-thienyl)thieno[3,4-*b*]pyrazine.** Sodium alkoxide was prepared by addition of NaH (0.40 g, 10.0 mmol, 60-65% in oil) to 20 mL of the specified alcohol and the mixture stirred for 2 h to ensure complete NaH consumption. The alkoxide solution was then added dropwise to **7** (0.49 g,

1.0 mmol) in 50 mL dry CH<sub>2</sub>Cl<sub>2</sub> and the mixture allowed to stir for 6 h. Saturated aq. NH<sub>4</sub>Cl was then added and the CH<sub>2</sub>Cl<sub>2</sub>/alcohol solvents removed by rotary evaporation and vacuum distillation as needed. The aqueous mixture was then extracted with CH<sub>2</sub>Cl<sub>2</sub>, after which the combined organic fractions were dried with MgSO<sub>4</sub> and concentrated.

**2,3-Bis(ethoxymethyl)-5,7-bis(2-thienyl)thieno[3,4-*b*]pyrazine (16a).** The crude product was purified by silica chromatography (100% CH<sub>2</sub>Cl<sub>2</sub>) to give 0.24-0.26 g of a red/purple solid (55-60%). mp 84-86 °C. <sup>1</sup>H NMR: δ 7.64 (dd, *J* = 1.2, 3.6 Hz, 2H), 7.36 (dd, *J* = 1.2, 5.2 Hz, 2H), 7.09 (dd, *J* = 3.6, 5.2 Hz, 2H), 4.86 (s, 4H), 3.67 (q, *J* = 6.8 Hz, 4H), 1.27 (t, *J* = 6.8 Hz, 6H); <sup>13</sup>C NMR: δ 152.3, 137.7, 134.6, 127.5, 126.8, 125.4, 125.0, 72.6, 66.7, 15.5; HRMS *m/z* 439.0581 [M + Na]<sup>+</sup> (calcd for C<sub>20</sub>H<sub>20</sub>N<sub>2</sub>O<sub>2</sub>S<sub>3</sub>Na 439.0579).

**2,3-Bis(hexyloxymethyl)-5,7-bis(2-thienyl)thieno[3,4-*b*]pyrazine (16b).** The crude product was purified by silica chromatography (50% CH<sub>2</sub>Cl<sub>2</sub>/hexanes) to give 0.29-0.32 g of a red-purple solid (55-60%). <sup>1</sup>H NMR: δ 7.64 (dd, *J* = 1.2, 3.6 Hz, 2H), 7.36 (dd, *J* = 1.2, 5.2 Hz, 2H), 7.09 (dd, *J* = 3.6, 5.2 Hz, 2H), 4.86 (s, 4H), 3.62 (t, *J* = 6.8 Hz, 4H), 1.68 (p, *J* = 6.8 Hz, 4H), 1.39 (m, 4H), 1.30 (m, 8H), 0.89 (t, *J* = 6.8 Hz, 6H); <sup>13</sup>C NMR: δ 152.4, 137.7, 134.6, 127.5, 126.7, 125.4, 125.0, 72.8, 71.6, 31.9, 30.0, 26.1, 22.8, 14.3; HRMS *m/z* 551.1846 [M + Na]<sup>+</sup> (calcd for C<sub>28</sub>H<sub>36</sub>N<sub>2</sub>NaO<sub>2</sub>S<sub>3</sub> 551.1831).

**2,3-Bis(*N,N*-diethylaminomethyl)-5,7-bis(2-thienyl)thieno[3,4-*b*]pyrazine (17).** Terthienyl **7** (0.24 g, 0.5 mmol) was added to dry CH<sub>2</sub>Cl<sub>2</sub> (25 mL) followed by the dropwise addition of *N,N*-diethylamine (25 mL, 242 mmol). The reaction was heated at reflux for 5 h. It was then quenched with distilled H<sub>2</sub>O and extracted with CH<sub>2</sub>Cl<sub>2</sub> (3 x 50 mL). The combined organics were washed with saturated aq. NaHCO<sub>3</sub> (2 x 100 mL) and brine (2 x 100 mL), dried with MgSO<sub>4</sub>, filtered and concentrated. The crude product was

purified by basic silica chromatography (prepared with 3% triethylamine/CH<sub>2</sub>Cl<sub>2</sub>, eluted with 100% CH<sub>2</sub>Cl<sub>2</sub>) to give 0.13-0.14 g of a dark red solid (55-60%). mp 63-66 °C; <sup>1</sup>H NMR: δ 7.63 (dd, *J* = 1.2, 3.6 Hz, 2H), 7.36 (dd, *J* = 1.2, 5.2 Hz, 2H), 7.09 (dd, *J* = 3.6, 5.2 Hz, 2H), 4.10 (s, 4H), 2.73 (q, *J* = 7.2 Hz, 8H), 1.06 (t, *J* = 7.2 Hz 12H); <sup>13</sup>C NMR: δ 154.6, 137.7, 135.0, 127.3, 126.5, 124.6, 124.5, 57.5, 46.6, 11.4; HRMS *m/z* 471.1707 [M + H]<sup>+</sup> (calcd for C<sub>24</sub>H<sub>31</sub>N<sub>4</sub>S<sub>3</sub> 471.1705).

## 2.5. Instrumentation

**UV-visible spectroscopy.** UV-visible spectra were measured on a dual beam scanning spectrophotometer using samples prepared as dilute CH<sub>3</sub>CN solutions in 1 cm quartz cuvettes. Oscillator strengths were determined from the visible spectra via spectral fitting to accurately quantify the area of each transition and then calculated using literature methods.<sup>71</sup>

**Electrochemistry.** Cyclic Voltammetry (CV) experiments were performed on a Bioanalytical Systems BAS 100B/W electrochemical analyzer. All electrochemical methods were performed utilizing a three-electrode cell consisting of platinum disc working electrode, a platinum wire auxiliary electrode, and a Ag/Ag<sup>+</sup> reference electrode (0.251 V vs. SCE).<sup>72</sup> Supporting electrolyte consisted of 0.10 M tetrabutylammonium hexafluorophosphate (TBAPF<sub>6</sub>) in dry CH<sub>3</sub>CN. Solutions were deoxygenated by sparging with argon prior to each scan and blanketed with argon during the measurements. All measurements were collected at a scan rate of 100 mV/s.

## 2.6. References

1. Rasmussen, S. C.; Mulholland, M. E.; Schwiderski, R. L.; Larsen, C. A. *J. Heterocyclic Chem.* **2012**, *49*, 479.
2. Rasmussen, S. C.; Schwiderski, R. L.; Mulholland, M. E. *Chem. Commun.* **2011**, *47*, 11394.
3. Rasmussen, S. C.; Pomerantz, M. In the *Handbook of Conducting Polymers*, 3rd ed.; Skotheim, T. A., Reynolds, J. R., Eds.; CRC Press: Boca Raton, FL, 2007; Vol. 1, Chapter 12.
4. Rasmussen, S. C.; Ogawa, K.; Rothstein, S. D. In the *Handbook of Organic Electronics and Photonics*, Nalwa, H. S., Ed.; American Scientific Publishers: Stevenson Ranch, CA, 2008; Vol. 1, Chapter 1.
5. Kitamura, C.; Tanaka, S.; Yamashita, Y. *J. Chem. Soc., Chem. Commun.* **1994**, 1585.
6. Kitamura, C.; Tanaka, S.; Yamashita, Y. *Chem. Mater.* **1996**, *8*, 570.
7. Delgado, M. C. R.; Hernandez, V.; Navarrete, J. T. L.; Tanaka, S.; Yamashita, Y. *J. Phys. Chem. B* **2004**, *108*, 2516.
8. Zhu, Z.; Champion, R. D.; Jenekhe, S. A. *Macromolecules* **2006**, *39*, 8721.
9. Schwiderski, R. L.; Rasmussen, S. C. *J. Org. Chem.* **2013**, *78*, 5453.
10. Wen, L.; Rasmussen, S. C. *J. Chem. Crystallogr.* **2007**, *37*, 387.
11. Xia, Y.; Luo, J.; Deng, X.; Li, X.; Li, D.; Zhu, X.; Yang, W.; Cao, Y. *Macromol. Chem. Phys.* **2006**, *207*, 511.
12. Karsten, B. P.; Viani, L.; Gierschner, J.; Cornil, J.; Janssen, R. A. J. *J. Phys. Chem. A.* **2008**, *112*, 10764.

13. Lee, W.; Cheng, K.; Wang, T.; Chueh, C.; Chen, W.; Tuan, C.; Lin, J. *Macromol. Chem. Phys.* **2007**, *208*, 1919.
14. Liu, C.; Tsai, J.; Lee, W.; Chen, W.; Jenekhe, S. A. *Macromolecules* **2008**, *41*, 6952.
15. Zhou, E.; Cong, J.; Yamakawa, S.; Wei, Q.; Nakamura, M.; Tajima, K.; Yang, C.; Hashimoto, K. *Macromolecules* **2010**, *43*, 2873.
16. Chao, C.; Lim, H.; Chao, C. *Polym. Prepr.* **2010**, *51(1)*, 715.
17. Perzon, E.; Wang, X.; Zhang, F.; Mammo, W.; Delgado, J. L.; de la Cruz, P.; Inganas, O.; Langa, F.; Andersson, M. R. *Synth. Met.* **2005**, *154*, 53.
18. Zhang, F.; Perzon, E.; Wang, X.; Mammo, W.; Andersson, M. R.; Inganas, O. *Adv. Funct. Mater.* **2005**, *15*, 745.
19. Admassie, S.; Inganas, O.; Mammo, W.; Perzon, E.; Andersson, M. R. *Synth. Met.* **2006**, *156*, 614.
20. Cai, T.; Zhou, Y.; Wang, E.; Hellstrom, S.; Zhang, F.; Xu, S.; Inganas, O.; Andersson, M. R. *Sol. Energy Mater. Sol. Cells* **2010**, *94*, 1275.
21. Tehrani, P.; Isaksson, J.; Mammo, W.; Andersson, M. R.; Robinson, N. D.; Berggren, M. *Thin Solid Films* **2006**, *515*, 2485.
22. Wienk, M. M.; Turbiez, M. G. R.; Struijk, M. P.; Fonrodona, M.; Janssen, R. A. J. *Appl. Phys. Lett.* **2006**, *88*, 153511.
23. Zoombelt, A. P.; Fonrodona, M.; Turbiez, M. G. R.; Wienk, M. M.; Janssen, R. A. J. *J. Mater. Chem.* **2009**, *19*, 5336.
24. Zoombelt, A. P.; Leenen, M. A. M.; Fonrodona, M.; Nicholas, Y.; Wienk, M. M.; Janssen, R. A. J. *Polymer* **2009**, *50*, 4564.

25. Petersen, M. H.; Hagemann, O.; Nielsen, K. T.; Jorgensen, M.; Krebs, F. C. *Sol. Energy Mater. Sol. Cells* **2007**, *91*, 996.
26. Petersen, M. H.; Gevorgyan, S. A.; Krebs, F. C. *Macromolecules* **2008**, *41*, 8986.
27. Helgesen, M.; Krebs, F. C. *Macromolecules* **2010**, *43*, 1253.
28. Mak, C. S. K.; Leung, Q. Y.; Chan W. K.; Djurišić, A. B. *Nanotechnology* **2008**, *19*, 424008.
29. Beaupre, S.; Breton, A.; Dumas, J.; Leclerc, M. *Chem. Mater.* **2009**, *21*, 1504.
30. Janietz, S.; Krueger, H.; Schleiermacher, H.; Wurfel, U.; Niggemann, M. *Macromol. Chem. Phys.* **2009**, *210*, 1493.
31. Yen, W.; Pal, B.; Yang, J.; Hung, Y.; Lin, S.; Chao, C.; Su, W. *J. Polym. Sci., Part A: Polym. Chem.* **2009**, *47*, 5044.
32. Mohamad, D.; Johnson, R. G.; Janeliunas, D.; Kirkus, M.; Yi, H.; Lidzey, D. G.; Iraqi, A. *J. Mater. Chem.* **2010**, *20*, 6990.
33. Lai, M.; Tsai, J.; Chueh, C.; Wang, C.; Chen, W. *Macromol. Chem. Phys.* **2010**, *211*, 2017.
34. Mak, C. S. K.; Cheung, W. K.; Leung, Q. Y.; Chan, W. K. *Macromol. Rapid Commun.* **2010**, *31*, 875.
35. Sonmez, G.; Shen, C. K. F.; Rubin, Y.; Wudl, F. *Angew. Chemie. Int. Ed.* **2004**, *43*, 1948.
36. Sonmez, G.; Sonmez, H. B.; Shen, C. K. F.; Wudl, F. *Adv. Mater.* **2004**, *16*, 1905.
37. Sonmez, G.; Sonmez, H. B.; Shen, C. K. F.; Jost, R. W.; Rubin, Y.; Wudl, F. *Macromolecules* **2005**, *38*, 669.



38. Tarkuc, S.; Unver, E. K.; Udum, Y. A.; Tanyeli, C.; Toppare, L. *Electrochim. Acta* **2010**, *55*, 7254.
39. Wen, L.; Nietfeld, J. P.; Amb, C. M.; Rasmussen, S. C. *J. Org. Chem.* **2008**, *73*, 8529.
40. Mulholland, M. E.; Schwiderski, R. L.; Rasmussen, S. C. *Polym. Bull.* **2012**, *69*, 291.
41. Sforza, S.; Dossena, A.; Corradini, R.; Virgili, E.; Marchelli, R. *Tetrahedron Lett.* **1998**, *39*, 711.
42. Baraznenok, I. L.; Nenajdenko, V. G.; Balenkova, E. S. *Tetrahedron* **2000**, *56*, 3077.
43. Charette, A. B.; Grenon, M. *Can. J. Chem.* **2001**, *79*, 1694.
44. Ghandi, M.; Salahi, S.; Hasani, M. *Tetrahedron Lett.* **2011**, *52*, 270.
45. Wuts, P. G. M.; Greene, T. W. *Greene's Protective Groups in Organic Synthesis*, 4th ed.; John Wiley & Sons: Hoboken, NJ, 2007, pp. 16-222.
46. Sigel, H.; Martin, R. B. *Chem. Rev.* **1982**, *82*, 385.
47. Fairlie, D. P.; Woon, T. C.; Wickramasinghe, W. A.; Willis, A. C. *Inorg. Chem.* **1994**, *33*, 6425.
48. Kheifets, G. M.; Kol'stov, A. I.; Khachaturov, A. S.; Gindin, V. A. *Russ. J. Org. Chem.* **2000**, *36*, 1373.
49. *CRC Handbook of Chemistry and Physics*; Weast, R. C, Ed.; CRC Press: Boca Raton, FL, 1987, pp. F-160.
50. Van Bolhuis, F.; Wynberg, H. *Synth. Met.* **1989**, *30*, 381.
51. *CRC Handbook of Chemistry and Physics*; Lide, D. R., Frederikse, H. P. R., Eds.; CRC Press: Boca Raton, FL, 1995, pp. 9-6.

52. Katritzky, A. R.; Pozharskii, A. F. *Handbook of Heterocyclic Chemistry*, 2nd Ed.; Pergamon Press: New York, 2000, p. 61.
53. Antolini, L.; Horowitz, G.; Kouki, F.; Garnier, F. *Adv. Mater.* **1998**, *10*, 382.
54. Herrema, J. K.; Wildeman, J.; van Bolhuis, F.; Hadziioannou, G. *Synth. Met.* **1993**, *60*, 239.
55. Evenson, S. J.; Pappenfus, T. M.; Delgado, M. C. R.; Radke-Wohlers, K. R.; Navarrete, J. T. L.; Rasmussen, S. C. *Phys. Chem. Chem. Phys.* **2012**, *14*, 6101.
56. Rasmussen, S. C.; Sattler, D. J.; Mitchell, K. A.; Maxwell, J. *J. Lumin.* **2004**, *190*, 111.
57. Mo, H.; Radke, K. R.; Ogawa, K.; Heth, C. L.; Erpelding, B. T.; Rasmussen, S. C. *Phys. Chem. Chem. Phys.* **2010**, *12*, 14585.
58. Turro, N. J. *Modern Molecular Photochemistry*, University Science Books: Sausalito, CA, 1991, p. 106.
59. Kenning, D. D.; Mitchell, K. A.; Calhoun, T. R.; Funfar, M. R.; Sattler, D. J.; Rasmussen, S. C. *J. Org. Chem.* **2002**, *67*, 9073.
60. Heth, C. L.; Tallman, D. E.; Rasmussen, S. C. *J. Phys. Chem. B* **2010**, *114*, 5275.
61. Meerholz, K.; Heinze, J. *Electrochim. Acta* **1996**, *41*, 1839.
62. Ramkumar, D.; Kalpana, M.; Varghese, B.; Sankararaman, S. *J. Org. Chem.* **1996**, *61*, 2247.
63. Zhou, Q.; Carroll, P. J.; Swager, T. M. *J. Org. Chem.* **1994**, *59*, 1294.
64. Bradshaw, J. D.; Solooki, D.; Tessier, C. A.; Youngs, Y. J. *J. Am. Chem. Soc.* **1994**, *116*, 3177.

65. Waltman, R. J.; Diaz, A. F.; Bargon, J. J. *Electrochem. Soc.* **1984**, *131*, 1452.
66. Waltman, R. J.; Bargon, J. *Can. J. Chem.* **1986**, *64*, 76.
67. Demanze, F.; Yassar, A.; Garnier, F. *Macromolecules* **1996**, *29*, 4267.
68. Zuman, P. *Substituent Effects in Organic Polarography*; Plenum Press: New York, 1967.
69. Pinhey, J. T.; Roche, E. G. *J. Chem. Soc. Perkins Trans 1*, **1988**, 2415.
70. Kaslow, C. E.; Marsh, M. M. *J. Org. Chem.* **1947**, *12*, 456.
71. Turro, N. J. *Modern Molecular Photochemistry*, University Science Books: Sausalito, CA, 1991, pp. 86-90.
72. Larson, R. C.; Iwamoto, R. T.; Adams, R. N. *Anal. Chim. Acta* **1961**, *25*, 371.

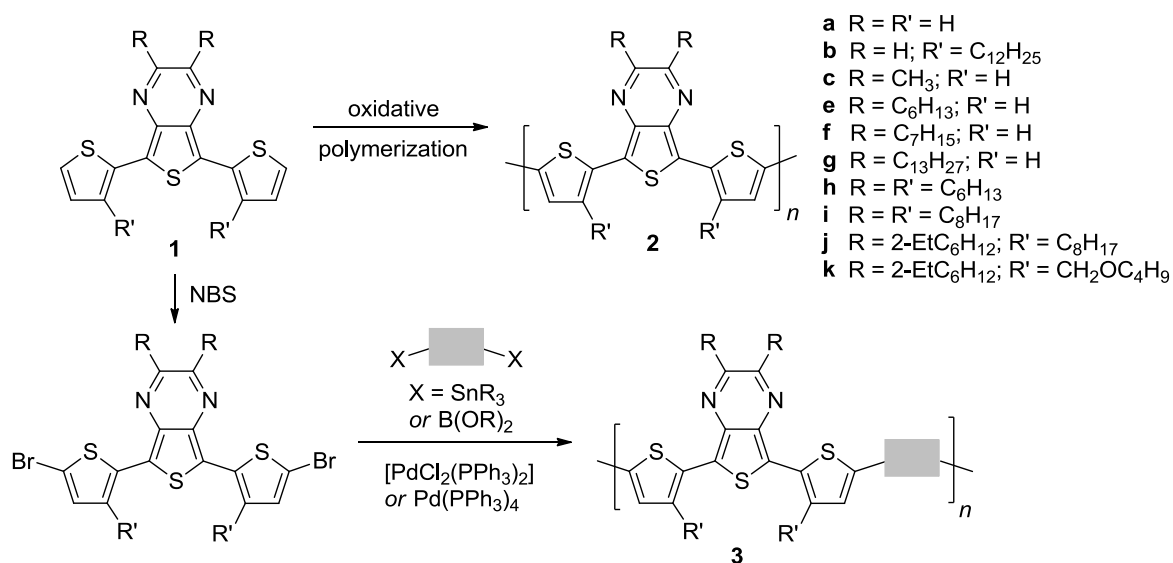
## CHAPTER 3. SIDE CHAIN TUNING OF FRONTIER ORBITALS IN POLYMERS OF THIENO[3,4-*b*]PYRAZINE-BASED TERTHIENYLS

### 3.1. Introduction

The property known as the band gap ( $E_g$ ) is one of the most critical parameters of conjugated organic materials and is defined as the energetic difference between the material's filled valence band and empty conduction band.<sup>1-4</sup> Thus, the band gap corresponds to the HOMO-LUMO gap of the bulk solid state material and determines many of the desirable properties of the material, such as the lowest energy absorption and the energy of any emitted light.<sup>1-4</sup> Control of the orbital energy levels allows tuning of the band gap as well as modulation of the redox properties because of the direct correlation between the band gap and the frontier orbitals. The redox properties of a material are crucial in determining environmental stability, as well as ensuring proper matching of energy levels with other electronic components in device applications. Therefore, control of these critical parameters is of great importance for the generation of technologically useful materials because this allows one to engineer materials for specific device applications.

The thieno[3,4-*b*]pyrazine (TP) unit has become a popular building block for the production of conjugated organic materials with a wide range of band gaps, which include both reduced band gap ( $E_g = 1.5-2.0$  eV) and low band gap ( $E_g < 1.5$  eV) polymers.<sup>4,5</sup> Although, incorporation of monomeric TP units have been demonstrated to be a successful approach to generating low band gap materials, TPs are oftentimes thought of as difficult to work with due to their somewhat reactive nature.<sup>4,6,7,8,9</sup> Because of this difficulty, many

researchers favor the application of TP-based terthienyl analogues, such as 5,7-bis(2-thienyl)thieno[3,4-*b*]pyrazine (Scheme 3.1, **1**, R = R' = H) as an alternative, in which the  $\alpha$ -positions of the central TP unit are substituted with 2-thienyl groups.<sup>4</sup> These materials actually undergo oxidation at lower potentials than the simple TP monomers due to the increased conjugation length of these TP-based terthienyls, which would lead one to believe that these materials would be more reactive. However, the combination of their increased size and a greater conjugation length results in slower reactivity, which fortuitously translates to a reduced production of unwanted byproducts via oxidative coupling or decomposition.



Scheme 3.1. Polymeric materials via TP-based terthienyls.

In 1994 Yamashita and co-workers reported the first examples of TP-based terthienyls, including terthienyls **1a**, **1c**, **1e**, and **1g**.<sup>6</sup> Polymerization of these terthienyls generated materials that were essentially alternating copolymers of TP and bithiophene

(Scheme 3.1, **2**). These initial polymeric materials were produced via electrochemical or chemical oxidation polymerizations and were successful in producing various 2,3-dialkyl functionalized TP-based terthienyl materials exhibiting low band gaps with  $E_g$  values between 1.00 eV and 1.50 eV.<sup>4,6-13</sup> There have been a number of various TP-based terthienyl analogs reported, which utilize central 2,3-diaryl-functionalized TP units with either external thiophenes or 3,4-ethylenedioxythiophene (EDOT) units in an attempt to further tune the properties of these materials.<sup>4,10-19</sup> Analogs that incorporated 2,3-diaryl substituted TP-based terthienyls resulted in materials with  $E_g$  values between 0.95 eV and 1.90 eV<sup>10-16</sup>, while the utilization of EDOT moieties in place of thiophene gave materials with  $E_g$  values between 0.77 eV and 1.30 eV.<sup>17-19</sup> In addition to the direct polymerization of various TP-based terthienyls, bromination of the terthienyls have allowed for their incorporation into more complex copolymeric materials via either Stille or Suzuki polymerizations (Scheme 3.1, **3**).<sup>4</sup> These multi-component alternating copolymeric systems generally lead to materials with higher band gaps, with a majority of the materials giving  $E_g$  values between 1.50 eV and 1.78 eV.<sup>4</sup>

It has been demonstrated that the use of TP-based terthienyls in conjugated polymers can be a very successful approach towards the production of both low band gap and reduced band gap materials. However, choice of functional groups for either the monomeric TPs, or the terthienyl analogues, are relatively limited due to the fact that the approach commonly utilized for the production of the TP units is the condensation of 3,4-diaminothiophene with available  $\alpha$ -diones.<sup>20-22</sup> Consequently, this has limited this class of compounds to either the dialkyl or diaryl analogues, which also limits the ability to tune the electronic and optical properties of the TP unit. As a means to overcome this

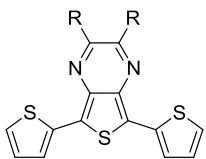
limitation, more versatile synthetic approaches to monomeric TPs were initially developed and reported by Rasmussen and coworkers in 2008.<sup>22,23</sup> We have recently applied these approaches to the analogous TP-based terthienyls to develop methods for the production of 2,3-ditriflato- and 2,3-bis(bromomethyl)-5,7-bis(2-thienyl)thieno[3,4-*b*]pyrazines.<sup>24</sup> These new reactive precursors allowed for the relatively simple production of a wide variety of TP-based terthienyls, which now afforded us the ability to incorporate electron-donating and electron-withdrawing substituents into the TP unit in an efficient manner. This provided an avenue for the production of conjugated materials based on these important building blocks with a much more pronounced tunability. In order to demonstrate the ability of these new TP-based terthienyls to tune the properties of low and reduced  $E_g$  materials, we report herein the electropolymerization of various TP-based terthienyls and characterization of the associated structure-function relationships.<sup>25-27</sup> Additional comparisons included the study of copolymers of TP-based terthienyls and fluorene, thus allowing both additional examples of side chain tuning and the effect of further diluting the TP content in such multi-component alternating copolymeric materials. The bulk of the work reported in this chapter has been published as paper in *Synthetic Metals*.<sup>28</sup> The final studies of Poly(5,7-bis(2-thienyl)thieno[3,4-*b*]pyrazine-*co*-fluorene)s has been published as a paper in *Polymer Bulletin*.<sup>44</sup>

### 3.2. Results and Discussion

**Electrochemical and optical properties of TP-based terthienyls.** The electrochemical and spectroscopic data for thieno[3,4-*b*]pyrazine-based terthienyls **4-8** are given in Table 3.1 so comparisons can be made with the polymers presented herein, and

clearly illustrate the effect of the side chains on the electronic and optical properties of these species.<sup>24</sup> The absorption properties of the TP-based terthienyls are consistent with results found during previous studies of monomeric TPs and are characterized by a broad, low energy transition, which can be formally assigned as an intramolecular charge transfer (ICT) band.<sup>5,22,29</sup> As is the case for the monomeric TPs, the ICT band results from a transition between the HOMO, which is now predominantly localized across the entire terthienyl backbone, and the LUMO, which is still derived mostly of contributions from the pyrazine.<sup>24</sup>

Table 3.1. TP-based terthienyl electrochemical and optical data.

	Terthienyl	R	Oxid. E <sub>pa</sub> , V <sup>a</sup>	Red. E <sub>1/2</sub> , V <sup>a</sup>	Abs nm (eV)
	<b>4</b>		OC <sub>6</sub> H <sub>13</sub>	0.45	-2.03
<b>5</b>		CH <sub>3</sub>	0.50	-1.68	492 (2.52)
<b>6</b>		CH <sub>2</sub> OC <sub>2</sub> H <sub>5</sub>	0.57	-1.48	511 (2.43)
<b>7</b>		CH <sub>2</sub> Br	0.62	-1.26	544 (2.28)
<b>8</b>		C <sub>6</sub> H <sub>5</sub>	0.54	-1.46	540 (2.30)

<sup>a</sup>All potentials vs. Ag/Ag<sup>+</sup>. Data collected from reference.<sup>24</sup>

It has been shown that changing the electronic nature of the side chains on the TP unit results in either stabilizing or destabilizing the resulting HOMO and LUMO energies of the TP-based terthienyl. However, as this effect is primarily inductive, the direct connection of the side chains to the pyrazine ring results in a more significant effect on the corresponding LUMO energies. Therefore, as the electron-withdrawing nature of the side chains are increased, such as from terthienyl **4** to **7**, the HOMO energy is stabilized, which results in a 170 mV more positive shift of the first oxidation potential. Comparatively, this also causes a stabilization of the corresponding LUMO energies by 770 mV, which in turn



results in a red shift of the ICT transitions by 100 nm. Because of the asymmetric affect these substitutions have on the HOMO and LUMO energies, not only can the choice of TP side chains can be used to tune the HOMO and LUMO energies, but also the corresponding HOMO-LUMO gap of these species.

**Electropolymerization and electrochemistry of poly(5,7-bis(2-thienyl)thieno[3,4-*b*]pyrazine)s.** In the 1980's, electropolymerization of heterocycles was a popular method for the production of numerous conjugated polymers, during which time a rapid growth of the conjugated polymer field was underway. Most current efforts tend to focus on the production of soluble, processable materials via various organometallic-catalyzed cross-coupling methods. However, electropolymerization still provides a simple and efficient method to study the structure-function relationships of materials as this allows for the production of polymer films directly onto electroactive substrates.<sup>25-27</sup> Electropolymerization not only provides a simple means for the electrochemical characterization of the resulting films, but also allows the direct comparison of a series of materials while minimizing the complicating effects of differences in solubility or processability. For these reasons, the electropolymerization of the terthienyls **4-8** were investigated as a means to quickly and efficiently study the effectiveness of side chain tuning on polymeric materials containing TP-based terthienyl units.

Potential cycling through the irreversible oxidation of the TP-based terthienyls resulted in the incremental growth of the corresponding polymer film on the surface of the working electrode. The oxidation wave of poly(2,3-bis(bromomethyl)-5,7-bis(2-thienyl)-thieno[3,4-*b*]pyrazine) (**P7**) resulted in a broadening of the redox response that corresponded to an increase in current and is shown in Figure 3.1. The shift of the

oxidation onset to lower potentials and an increased current response is indicative of increased conjugation length resulting from polymer growth. Interestingly, the fact that the  $E_{pa}$  of the polymer is essentially the same as that of the initial TP-based terthienyl is indicative of the polymer film containing either significant segments of lower conjugation length or some portion of unpolymerized terthienyl trapped within the polymeric matrix. When compared to previous work, this lack of a significant shift in the polymer  $E_{pa}$  versus the initial TP-based terthienyl is consistent with the reports of Yamashita and coworkers.<sup>6,7</sup>

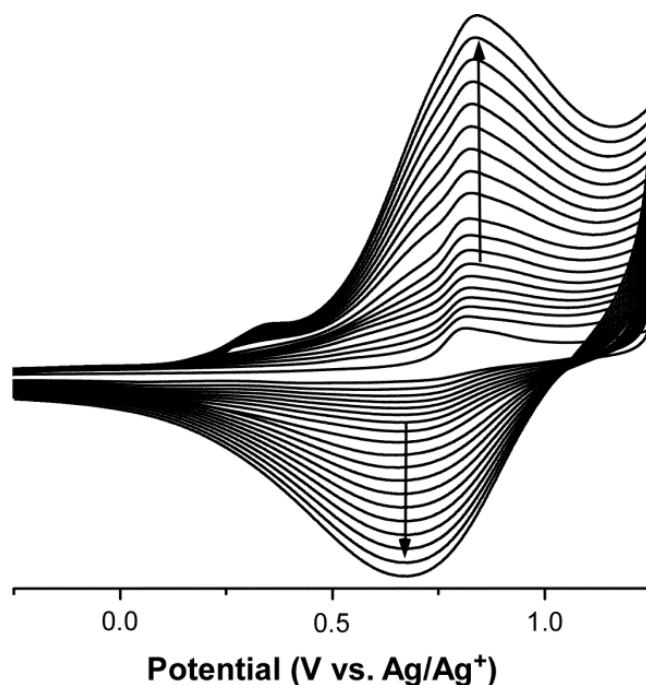


Figure 3.1. Growth of polymer **P7** with potential cycling.<sup>28</sup>

It should be noted, however, that one weakness of the electropolymerization technique arises from the possibility for the inclusion of defects resulting from  $\alpha$ - $\beta$  coupling in the polymer product, as shown below in Figure 3.2. In the case of monomeric

thiophenes, the desired  $\alpha$ - $\alpha$  coupling is highly favored with the relative reactivity of the  $\alpha$ - and  $\beta$ -positions being about 95:5 ( $\alpha$ : $\beta$ ).<sup>30</sup> Computational studies have suggested that as the oligomer length increases, the increased conjugation length enhances delocalization, which would result in reduced unpaired electron density at the  $\alpha$ -position.<sup>26,31,32</sup> These higher oligomer species would still favor reactivity at the  $\alpha$ -position, however, the diminished reactivity of the  $\alpha$ -position would in turn decrease the  $\alpha$ : $\beta$  selectivity.<sup>26,30</sup> Therefore, the decreased  $\alpha$ : $\beta$  selectivity could potentially lead to a statistical increase of the number of  $\alpha$ - $\beta$  couplings that would cause a decrease of the mean conjugation length in the resulting polymer film.<sup>26,30</sup> The electropolymerizations reported in this study start with a terthienyl backbone, so it is conceivable that decreased selectivity could be observed that would result in an increase of such  $\alpha$ - $\beta$  defects, which would lead to the production of polymer segments of lower conjugation length. However, the large shift of the oxidative onset, as illustrated in Figure 3.1, would confirm the presence of polymer segments consisting of considerably higher conjugation lengths as well.

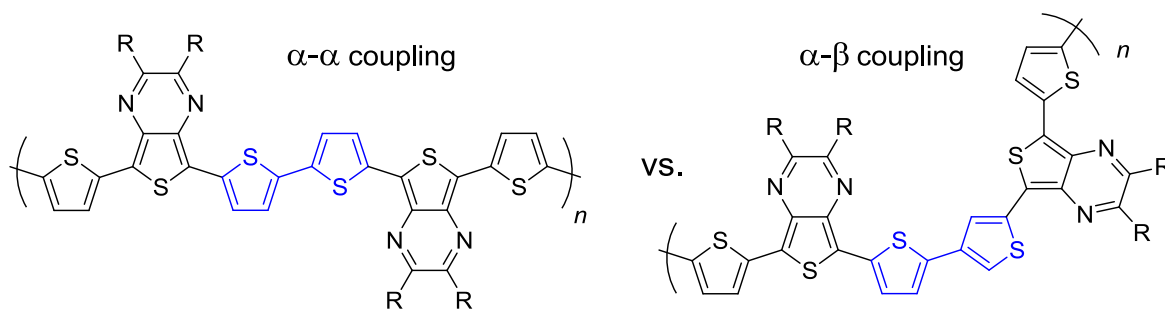


Figure 3.2. Depiction of  $\alpha$ - $\alpha$  and  $\alpha$ - $\beta$  coupling in TP-based terthienyl polymers.

The electrochemical data for the resulting electropolymerized polymers **P4-P8** are summarized in Table 3.2 with representative cyclic voltammograms (CVs) shown in Figure 3.3. The resulting polymer films exhibit amphoteric redox properties consisting of relatively broad oxidation waves with sharper, more well-defined reductions that are typical of the majority of TP-based materials. For two polymers, **P4** and **P7**, the typical reduction processes are not observed in the corresponding CVs under normal conditions, although quasireversible reductions are observed for the original terthienyls **4** and **7**. In the case of **P4**, this is expected as the strongly electron-donating alkoxy side chains result in a significant destabilization of the LUMO energy level, which results in the reduction now lying outside the solvent window. This is also consistent with the previously reported TP homopolymer containing similar alkoxy side chain functionalities.<sup>23</sup>

Table 3.2. Electrochemical data of poly(5,7-bis(2-thienyl)thieno[3,4-*b*]pyrazine) films.<sup>a</sup>

Polymer	R	Oxidation		Reduction		E <sub>HOMO</sub> , eV <sup>c</sup>	E <sub>LUMO</sub> , eV <sup>d</sup>	E <sub>g</sub> <sup>elec</sup> , eV
		E <sub>pa</sub> , V	E <sub>onset</sub> , V	E <sub>pc</sub> , V	E <sub>onset</sub> , V			
<b>P4</b>	OC <sub>6</sub> H <sub>13</sub>	0.37	0.18	<i>nws</i>	<i>nws</i>	-5.23	-	-
<b>P5</b>	CH <sub>3</sub>	0.54, 0.85	0.32	-1.48, -1.82	-1.24	-5.37	-3.81	1.56
<b>P6</b>	CH <sub>2</sub> OC <sub>2</sub> H <sub>5</sub>	0.59, 0.99	0.37	-1.44, -1.63	-1.14	-5.42	-3.91	1.51
<b>P7</b>	CH <sub>2</sub> Br	0.71	0.41	-1.15 <sup>b</sup>	-0.90 <sup>b</sup>	-5.46	-4.13	1.31
<b>P8</b>	C <sub>6</sub> H <sub>5</sub>	0.58	0.33	-1.39	-1.00	-5.38	-4.05	1.33

<sup>a</sup>All potentials vs. Ag/Ag<sup>+</sup>. *nws* = not within solvent window. <sup>b</sup>Observable only with the addition of KPF<sub>6</sub>. <sup>c</sup>E<sub>HOMO</sub> = -(E<sub>[onset, ox vs. Fc+/Fc]</sub> + 5.1)(eV).<sup>33</sup>

<sup>d</sup>E<sub>LUMO</sub> = -(E<sub>[onset, red vs. Fc+/Fc]</sub> + 5.1)(eV).<sup>33</sup>

In the case of polymer **P7**, the reduction can be observed during the initial electropolymerization, but shifts to higher negative potential as the polymer film forms and increases in thickness, which ultimately falls outside of the solvent window so it can no longer be observed. Previous studies have shown that the size of the electrolyte ions can

significantly change the electrochemistry of thin films due to differences in the ability of the counter ions to diffuse into the film during redox processes.<sup>34</sup> In the case of **P7**, it is believed that the larger steric size of the bromomethyl side chains inhibit the diffusion of the bulky tetrabutylammonium cation into the film during the attempted reduction. In turn, this would prohibit charge balance, which would result in a significant over potential that would shift the reduction outside of the solvent window. In order to verify this concept,  $\text{KPF}_6$  was added as a secondary electrolyte, which contains the much smaller  $\text{K}^+$  cation. Although the corresponding current response was reduced in comparison to that observed for the other polymeric films in the series, the polymer reduction was now observable in the presence of the  $\text{KPF}_6$  indicating that counter ion diffusion issues are present with the bulky TP side chains.

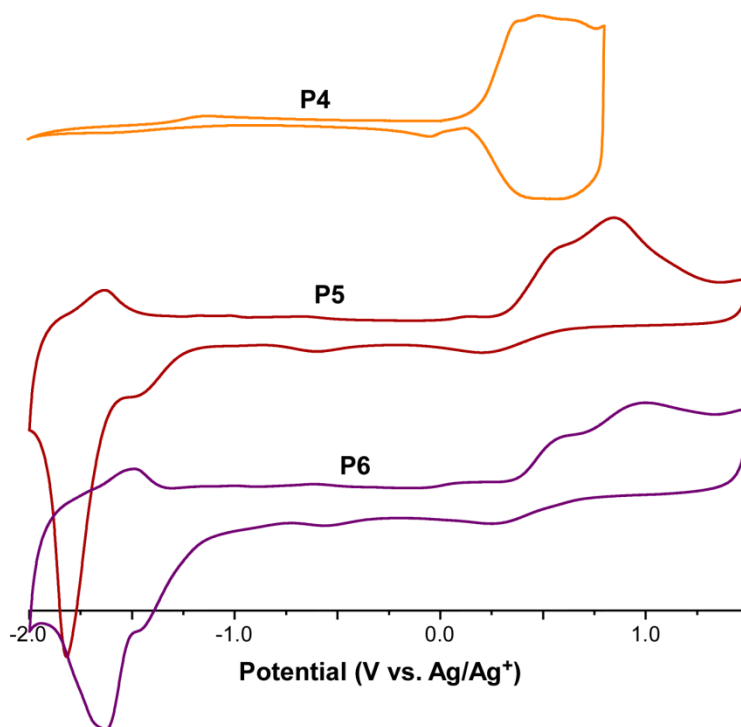


Figure 3.3. Cyclic voltammograms for polymers **P4-P6**.<sup>28</sup>

The general trends in side chain effects observed for the terthienyl oligomers are shown in Table 3.1 and seem to carry through to the resulting polymers. The electropolymerized polymers containing electron-donating groups, such as **P4**, oxidize at lower potentials in comparison to the analogous dialkyl polymer **P5** (0.37 V vs. 0.54 V). In the same way, polymers with more electron-withdrawing functional groups, such as **P6** and **P7**, oxidize at higher potentials and are more easily reduced than polymer **P5**. Similar to the TP-based terthienyls shown above in Table 3.1, the effect of the electronic nature of the side chain has been shown to have a more significant role in tuning the LUMO energies. However, it is clear that even though the substitutions are spatially separated from the thiophene-rich backbone, which is where the HOMO is predominantly concentrated, a measurable effect is still observed on the HOMO energies as well.

As a means to further compare the electronic effects of the various side chains on the frontier orbitals of the polymeric materials, the potential onsets were plotted against the respective Hammett substituent constants ( $\sigma_p^+$  or  $\sigma_p^-$ ) and are shown in Figure 3.4. The shifts in redox potentials of comparable molecular species are dependent on the polar, steric, and mesomeric effects exerted on the molecules by the substituents and can be described by the Hammett–Taft equation:

$$E = \rho\pi\sigma + S$$

where  $\rho\pi\sigma$  describes the polar-mesomeric parameters and  $S$  accounts for the steric factors.<sup>22,24-26,35-37</sup> In the case where functional groups are of low or comparable steric strain (i.e.,  $S$  is constant), linear relationships are found between the potential of oxidation and  $\sigma_p^+$ , as well as between the reduction potential and  $\sigma_p^-$ .

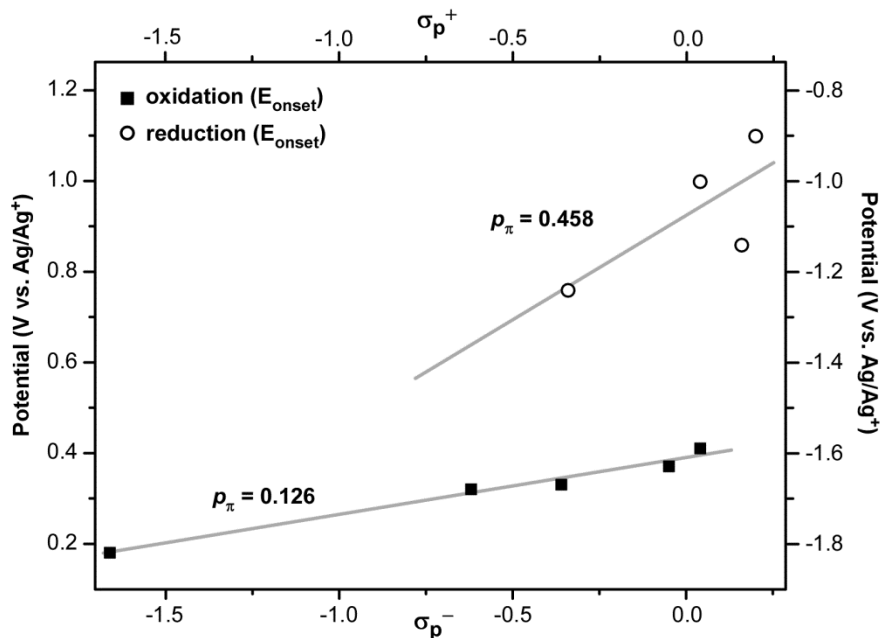


Figure 3.4. Hammett plot of for polymers **P4-P8**.<sup>28</sup>

As seen in Figure 3.4, both the plots of oxidation onset vs  $\sigma_p^+$  and the reduction onset vs  $\sigma_p^-$ , give linear relationships with respective R values of 0.989 and 0.752. In terms of the oxidation onsets, the plot gives a  $\rho_\pi$  value of 0.126, which is in good agreement with the value previously found for the corresponding TP-based terthienyl monomers ( $\rho_\pi = 0.113$ ).<sup>24</sup> Also similar to the trend observed for the TP-based terthienyl monomers, the plot of the reduction onsets gives a higher value for  $\rho_\pi$  value of 0.458. While this value is not as high as that previously found for the analogous TP-based terthienyl monomers ( $\rho_\pi = 0.694$ ), the current study utilizes a smaller dataset that could potentially result in a less accurate correlation, which is also indicated by the lower associated R value.<sup>24</sup> Nonetheless, comparisons of the  $\rho_\pi$  values for both processes shows that the TP side chains have approximately four times the effect on the polymer reduction, or LUMO energy, when compared to the polymer oxidation, or HOMO energy.

**Optical properties of poly(5,7-bis(2-thienyl)thieno[3,4-*b*]pyrazine)s.** In order to further characterize these new TP-based materials, terthienyls **4-8** were electropolymerized onto indium tin oxide (ITO) coated glass slides, which allowed for the measurement of the absorption spectra of these materials as thin films deposited on the transparent ITO substrate. The collected optical data is given in Table 3.3 with the corresponding spectra shown in Figure 3.5. For all of the terthienyls, a low energy transition in the visible to NIR portion of the spectrum that is common for TP-based materials was exhibited, along with a second transition in the high energy region of the visible spectrum. The low energy transition is considerably broad, except in the case for polymer **P4**, and can be assigned as an ICT transition from the polythiophene backbone to the pyrazine of the TP units. It is interesting to note that the polymer **P4** shows significant vibronic character, thus it is unclear as to what extent charge transfer character is involved in the low energy transition of this polymer.

Table 3.3. Optical data for poly(5,7-bis(2-thienyl)thieno[3,4-*b*]pyrazine) films.<sup>a</sup>

Polymer	R	$\lambda_{\text{max}}$ , nm	$\lambda_{\text{onset}}$ , nm	$E_g^{\text{opt}}$ , eV
<b>P4</b>	OC <sub>6</sub> H <sub>13</sub>	565	700	1.77
<b>P5</b>	CH <sub>3</sub>	626	850	1.46
<b>P6</b>	CH <sub>2</sub> OC <sub>2</sub> H <sub>5</sub>	697	990	1.25
<b>P7</b>	CH <sub>2</sub> Br	708	1100	1.13
<b>P8</b>	C <sub>6</sub> H <sub>5</sub>	712	1230	1.01

<sup>a</sup>All spectra measured as thin films on ITO slides.

The optical band gap ( $E_g^{\text{opt}}$ ) values measured for these polymers show excellent agreement with the trends found in the TP-based terthienyl precursors. As can be seen in



Table 3.3 and Figure 3.5, the polymer **P4** exhibits an  $E_g^{\text{opt}}$  of 1.77 eV and the analogous  $E_g^{\text{opt}}$  values decrease with the addition of increasing electron-withdrawing functionalities. Also, as the electron-withdrawing nature of the side chains is increased, there is a significant red-shift ( $\sim 400$  nm) in the onset of the low-energy transition, which corresponds to a sizable decrease in band gap. For instance, there is a decrease of 0.64 eV going from the electron-donating alkoxy (**P4**  $E_g^{\text{opt}} = 1.77$  eV) functionality to the much more electron-withdrawing bromomethyl (**P7**  $E_g^{\text{opt}} = 1.13$  eV) side chains. The  $E_g^{\text{opt}}$  value of 1.46 eV for polymer **P5** is slightly higher than that previously reported by Yamashita and coworkers, but still within good agreement.<sup>6,7</sup>

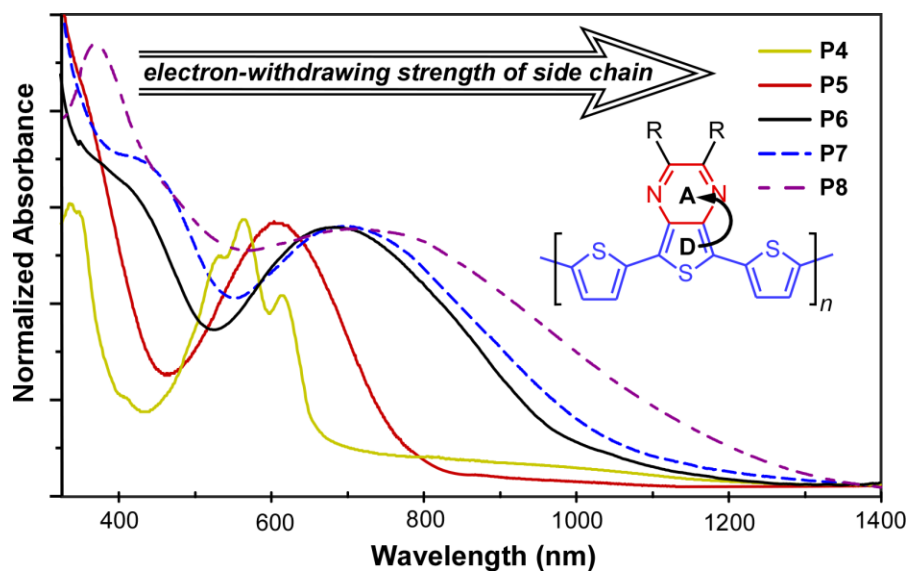


Figure 3.5. Thin film vis-NIR spectra for polymers **P4-P8**.<sup>28</sup>

The optical data presented here supports the claim that TP-based terthienyl materials can be synthetically manipulated to tune their optical and electronic properties based on the electronic nature of the substituents. Oxidative spectral electrochemistry was

performed on the electropolymerized polymers **P5** and **P7** in order to characterize the effect of oxidative doping on the absorption profile. The corresponding absorption profiles were measured over a range of 200 to 1300 mV in stepwise 100 mV increments. No changes in the measured spectra were observed in the initial range, from 200 to 500 mV, so only the steps from 500 to 1300 mV are shown in Figure 3.6 and Figure 3.7. In the neutral state of polymer **P5**, two absorption bands were observed, at approximately 410 and 625 nm, which corresponds to a dark blue polymer film. Bleaching of the peaks at 410 and 625 nm occurred upon the incremental oxidation of the polymer film, while broad peaks at approximately 800 nm and 1050 nm began to develop and extended out into the infrared region of the electromagnetic spectrum. New transitions at approximately 875 and 990 nm began to grow in at potentials above 1000 mV that were very broad and exhibited absorption across the full visible-NIR spectrum. As these final transitions are quite intense and the strongly oxidized film absorbs across the full visible-NIR spectrum, it appeared as a greenish film.

The spectroelectrochemistry of polymer **P7** exhibited similar transitions to **P5**, which were red-shifted in the neutral film in comparison, but with absorption bands observed at approximately 380 and 700 nm with a greenish color to the film. Bleaching of the peaks at 380 and 700 nm occurred upon incremental oxidation of the polymer film while a broad peak at approximately 920 nm developed and extended out into the infrared region of the electromagnetic spectrum. The NIR transition in **P5** exhibited significant structure, whereas the corresponding transition in **P7** was quite broad and featureless. As was the case with **P5**, this NIR transition observed for **P7** was intense and the strongly oxidized film absorbed across the full visible-NIR spectrum to give a gray-colored film.

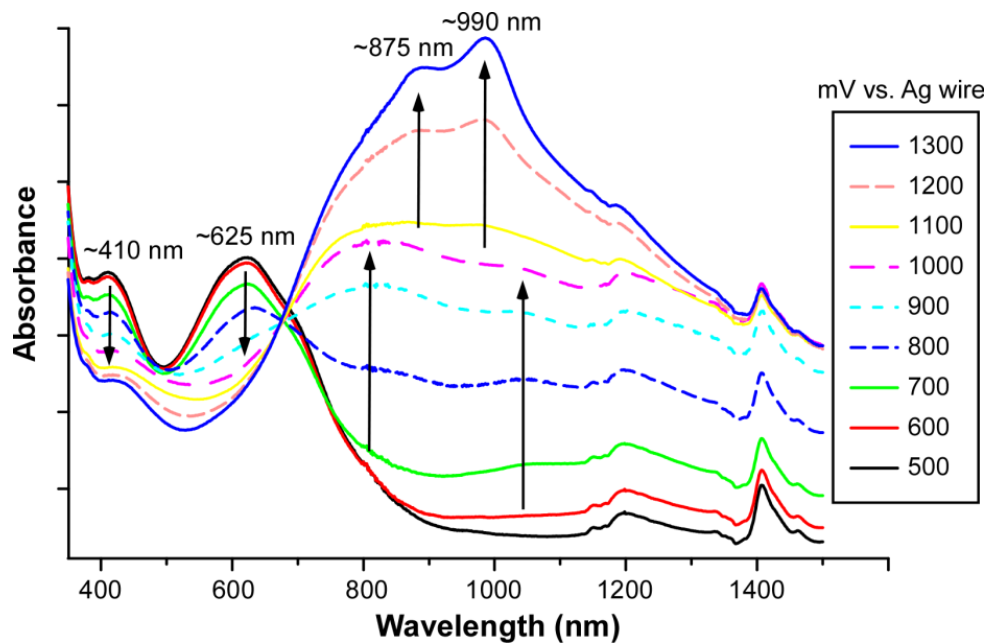


Figure 3.6. Spectroelectrochemistry of polymer **P5**.<sup>28</sup>

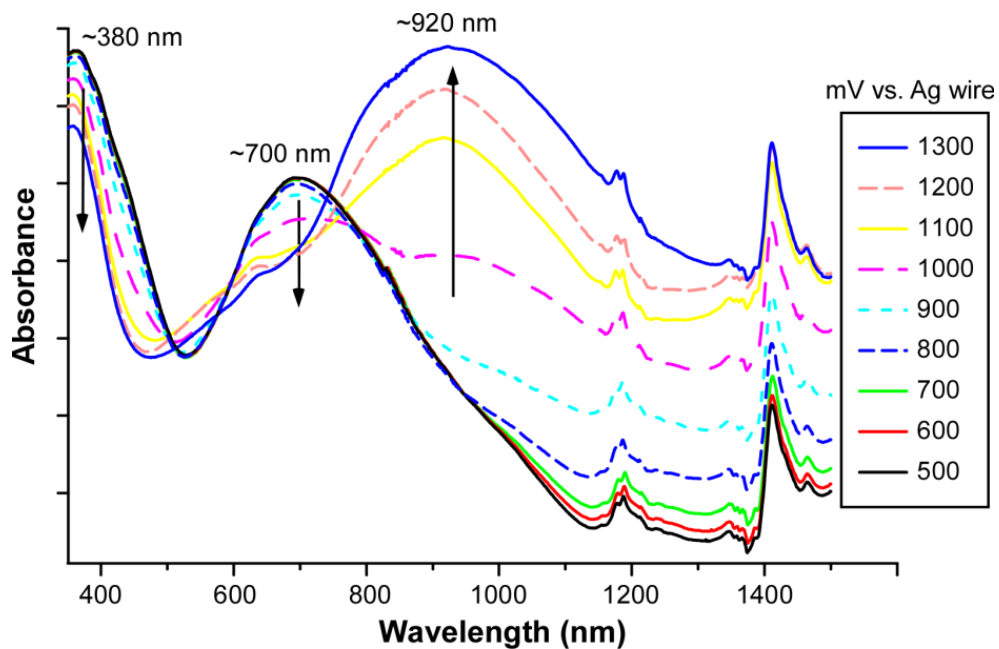


Figure 3.7. Spectroelectrochemistry of polymer **P7**.<sup>28</sup>

**Copolymers of 5,7-bis(2-thienyl)thieno[3,4-*b*]pyrazine and fluorene.** The ability to incorporate electron-donating and electron-withdrawing functionalities on TPs has demonstrated a great deal of tunability of the optical and electronic properties of the resultant homopolymeric TP materials.<sup>23</sup> As discussed previously, initial results from the electropolymerization of poly(5,7-bis(2-thienyl)thieno[3,4-*b*]pyrazine)s have demonstrated the ability to use the electronic nature of the side chains on a central TP unit to tune the electronic properties of the resultant TP-based terthienyl materials, which are essentially copolymers comprised of TP and bithiophene units. The effects of side chains on a series of these TP-based terthienyls are reported and their application to copolymeric materials was investigated, which utilized the well-studied poly(5,7-bis(2-thienyl)thieno[3,4-*b*]pyrazine-*co*-fluorene) framework (Figure 3.8).<sup>9,38-44</sup>

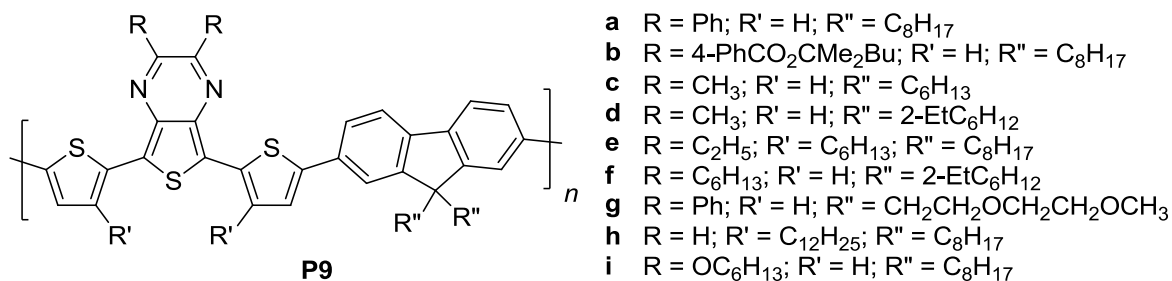
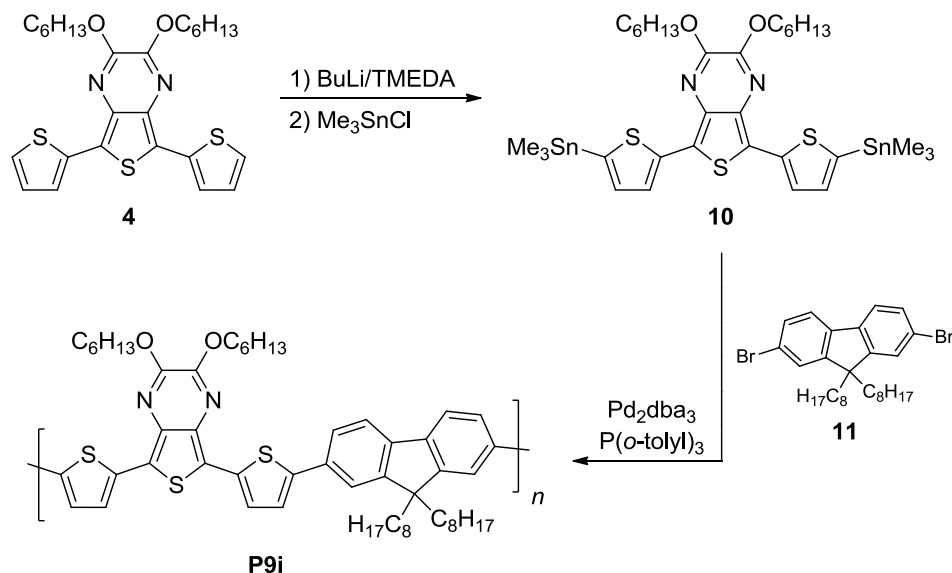


Figure 3.8. Poly(5,7-bis(2-thienyl)thieno[3,4-*b*]pyrazine-*co*-fluorene)s.<sup>45</sup>

To further evaluate the effect of the TP side chains in copolymeric materials, the 2,3-dihexyloxy-functionalized terthienyl **4** was converted to the corresponding trimethylstannyl analogue **10** and copolymerized with dibromofluorene **11** via Stille coupling to give polymer **P9i**, as detailed in Scheme 3.2. The poly(5,7-bis(2-thienyl)thieno[3,4-*b*]pyrazine-*co*-fluorene) framework was chosen because it is one of the

most well studied of the TP-based terthienyl copolymeric materials. As a result, there are a number of analogous materials available in the literature for easy comparison.



Scheme 3.2. Synthesis of poly(2,3-dihexyloxy-5,7-bis(2-thienyl)thieno[3,4-*b*]pyrazine-*co*-9,9-dioctyl-9*H*-fluorene).<sup>45</sup>

The electronic properties of **P9i** and various other previously reported analogues are given in Table 3.4. For the most part, the majority of reported materials with this TP-based terthienyl-*co*-fluorene copolymeric framework are reduced band gap polymers with band gaps close to 1.6 eV.<sup>4</sup> As expected from the previous trends both in the monomeric TPs and in the TP-based terthienyls discussed above, the switch to alkoxy side chains resulted in a destabilization of both the HOMO and LUMO energy levels. In addition, this switch to a more electron-donating functionality resulted in a corresponding increase in the material band gap, with a material that now exhibits a band gap above 2 eV.<sup>45,46</sup>

Table 3.4. Optical and electronic data for poly(5,7-bis(2-thienyl)thieno[3,4-*b*]-pyrazine-*co*-fluorene)s.<sup>45,46</sup>

Polymer	R	$\lambda_{\text{max}}$ , (film, nm)	$E_{\text{g}}^{\text{opt}}$ , eV	$E_{\text{HOMO}}$ , eV <sup>a</sup>	$E_{\text{LUMO}}$ , eV <sup>b</sup>
<b>P9i</b>	OC <sub>6</sub> H <sub>13</sub>	350, 400, 440	2.25	-5.3	-3.2
<b>P9a</b>	Ph	616	1.61	-5.2	-3.7
<b>P9d</b>	CH <sub>3</sub>	600	1.61	-5.6	-3.8
<b>P9h</b>	H	667	1.60	-5.7	-3.6
<b>P9b</b>	<i>p</i> -PhCO <sub>2</sub> R'	710	1.37	<i>nr</i>	<i>nr</i>

*nr* = not reported

$${}^a E_{\text{HOMO}} = - (E_{[\text{onset,ox vs. Fc}^+/\text{Fc}]} + 5.1)(\text{eV}).^{33}$$

$${}^b E_{\text{LUMO}} = - (E_{[\text{onset,red vs. Fc}^+/\text{Fc}]} + 5.1)(\text{eV}).^{33}$$

Interestingly, Helgesen and Krebs reported polymer **P9b** that incorporates phenylester side chains on the TP unit.<sup>42</sup> These phenylesters were incorporated as thermocleavable side chains and not for the intention to tune the electronic properties of the polymer. However, the considerable electron-withdrawing nature of these side chains resulted in a reduction of the band gap in comparison to the alkyl and aryl analogues. As a consequence of the phenylester side chains applied, a polymeric framework that normally resulted in reduced band gap materials was then able to generate a true low band gap material with an  $E_{\text{g}}$  of 1.37 eV. Even though they did not report the electrochemistry, it would be expected from the trends above that this type of functionality would have resulted in a stabilization of both the HOMO and LUMO energy levels of the material.

### 3.3. Conclusion

The ability to produce thieno[3,4-*b*]pyrazine-based terthienyls beyond the simple dialkyl or diaryl analogues allows for the ability to significantly tune the optical and electronic properties of the corresponding polymeric materials, while also minimizing the loss of starting materials through unwanted reactivity. Contrary to the trends commonly

observed with polythiophene materials, the addition of electron-donating groups results in higher HOMO-LUMO energies in the monomers, as well as higher  $E_g$  values in the resulting polymers. Correspondingly, the use of electron withdrawing groups provides reduced HOMO-LUMO energies, as well as lower  $E_g$  values. The application of these tunable TP-based terthienyl building blocks towards the production of conjugated materials appears to be a promising approach for controlling the corresponding frontier orbitals and band gaps of the final polymeric materials.

In the application of TP-based terthienyls into copolymeric systems with fluorene, the effect of the side chains on the HOMO is diminished. Even though the effect on the HOMO is weakened, the TP unit is essentially the factor that determines the LUMO energy of the resultant material and as a result the material's band gap as well. The ability to modulate the optical and electronic properties of materials via TP functional groups would allow for the production of systems that are much more structurally and synthetically simple. Also, this would provide a means to accomplish the desired electronic and optical property modifications for various device applications while holding the backbone structure constant, which would result in a reduction of issues that arise from morphological changes of structurally different materials.

### **3.4. Experimental**

**General.** Unless noted, all materials were reagent grade and used without further purification. Toluene was distilled from sodium benzophenone prior to use. The  $\text{CH}_3\text{CN}$  was dried over CaH and distilled prior to use. All electrochemical glassware was oven dried and cooled in a desiccator. Chromatographic separations were performed using

standard column methods with silica gel (230–400 mesh). Basic silica gel was prepared by pretreating the silica with 3% Et<sub>3</sub>N in CH<sub>2</sub>Cl<sub>2</sub>. Unless otherwise stated, all other materials were reagent grade and used without further purification. All reactions were performed under a nitrogen atmosphere using oven dried glassware. Unless otherwise stated, NMR spectra were obtained in CDCl<sub>3</sub> on a 400 MHz spectrometer and referenced to the chloroform signal. The <sup>1</sup>H NMR and <sup>13</sup>C NMR were completed on a 400 MHz spectrometer. All NMR data was referenced to the chloroform signal and peak multiplicity was reported as follows: s = singlet, d = doublet, t = triplet, q = quartet, p = pentet, dd = doublet of doublets, m = multiplet and br = broad.

**Materials.** Dihexyloxy-5,7-bis(2-thienyl)thieno[3,4-*b*]pyrazine (**4**), 2,3-dimethyl-5,7-bis(2-thienyl)-thieno[3,4-*b*]pyrazine (**5**), 2,3-bis(ethoxymethyl)-5,7-bis(2-thienyl)thieno[3,4-*b*]-pyrazine (**6**), 2,3-bis(bromomethyl)-5,7-bis(2-thienyl)thieno[3,4-*b*]pyrazine (**7**), 2,3-diphenyl-5,7-bis(2-thienyl)thieno[3,4-*b*]pyrazine (**8**), and 2,7-dibromo-9,9-dioctyl-9*H*-fluorene (**11**) were all prepared as previously described.<sup>24,47</sup>

**2,3-Dihexyloxy-5,7-bis(5-trimethylstannyl-2-thienyl)thieno[3,4-*b*]pyrazine (**10**).** Dry hexanes (60 mL) was added via syringe to a flask containing **4** (0.06 g, 0.12 mmol) and the solution was cooled to 0 °C. TMEDA (0.05 mL, 0.35 mmol) was then added followed by BuLi (0.13 mL, 0.33 mmol) and the solution was stirred for 2 h. Me<sub>3</sub>SnCl (0.3 mL, 0.33 mmol) was syringed into the solution and the reaction was allowed to stir overnight. The solution was poured over Et<sub>3</sub>N treated silica gel, filtered, and rinsed with 100 mL hexanes. The solution was concentrated via rotary evaporation to yield a yellow liquid (99%). <sup>1</sup>H NMR: δ 7.44 (d, J = 3.2, 2 H), 7.099 (d, J = 1.6, 2H), 4.40 (t, J = 6.4, 4H), 1.81 (m, J = 6.8, 4H), 1.53–1.20 (m, 16 H), 0.86 (t, J = 6.8, 6 H), 0.40 (s, 18H).



**Poly[2,3-dihexyloxy-5,7-bis(2-thienyl)thieno[3,4-*b*]pyrazine-co-9,9-dioctyl-9H-fluorene] (4i).** Fluorene **11** (0.06 g, 0.12 mmol), **10** (0.10 g, 0.12 mmol), Pd<sub>2</sub>dba<sub>3</sub> (0.002 g, 0.002 mmol), and P(*o*-tolyl)<sub>3</sub> (0.02 g, 0.08 mmol) were combined in a flask. N<sub>2</sub> purged toluene (15 mL) was then added by syringe and the solution evacuated and backfilled with N<sub>2</sub>. The reaction was then placed in an oil bath (95 °C) and allowed to react for 4 days. The reaction was then cooled, poured into 300 mL methanol, and filtered. The soluble fraction of polymer was collected in CHCl<sub>3</sub> and isolated by rotary evaporation. Further purification was accomplished by further washes with MeOH yielding a red solid (75%). <sup>1</sup>H NMR: δ 7.50 (m), 7.44 (m), 7.30 (m), 4.55 (br t), 1.92 (m), 1.6-0.6 (m). GPC: M<sub>w</sub> = 4000, M<sub>n</sub> = 2700, PDI = 1.48.

**Electropolymerizations.** Electropolymerizations for the electrochemical experiments were carried out in a three-electrode cell consisting of a platinum disc working electrode, a platinum wire auxiliary electrode, and a Ag/Ag<sup>+</sup> reference electrode. Solutions consisted of oligomer (0.05 M) dissolved in anhydrous CH<sub>3</sub>CN containing 0.10 M tetrabutylammonium hexafluorophosphate (TBAPF<sub>6</sub>). The solutions were deoxygenated by sparging with argon prior to each scan and blanketed with argon during the polymerizations. The platinum disc working electrode was polished with 0.05 mm alumina and washed well with deionized water and dry CH<sub>3</sub>CN prior to each film growth. The films were grown by cyclic voltammetry scanning through the E<sub>pa</sub> region for each oligomer.

Electropolymerizations for optical experiments were carried out in the same manner as discussed above except an indium tin oxide (ITO) coated glass plate was used as the working electrode. Polymer films were grown by continuous repeated potential

cycling around the  $E_{pa}$  for each monomer until a suitable film was obtained and then held at a fixed potential corresponding to the neutral form of the polymer under investigation.

### 3.5. Instrumentation

**Electropolymerization study.** UV–vis spectra were measured on a dual beam scanning spectrophotometer using samples prepared as polymer films on ITO coated glass plates. The spectroelectrochemical measurements were performed on a BAS 100B/W utilizing a platinum wire auxiliary electrode, a silver wire quasi-reference electrode and an ITO coated glass working electrode. All other electrochemical measurements were performed on a BAS utilizing a platinum wire auxiliary electrode, either silver wire or  $Ag/Ag^+$  reference electrode (0.251 V vs SCE) and either a platinum disc or an indium tin oxide coated glass working electrode. The supporting electrolyte consisted of 0.10 M TBAPF<sub>6</sub> in dry CH<sub>3</sub>CN. Solutions were deoxygenated by sparging with argon prior to each scan and blanketed with argon during the measurements. All measurements were collected at a scan rate of 100 mV/s.

**TP-terthienyl-*co*-fluorene polymer study.** Electrochemical measurements were performed on an EC Epsilon potentiostat using a Pt disc working electrode and a Pt wire counter electrode. Solutions consisted of 0.1 M TBAPF<sub>6</sub> in CH<sub>3</sub>CN and were sparged with argon for 20 min prior to data collection and blanketed with argon during the experiment. Terthiophene samples were measured as millimolar solutions and polymeric samples were measured as solid-state films drop-cast onto the Pt disc working electrodes. All potentials are referenced to a  $Ag/Ag^+$  reference (0.1 M AgNO<sub>3</sub>/0.1 M TBAPF<sub>6</sub> in CH<sub>3</sub>CN; 0.320 V vs. SCE).<sup>48</sup> UV–visible spectra were measured on a dual-beam scanning

spectrophotometer using samples prepared as dilute solutions in 1-cm quartz cuvettes or thin films spun onto glass slides.

### 3.6. References

1. Rasmussen, S. C. In *The Encyclopedia of Polymeric Nanomaterials*; Kobayashi, S., Muellen, K., Eds.; Springer-Verlag: Berlin, Germany, 2015; Chapter 57.
2. Rasmussen, S. C.; Pomerantz, M. In the *Handbook of Conducting Polymers*, 3rd ed.; Skotheim, T. A., Reynolds, J. R., Eds.; CRC Press: Boca Raton, FL, 2007; Vol. 1, Chapter 12.
3. Rasmussen, S. C.; Ogawa, K.; Rothstein, S. D. In the *Handbook of Organic Electronics and Photonics*, Nalwa, H. S., Ed.; American Scientific Publishers: Stevenson Ranch, CA, 2008; Vol. 1, Chapter 1.
4. Rasmussen, S. C.; Schwiderski, R. L.; Mulholland, M. E. *Chem. Commun.* **2011**, 47, 11394.
5. Rasmussen, S. C.; Mulholland, M. E.; Schwiderski, R. L.; Larsen, C. A. *J. Heterocyclic Chem.* **2012**, 49, 479.
6. Kitamura, C.; Tanaka, S.; Yamashita, Y. *J. Chem. Soc., Chem. Commun.* **1994**, 1585.
7. Kitamura, C.; Tanaka, S.; Yamashita, Y. *Chem. Mater.* **1996**, 8, 570.
8. Delgado, M. C. R.; Hernandez, V.; Navarrete, J. T. L.; Tanaka, S.; Yamashita, Y. *J. Phys. Chem. B* **2004**, 108, 2516.
9. Zhu, Z.; Champion, R. D.; Jenekhe, S. A. *Macromolecules* **2006**, 39, 8721.
10. Cai, T.; Zhou, Y.; Wang, E.; Hellstrom, S.; Zhang, F.; Xu, S.; Inganas, O.; Andersson, M. R. *Sol. Energy Mater. Sol. Cells* **2010**, 94, 1275.

11. Wienk, M. M.; Turbiez, M. G. R.; Struijk, M. P.; Fonrodona, M.; Janssen, R. A. J. *Appl. Phys. Lett.* **2006**, *88*, 153511.
12. Zoombelt, A. P.; Fonrodona, M.; Turbiez, M. G. R.; Wienk, M. M.; Janssen, R. A. J. *J. Mater. Chem.* **2009**, *19*, 5336.
13. Zoombelt, A. P.; Leenen, M. A. M.; Fonrodona, M.; Nicholas, Y.; Wienk, M. M.; Janssen, R. A. J. *Polymer* **2009**, *50*, 4564.
14. Sonmez, G.; Shen, C. K. F.; Rubin, Y.; Wudl, F. *Angew. Chemie. Int. Ed.* **2004**, *43*, 1948.
15. Sonmez, G.; Sonmez, H. B.; Shen, C. K. F.; Wudl, F. *Adv. Mater.* **2004**, *16*, 1905.
16. Sonmez, G.; Sonmez, H. B.; Shen, C. K. F.; Jost, R. W.; Rubin, Y.; Wudl, F. *Macromolecules* **2005**, *38*, 669.
17. Tarkuc, S.; Unver, E. K.; Udum, Y. A.; Tanyeli, C.; Toppare, L. *Electrochim. Acta* **2010**, *55*, 7254.
18. Berlin, A.; Zotti, G.; Zecchin, S.; Schiavon, G.; Vercelli, B.; Zanelli, A. *Chem. Mater.*, **2004**, *16*, 3667.
19. Casado, J.; Ortiz, R. P.; Delgado, M. C. R.; Hernandez, V.; Navarrete, J. T. L.; Raimundo, J.; Blanchard, P.; Allain, M.; Roncali, J. *J. Phys. Chem. B* **2005**, *109*, 16616.
20. Kenning, D. D.; Mitchell, K. A.; Calhoun, T. R.; Funfar, M. R.; Sattler, D. J.; Rasmussen, S. C. *J. Org. Chem.* **2002**, *67*, 9073
21. Wen, L.; Nietfeld, J. P.; Amb, C. M.; Rasmussen, S. C. *Polym. Prepr.* **2008**, *49*, 633.
22. Wen, L.; Nietfeld, J. P.; Amb, C. M.; Rasmussen, S. C. *J. Org. Chem.* **2008**, *73*, 8529.

23. Wen, L.; Nietfeld, J. P.; Amb, C. M.; Rasmussen, S. C. *Synth. Met.* **2009**, *159*, 2299.
24. Schwiderski, R. L.; Rasmussen, S. C. *J. Org. Chem.* **2013**, *78*, 5453-5462.
25. Waltman, R. J.; Diaz, A. F.; Bargon, J. *J. Electrochem. Soc.* **1984**, *131*, 1452.
26. Waltman, R. J.; Bargon, J. *Can. J. Chem.* **1986**, *64*, 76.
27. Gurunathan, K.; Vadivel Murugan, A.; Marimuthu, R.; Mulik, U. P.; Amalnerkar, D. *P. Mater. Chem. Phys.* **1999**, *61*, 173.
28. Schwiderski, R. L.; Rasmussen, S. C. *Synth. Met.* **2014**, *193*, 58.
29. Rasmussen, S. C.; Sattler, D. J.; Mitchell, K. A.; Maxwell, J. *J. Lumin.* **2004**, *190*, 111.
30. Roncali, J. *Chem. Rev.* **1992**, *92*, 711.
31. Waltman, R. J.; Bargon, J. *Tetrahedron* **1984**, *40*, 3963.
32. Smith, J. R.; Cox, P. A.; Campbell, S. A. *J. Chem. Soc. Faraday Trans.* **1995**, *91*, 2331.
33. Cardona, C. M.; Li, W.; Kaifer, A. E.; Stockdale, D.; Bazan, G. C. *Adv. Mater.* **2011**, *23*, 2367.
34. Wang, X.; Wang, L.; Wang, J.; Chen, T. *J. Appl. Polym. Sci.* **2006**, *101*, 515.
35. Heth, C. L.; Tallman, D. E.; Rasmussen, S. C. *J. Phys. Chem. B* **2010**, *114*, 5275.
36. Demanze, F.; Yassar, A.; Garnier, F. *Macromolecules* **1996**, *29*, 4267.
37. P. Zuman, *Substituent Effects in Organic Polarography*, Plenum Press: New York, 1967.
38. Perzon, E.; Wang, X.; Zhang, F.; Mammo, W.; Delgado, J. L.; de la Cruz, P.; Inganas, O.; Langa, F.; Andersson, M. R. *Synth. Met.* **2005**, *154*, 53.

39. Zhang, F.; Perzon, E.; Wang, X.; Mammo, W.; Andersson, M. R.; Inganas, O. *Adv. Funct. Mater.* **2005**, *15*, 745.
40. Admassie, S.; Inganas, O.; Mammo, W.; Perzon, E.; Andersson, M. R. *Synth. Met.* **2006**, *156*, 614.
41. Lee, W.; Cheng, K.; Wang, T.; Chueh, C.; Chen, W.; Tuan, C.; Lin, J. *Macromol. Chem. Phys.* **2007**, *208*, 1919.
42. Helgesen, M.; Krebs, F. C. *Macromolecules* **2010**, *43*, 1253.
43. Zhou, E.; Cong, J.; Yamakawa, S.; Wei, Q.; Nakamura, M.; Tajima, K.; Yang, C.; Hashimoto, K. *Macromolecules* **2010**, *43*, 2873.
44. Chao, C-Y.; Lim H.; Chao, C-H. *Polym. Prepr.* **2010**, *51(1)*, 715.
45. Mulholland, M. E.; Schwiderski, R. L.; Rasmussen, S. C. *Polym. Bull.* **2012**, *69*, 291.
46. Mulholland, M. E.; Schwiderski, R. L.; Evenson, S. J.; Rasmussen, S. C. *PMSE preprint*, **2012**, *107*, 36.
47. Cho, S. Y.; Grimsdale, A. C.; Jones, D. J.; Watkins, S. E.; Holmes, A. B. *J. Am. Chem. Soc.* **2007**, *129*, 11910.
48. Larson, R. C.; Iwamoto, R. T.; Adams, R. N. *Anal. Chim. Acta* **1961**, *25*, 371.

# CHAPTER 4. EXTENDED FUSED-RING THIENO[3,4-*b*]PYRAZINES WITH SOLUBILIZING CHAINS

## 4.1. Introduction

The fused pyrazine ring of thieno[3,4-*b*]pyrazines (TPs) is known to stabilize the quinoidal resonance form of the thiophene backbone, which results in a significant reduction in band gap in the corresponding polymeric materials.<sup>1-3</sup> Consequently, a great deal of effort has been applied towards the development of more extended fused-ring TP analogs as these extended fused-ring building blocks show much promise in regards to the production of low band gap materials. The earliest known extended fused-ring TP analog is thieno[3,4-*b*]quinoxalines (**1**) and was synthesized in 1977 by Roland and Anderson, but were only observed via trapping experiments (Figure 4.1).<sup>4</sup> Later, in 1995 Cava and coworkers reported the successful synthesis and isolation and the first extended fused-ring TP analog was characterized.<sup>5</sup> Since then, very few extended fused-ring TP materials have been produced because of the limited solubility of these systems and the significant efforts required to produce the functionalized diones required for their synthesis.

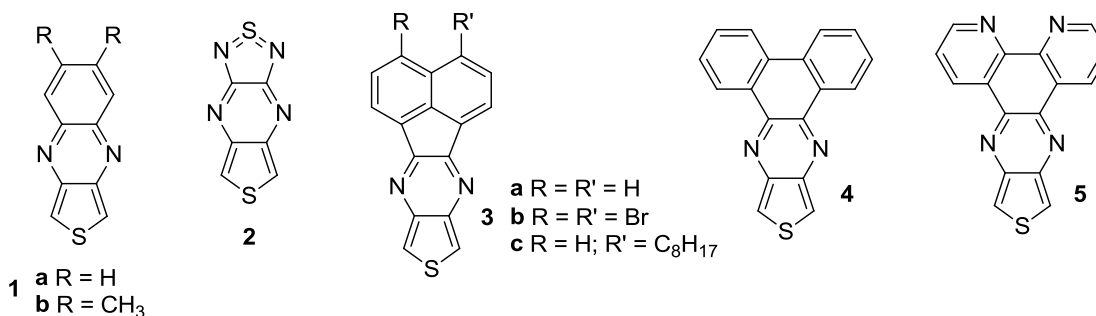


Figure 4.1. Extended fused-ring thieno[3,4-*b*]pyrazine monomers.<sup>5,6,10,11</sup>

Some of the other common examples of extended fused-ring TPs include [1,2,5]thiadiazolo[3,4-*b*]thieno[3,4-*e*]pyrazine (**2**), acenaphtho[1,2-*b*]thieno[3,4-*e*]pyrazine (**3**), dibenzo[*f,h*]thieno[3,4-*b*]quinoxaline (**4**), and thieno[3',4':5,6]pyrazino[2,3-*f*][1,10]phenanthroline (**5**), which are shown in Figure 4.1.<sup>4-11</sup> Because of the limited solubility of these TP monomers and the bulkiness of the extended ring system, researchers have favored the use of the 5,7-di(2-thienyl)thieno[3,4-*b*]pyrazine analogs as an alternative. As a consequence, there are far more examples of the extended fused-ring TP-based terthienyl oligomers as compared to the TP monomers (Figure 4.2).<sup>11</sup> However, like their monomeric counterparts, these oligomers also suffer from reduced solubility so the addition of solubilizing chains is necessary. Most often, the solubilizing chains are included on the exterior thiophenes, which unfortunately cause steric interactions and torsional rotation about the interannular bonds that are responsible for a reduction in conjugation and a blue shift in absorbance (as exhibited in **7a** → **b,c**; **8a** → **e**), with representative examples listed in Table 4.1.<sup>11</sup>

Table 4.1. Collected data for extended fused-ring TPs and corresponding TP-based terthienyl analogs.

Compound	$\lambda_{\max}$ (nm)	Compound	$\lambda_{\max}$ (nm)	Compound	$\lambda_{\max}$ (nm)
<b>1</b>	371 <sup>c</sup>	<b>6a</b>	990 <sup>a</sup>	<b>7c</b>	483 <sup>b</sup>
<b>2</b>	581 <sup>a</sup>	<b>6b</b>	853 <sup>a</sup>	<b>8a</b>	641
<b>3a</b>	375	<b>6c</b>	1345 <sup>a</sup>	<b>8b</b>	648
<b>3c</b>	376	<b>6d</b>	800 <sup>a</sup>	<b>8c</b>	622
<b>4</b>	426	<b>7a</b>	548	<b>8e</b>	622
<b>5</b>	418	<b>7b</b>	495 <sup>b</sup>	<b>11a</b>	655 <sup>a</sup>

<sup>a</sup> In CH<sub>2</sub>Cl<sub>2</sub>. <sup>b</sup> In dichlorobenzene. <sup>c</sup> In ethanol. All other  $\lambda_{\max}$  measured in CHCl<sub>3</sub>.<sup>11</sup>



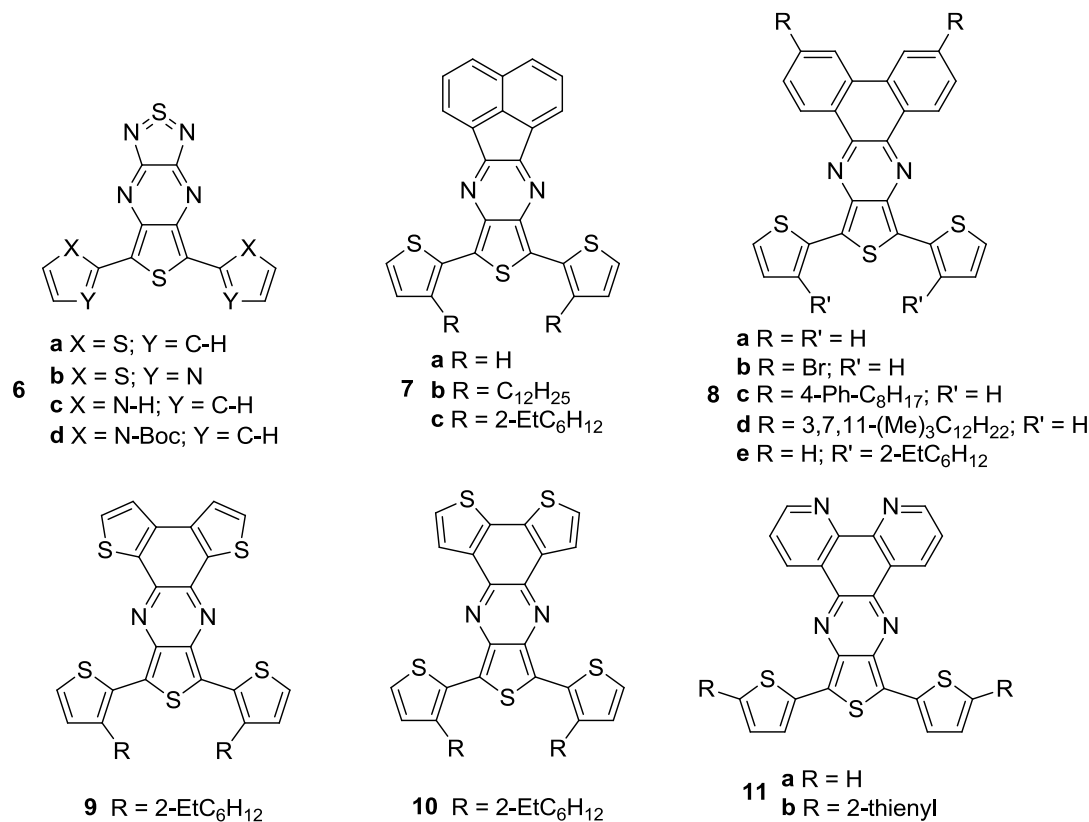


Figure 4.2. Extended fused-ring thieno[3,4-*b*]pyrazine oligomers.

The monomeric TPs (**1-5**) share similar optical properties with the TP-based oligomers (**6-11**), but with a red shift in absorbance due to the extended conjugation length of the oligomers. The monomers exhibit increasing red shifts from **1** → **3** → **5** → **4** → **2** and the corresponding oligomers follow the same trend closely with increasing red shifts from **7** → **8** → **11** → **6**. Since the LUMO energy is determined predominantly from the pyrazine contributions, the reduction potentials of analogous monomeric and oligomeric TPs should be nearly identical. This is clearly observed for **3a** vs. **7b** (-1.67 V vs. -1.85 V), **4** vs. **8a** (-1.51 V vs. -1.44 V), and **5** vs. **11a** (-1.27 V vs. -1.24 V), as shown in Table 4.2. However, because the HOMO is located on the thiophene of the monomer and

thiophene backbone of the terthienyl oligomer, notable effects on the potential of oxidation of the monomers vs. oligomers is observed, where **3a** → **7b** decreases from 1.18 V to 0.43 V, **4** → **8a** decreases from 0.98 V to 0.25 V, and **5** → **11a** decreases from 1.45 V to 0.48 V (Table 4.1).<sup>11</sup> The structural modifications made to these extended fused-ring TPs understandably affects the corresponding materials when they are incorporated into polymeric systems.

Table 4.2. Collected data for extended fused-ring TPs and their corresponding terthienyl analogs.<sup>11</sup>

Compound	Oxidation	Reduction	HOMO-LUMO gap <sup>a</sup> , eV
	$E_{pa}$ , V	$E_{1/2}$ , V	
<b>3a</b>	1.18	-1.67	3.31
<b>7b</b>	0.43	-1.85	2.51
<b>4</b>	0.98	-1.51	2.91
<b>8a</b>	0.25	-1.44	1.93
<b>5</b>	1.45	-1.27	2.97
<b>11a</b>	0.48	-1.24	1.89

<sup>a</sup>Values based optical  $\lambda_{max}$ . Electrochemical data vs. Ag/Ag<sup>+</sup>. Values reported vs. other references converted for comparison.

The net effect on the electronic properties due to the addition of the external thiophenes of the oligomers is to decrease the HOMO-LUMO gap of these systems because the extended conjugation imparted by the extra thiophenes causes a significant decrease of the potential of oxidation. One could reasonably expect that this would lead to a decreased band gap in the polymers by virtue of the donor-acceptor (D-A) model of copolymers. In the D-A model it is thought that the HOMO energy level is determined by the electron-rich donor and the LUMO energy level determined by the electron-poor

acceptor, where in this case the TP acts as the acceptor moiety and the bithiophene acts as the donor moiety. It is thought that a combination of these moieties would produce polymers with decreased band gaps. However, the opposite trend is actually observed with the homopolymeric materials giving significantly smaller  $E_g$  values in comparison to their copolymeric counterparts and is illustrated below in Figure 4.3. This fact is demonstrated by the observation of a significant blue shift in absorbance from the homopolymeric **12** (910 nm) to the copolymeric **13** (716 nm) and **14** (576 nm) as well as an increase in band gap from **12** (0.50 eV)  $\rightarrow$  **13** (1.33 eV)  $\rightarrow$  **14** (1.83 eV).<sup>11</sup>

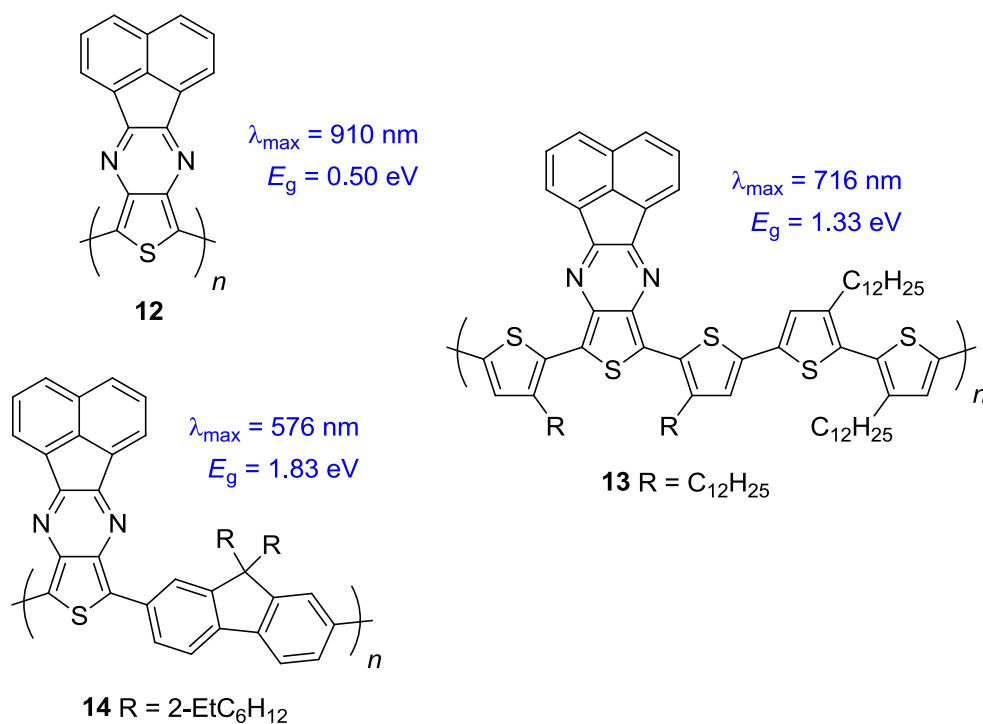


Figure 4.3. Solid-state absorbance and electrochemical band gap of homopolymeric and copolymeric acenaphtho[1,2-*b*]thieno[3,4-*e*]pyrazines.<sup>11</sup>

While most research in the literature views TPs as ‘acceptor’ units, Janssen and coworkers suggested that TPs also act as ‘donor’ unit.<sup>12</sup> Meanwhile Rasmussen and coworkers have not only shown that TPs can act as ‘donor’ units, but are in fact better donors than most traditional donors, thus the degree of TP content determines much of the properties of the corresponding material.<sup>13</sup> Rasmussen went on to demonstrate that both the HOMO and LUMO energy levels are determined by the TP and because in most cases the combination reduces the donor character of the polymer backbone TP is a stronger donor than the comonomer. Consequently, the traditional model of donor-acceptor copolymers, where the band gap is determined as a result of a charge transfer between the donor unit and TP, is in reality more correct to think of as a charge transfer between the polymer backbone and the TP-based LUMO energy level.<sup>13</sup>

The decrease in donor character with the copolymeric systems results in a stabilization of the HOMO, which leads to an increase in the energy of the charge transfer transition, or a larger band gap.<sup>13</sup> This sentiment is echoed with the acenaphtho[1,2-*b*]thieno[3,4-*e*]pyrazine-based polymers shown above. As the TP content decreases from **12** to **13** and **14**, there is also a corresponding increase in energy of the charge transfer transition, as well as an increase in band gap (Figure 4.3). Because of this, in order to produce extended fused-ring TP-based materials with very low band gaps ( $E_g < 1$  eV), while also retaining solubility, homopolymeric materials with solubilizing chains must be used instead of incorporating comonomers for added solubility.

However, as with all conjugated materials, a critical aspect to consider when designing these materials is side chain-induced steric effects. While side chains are necessary to overcome the limited solubility of these materials, their inclusion can also

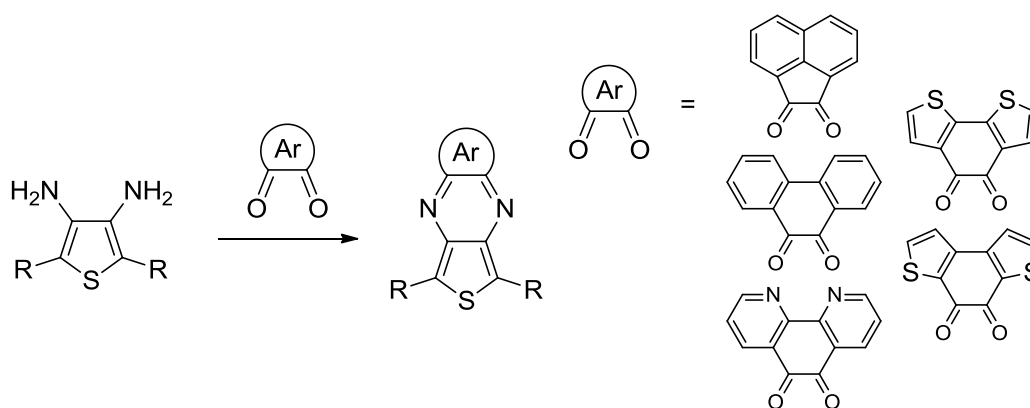
result in undesirable steric interactions that inhibit backbone planarity. Oftentimes, trends in band gaps for conjugated materials are attributed to increased or decreased charge transfer effects, while the critical effect of side chain steric interactions is routinely overlooked.<sup>11</sup> Minimizing the steric interactions in hopes of decreasing the band gap is inherently limited, but ignoring the contributions of unfavorable steric interactions can quickly overpower any potential benefits from the extended fused-ring TP unit. Therefore, the generation of extended fused-ring TPs containing solubilizing chains, that have minimal impacts on the optical and electronic properties of the corresponding polymers, is of great interest.

## 4.2. Results and Discussion

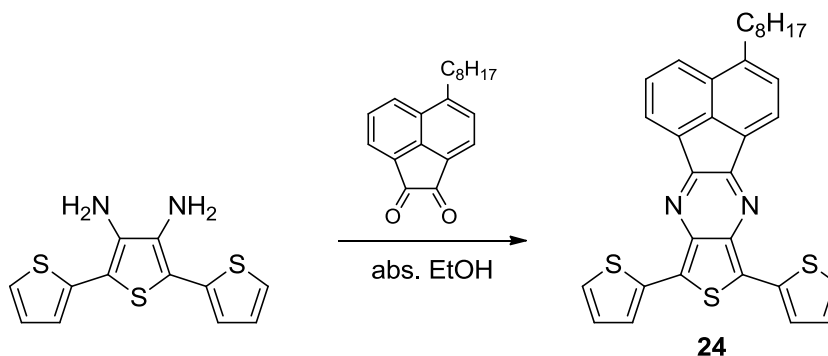
**Synthesis.** With the exception of compounds **1**, **2**, and **6**, the extended fused-ring TPs are generated via a simple condensation reaction between a thiophene-based diamine and their corresponding polycyclic  $\alpha$ -dione as outlined in Scheme 4.1.<sup>11</sup> A vast majority of these species do not contain the added alkyl chains on the TP unit itself and instead rely on other means for solubilization, with the only analogs to incorporate such functionalities being **3c**, **8c**, and **8d**. Therefore, methods were sought for the production of extended fused-ring  $\alpha$ -diones that incorporate solubilizing functionalities so soluble, solution processable derivatives of TPs could be achieved.

An example of an extended fused-ring TP terthienyl was synthesized with the 5-octylacenaphthylene-1,2-dione as a means to produce a soluble TP-terthienyl analog. The reaction was a straightforward condensation between the dione and 3',4'-diamino-2,2':5',2''-terthiophene, as shown in Scheme 4.2, in which 3-octyl-8,10-bis(2-

thienyl)acenaphtho[1,2-*b*]thieno[3,4-*e*]pyrazine (**24**) was produced in good yield. The TP-terthienyl **24** exhibited properties similar to those of other extended fused-ring TP-terthienyls.



Scheme 4.1. General synthesis of extended fused-ring thieno[3,4-*b*]pyrazines.

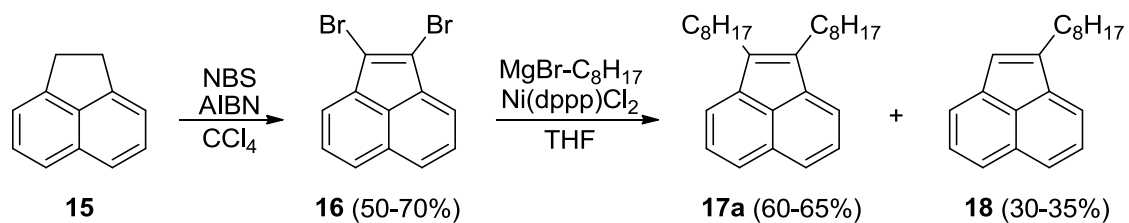


Scheme 4.2. Synthesis of extended fused-ring 3-octyl-8,10-bis(2-thienyl)acenaphtho[1,2-*b*]thieno[3,4-*e*]pyrazine.

The optical properties of terthienyl **24** are nearly identical to those found for the unfunctionalized analog **7a**, with exhibited  $\lambda_{\text{max}}$  values of 545 nm and 548 nm respectively.<sup>11</sup> Unfortunately, the electronic properties of **24** cannot be compared directly

to those of **7a** because they were never published. However, compound **24** has an alkyl chain attached at the central TP unit and the external thiophenes remain unsubstituted. While for **7b** the opposite is true where the central TP unit is free of substitution and the alkyl chains are attached to the external thiophenes, so inferences can be made as to the extent the location of alkyl substitutions affect the optical and electronic properties of the material. A blue shift of approximately 50 nm is observed in the lowest energy absorbance from **24** to **7b**, which is 545 nm versus 495 nm.<sup>11</sup> Also, electrochemical differences are observed, where **24** exhibits a shift to more positive potentials for both the first oxidation, 0.83 V versus 0.43 V, and the first reduction, -1.34 V versus -1.85 V, for **7b**.<sup>11</sup>

A synthetic approach towards the production of 1,2-dibromoacenaphthylene (**16**) was previously established via the radical bromination of acenaphthene (**15**) and is illustrated in Scheme 4.3.<sup>25</sup> X-ray quality crystals were grown to confirm the structure of **16** and is shown below in Figure 4.4. Using the same methodology as a starting point, the approach was applied towards the generation of 1,2-dioctylacenaphthylene (**17a**). Utilizing a Kumada coupling reaction, dibromide **16** was reacted with an octyl Grignard reagent and a nickel catalyst that produced a mixture of approximately 2:1 of the di-coupled **17a** and mono-coupled **18** products. The di- and mono-coupled products could not be separated via column chromatography and possessed boiling points that were too high for vacuum distillation. As a result, this series of reactions produced an inseparable mixture that was not suitable for the next step. Due to the generation of impure materials as well as the high cost of starting materials, reactants, and solvents needed for these transformations, this process was abandoned in favor of a more cost-effective approach for the generation the 1,2-disubstituted acenaphthylenes.



Scheme 4.3. Synthesis of 1,2-dioctylacenaphthylene via radical bromination.

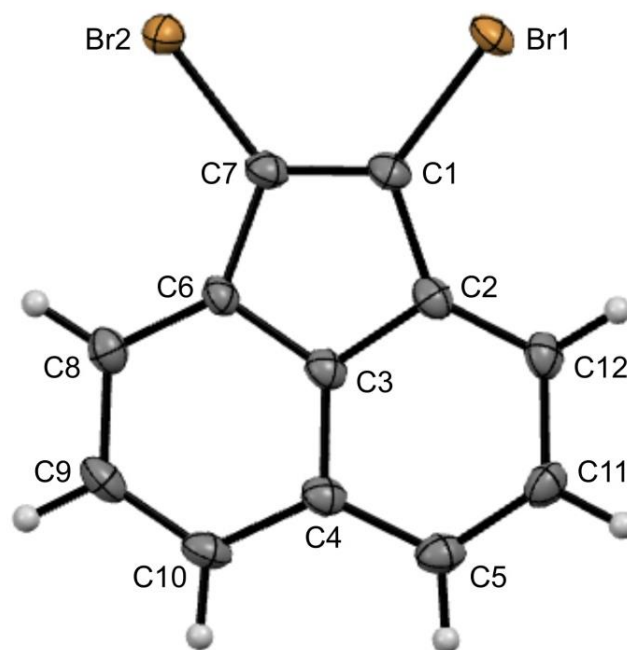
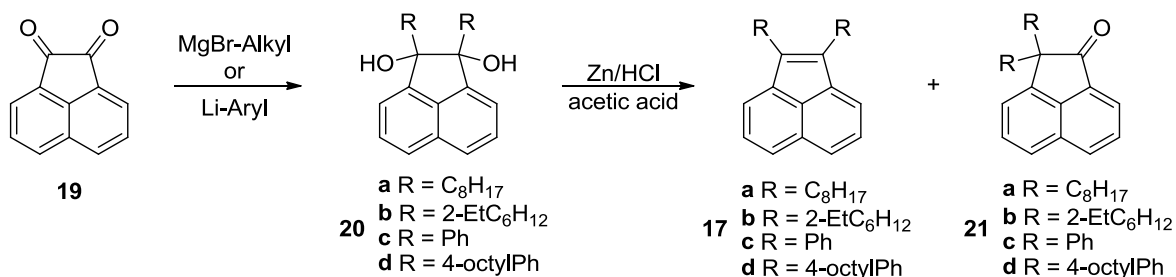


Figure 4.4. Thermal ellipsoid plot of 1,2-dibromoacenaphthylene, **16** at the 50% probability level.

An appropriate method for the generation of 1,2-disubstituted acenaphthylene analogs was successfully developed. This approach utilized acenaphthenequinone (**19**) that was reacted with either alkyl Grignard reagents to produce 1,2-dialkyl-1,2-dihydroxyacenaphthenes (**17a** and **17b**) or aryllithium reagents to produce 1,2-diaryl-1,2-dihydroxyacenaphthenes (**17c** and **17d**) as racemic mixtures (Scheme 4.4). With the



standard Grignard approach the generation of the dioctyl **20a**, and to a lesser extent bis(2-EtC<sub>6</sub>H<sub>12</sub>) **20b**, were produced in moderate yields. The dioctyl derivative was a white powder that could be easily purified by filtration and washing with hexane to produce **20a** in 30-40% yield. The bis(2-EtC<sub>6</sub>H<sub>12</sub>) was a bit more difficult to work with as product **20b** was an orange oil that was soluble in hexanes and could not be separated from the various greasy byproducts of the reaction.

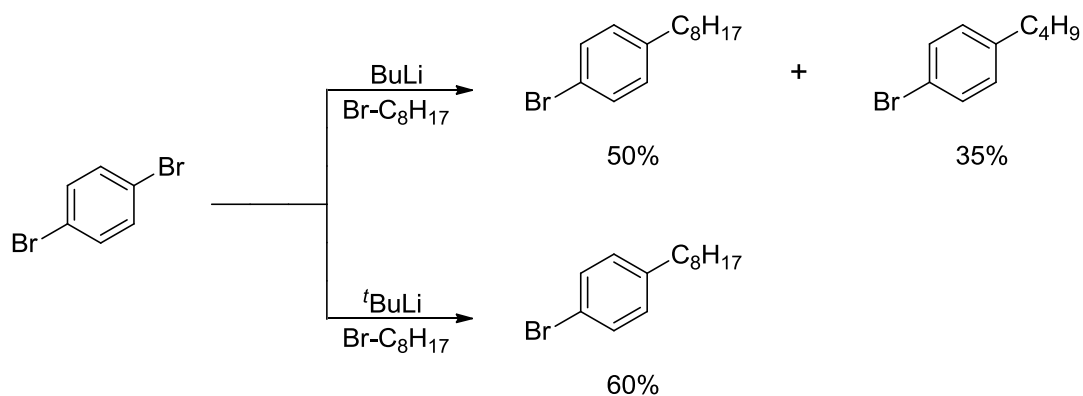


Scheme 4.4. Synthesis of various 1,2-disubstituted acenaphthylenes.

The production of the diaryl products **20c** and **20d** were achieved through the reaction of the aryllithium intermediate with acenaphthenequinone **19**. In the case of **20c**, bromobenzene was commercially available so the production of the phenyllithium intermediate was achieved via typical procedures using butyllithium. Upon reaction of phenyllithium, diphenyl derivative **20c** was produced in good yield (~80-85%) as a white powder that was easily purified by filtration and washing with hexanes. In the case of **20d**, 1-bromo-4-octylbenzene was not commercially available so it had to be synthesized from commercially available 1,4-dibromobenzene prior to use as outlined below in Scheme 4.5.

The use of butyllithium as the reagent for lithium halogen exchange with the 1,4-dibromobenzene led to the formation of an appreciable amount of the butyl substituted

benzene. This can be attributed to the production of butyl bromide upon lithium halogen exchange with the aryl bromide species, which can then react with the aryllithium base. It has been shown that at higher temperatures the butyl bromide generated upon lithium halogen exchange can react with bromobenzenes to produce the butyl-substituted products.<sup>14</sup> However, it was thought that the low temperatures employed here (-78 °C) would be enough to inhibit this unwanted side reaction due to the difference in solubility of the butyl bromide versus the octyl bromide species. Since the aryllithium base does not react with either alkyl halide selectively and there is not an appreciable difference in solubility of the alkyl bromides, a near stoichiometric ratio of products was observed.



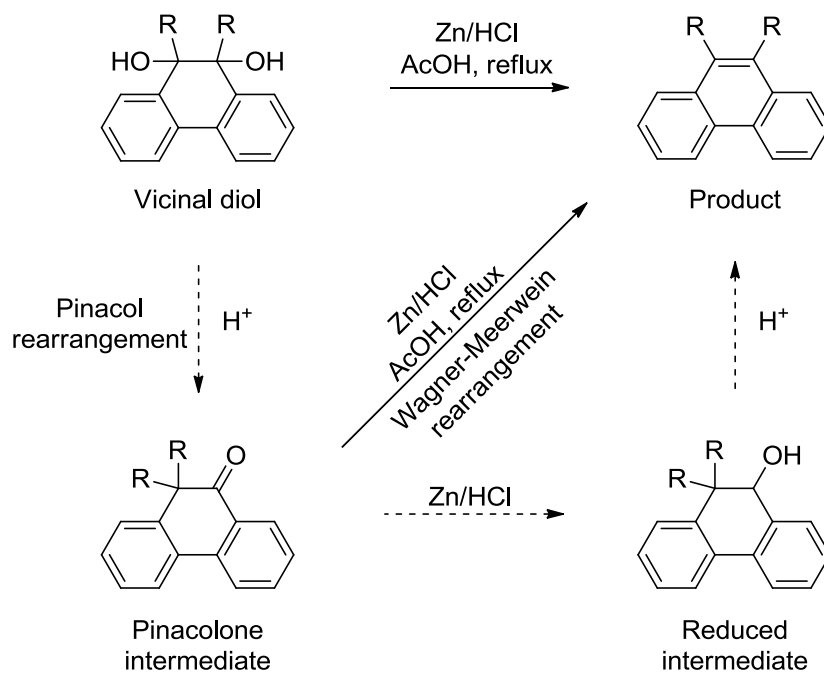
Scheme 4.5. Synthesis of 1-bromo-4-octylbenzene.

Therefore, the use of *t*-butyllithium is required as the *t*-butyl bromide that is generated upon lithium-halogen exchange reacts with another equivalent of *t*-butyllithium to form isobutene, isobutane, and lithium bromide, thus allowing for the selective reaction of the aryllithium base with octyl bromide.<sup>15</sup> The reaction only produced moderate yields of the 1-bromo-4-octylbenzene (60%) with a great deal of unreacted octyl bromide (~35%)

and purification via column chromatography was not able to separate these compounds. However, this mixture was utilized for the production of **20d** since lithium-halogen exchange reactions are kinetically controlled with the position of the equilibrium determined by the stabilities of the carbanion intermediates involved in this process, with  $sp \gg sp^2 \gg sp^3$ .<sup>15</sup> Therefore, the unreacted octyl bromide should not interfere with the lithium-halogen exchange of the aryl bromide. Upon reaction of this aryllithium with acenaphthene quinone **19**, **20d** was produced in excellent yield (~95%) which could be easily purified as a very thick, light yellow oil via column chromatography using a solvent gradient from 100% hexanes  $\rightarrow$  100%  $CH_2Cl_2$ . The oil turned to a white, hard, waxy solid after solidification was induced by freezing.

Once **20a-d** were prepared, a method for the efficient reductive dehydration to their corresponding **17a-d** derivatives was sought. Reductive dehydrations have been shown to successfully produce aromatic, fused-ring benzenes from 1,4-diols using sodium hypophosphite, potassium iodide, and trifluoroacetic acid in glacial acetic acid.<sup>16,17</sup> When these reaction conditions were applied to the vicinal diol **20a**, as shown in Scheme 4.4, a mixture of products was observed in ratios between 3:1 to 1:1 of the desired **17a** versus the rearranged ketone byproduct **21a** that were extremely difficult to separate via column chromatography. When 1.1 equivalents of sodium hypophosphite and potassium iodide with catalytic amounts of trifluoroacetic acid (versus **20a**) were used, a ratio of 3:1 of product versus byproduct was observed with a shift towards a 1:1 ratio when 10 equivalents of the reagents were employed. Based on the large amounts of the rearranged ketone byproduct produced under these reaction conditions, another method utilizing zinc metal and hydrochloric acid was developed.

Müllen and coworkers showed that the vicinal 9,10-diol of 9,10-diaryl substituted phenanthrenes could undergo efficient reductive dehydration using the well-known Zn/H<sup>+</sup> system, which could be done in one step while also avoiding the pinacol rearrangement to the ketone.<sup>18</sup> They described the reaction as a process in which the vicinal diol first undergoes a typical pinacol rearrangement to the pinacolone intermediate in the presence of an acid, with a proposed reaction pathway shown in Scheme 4.6.<sup>18</sup> This intermediate is then reduced by Zn/H<sup>+</sup> and is rapidly converted to the product via a Wagner-Meerwein rearrangement.<sup>18</sup> They showed that the pinacolone was a key intermediate in this process by performing its reduction and also by obtaining the desired product in excellent yields. In addition, a strong acid and the presence of water were crucial for the reaction to proceed efficiently, with hydrochloric acid producing the highest yields.



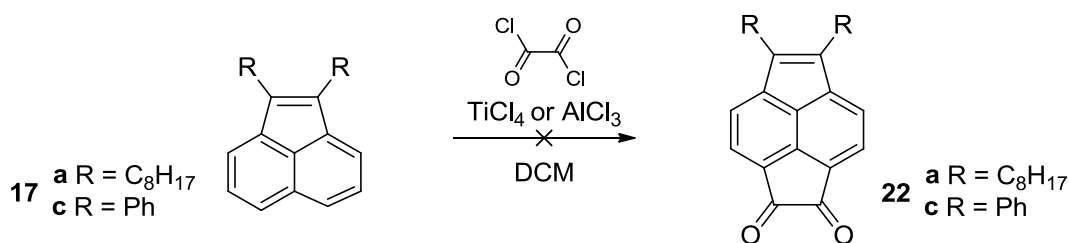
Scheme 4.6. Reductive dehydration of a vicinal phenanthrene diols with proposed routes and intermediates.<sup>18</sup>

These reaction conditions were applied to the vicinal acenaphthene diol systems presented here to investigate the occurrence of a pinacol rearrangement, which would suggest the acenaphthene systems undergo reductive dehydration via a similar mechanism as the phenanthrenes. To confirm that the byproduct produced from the sodium hypophosphite reductions was most likely the pinacol-rearranged ketone, a sample of the purified byproduct was subjected to the  $\text{Zn}/\text{H}^+$  reduction conditions where this byproduct was converted to 91% of the desired product with only 9% being the recovered byproduct. This fact led us to believe the byproduct produced in our reactions was indeed the pinacol-rearranged ketone and that the conditions developed by Müllen and coworkers would be successful for the acenaphthene systems.

Reactions with **20a** were then attempted using 10 equivalents of zinc granules, which were added in two portions of 5 equivalents each, with 4.8 equivalents of concentrated hydrochloric acid, which was also added in two portions of 2.4 equivalents each. Diol **20a** was added to glacial acetic acid and heated to near reflux with the addition of the zinc immediately followed by HCl. The reaction mixture was then allowed to heat at reflux for 30 minutes, at which point a second addition of Zn/HCl was used, followed by continued heating for approximately 24 hours. Upon workup, the concentrated residue from the reaction was purified via filtration through silica gel with hexanes as the eluent. The reaction produced an orange oil that was determined by GC-MS to contain 80% the desired **17a** and 20% of the rearranged ketone **21a**, in an overall reaction yield of approximately 70%. The reaction was attempted again using the same conditions but this time with 15 equivalents of zinc and 7.2 equivalents of hydrochloric acid, each added sequentially in three equal portions and in one hour intervals. Under these modified

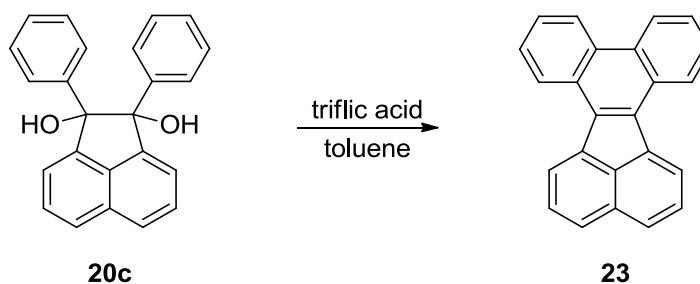
conditions, the reaction produced an orange oil, in a yield of 80%, that was determined to be 96% **17a** and 4% **21a**. Similar outcomes were found for **20b-d** using these reaction conditions, with overall reaction yields between 70-80% with conversions to **17b-d** greater than 95%.

Finally, the 1,2-disubstituted acenaphthylenes were subjected to Friedel-Crafts reactions to produce the dione intermediate necessary to generate extended fused-ring TPs. Two of the acenaphthylene analogs, **17a** and **17c**, were used in Friedel-Crafts acylations with oxalyl chloride and a titanium(IV) tetrachloride or aluminum(III) trichloride lewis acid, as shown below in Scheme 4.7. Acenaphthylene **17c** was used in a majority of these syntheses because it was the easiest analog to produce and because it was a solid, the easiest to work with as well. In all attempts to produce diones **22a** and **22c**, no product was observed with large amounts of unrecognizable byproducts present. Small amounts of the pinacol rearranged ketone were isolated but it was unclear if it was because the reaction conditions caused this rearrangement or if they were present in the starting materials. A variety of other reaction conditions should be screened to determine if a Friedel-Crafts acylation of these acenaphthylene systems is indeed possible, or if they promote side reactions that interfere with the synthesis of such diones.



Scheme 4.7. Friedel-Crafts acylation of 1,2-disubstituted acenaphthylenes.

Dehydrative cyclizations have been shown to occur with aryl pinacols in the presence of trifluoromethanesulfonic acid (triflic acid) as a general route for the production of substituted phenanthrenes.<sup>19,20</sup> This was an interesting avenue to pursue as it would allow for extended fused-ring systems with even greater conjugation, as well as provide a means to inhibit pinacol rearrangement. Obviously, the system presented in Scheme 4.8 would suffer from decreased solubility with such highly planar, rigid systems, but one could envision using alkylated phenyl functionalities that would incorporate solubilizing chains. The other issue that arises is the selectivity of the Friedel-Crafts acylation where the preference between the formations of the 6-membered rings, which are typically more favored, versus 5-membered rings would dictate whether or not this is a viable pathway.<sup>21</sup> One could envision incorporating bulky alky side chains on the phenanthrene portion of the compound to block the formation of the 6-membered ring, but this could have the unwanted consequence of inhibiting the dehydrative cyclization as well.



Scheme 4.8. Reductive dehydration of **20c** utilizing triflic acid.

The successful dehydrative cyclization of **20c** was accomplished using 15.1 equivalents of triflic acid in dry toluene, but fluorene **23** was generated in very low

yield (8%). X-ray quality crystals of **23** were grown from slow evaporation in chloroform to confirm the structure as its diminished solubility made it difficult to characterize by traditional means (Figure 4.5).

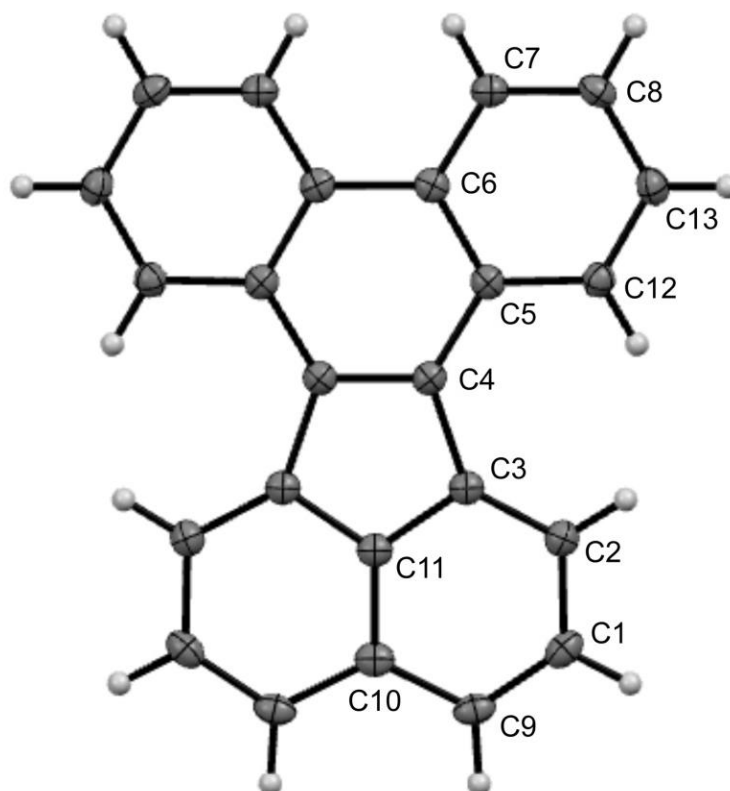


Figure 4.5. Thermal ellipsoid plot of Dibenzo[*j,l*]fluoranthene, **23** at the 50% probability level.

It was found that the major product of this reaction was ketone, **21c**, which is a result of the pinacol rearrangement, and attributed to approximately 80% of the recovered material. This could be an indication of the presence of water in the reaction as this would result in a weakened acid system, in which the acid strength of the reaction medium is required to have a  $H_o \geq -12$  in order to prevent the pinacol rearrangement.<sup>19,20</sup> Pure triflic



acid has been estimated to have a  $H_o = -14$ , so it is critical that the reaction be done under an inert atmosphere and with anhydrous reagents.<sup>22</sup> This reaction was only attempted once so further optimization is required for this avenue to be fruitful.

### 4.3. Conclusions

The work presented here describes the synthesis and characterization of a new extended fused-ring TP-based terthienyl, 3-octyl-8,10-bis(2-thienyl)acenaphtho[1,2-*b*]thieno[3,4-*e*]pyrazine, which contains a solubilizing chain attached to the central TP unit. In TP-based terthienyls, the introduction of solubilizing chains on the external thiophenes introduces complicating factors, such as sterics that cause decreased conjugation along the backbone because of torsional rotation about the interannular bonds, which would lead to undesirable consequences in materials prepared from these species. It was shown that the addition of solubilizing chains on the central TP unit would increase the solubility of these monomers while also still maintaining the desirable characteristics of their unfunctionalized counterparts. Therefore, the incorporation of alkyl chains on the central TP unit as a means to increase the solubility of these oligomers while maintaining their desirable optical and electronic properties is a promising approach to developing low band gap materials with enhanced solubility.

Also, methods have been developed towards the production of extended fused-ring diones via 1,2-dialkyl- and 1,2-diaryl-acenaphthylenes that can be used to develop TPs with even greater solubility in common organic solvents. Progress was made towards the production of four 1,2-disubstituted- acenaphthylene analogs with the successful synthesis of the alkyl substituted 1,2-bis(2-ethylhexy)- and 1,2-dioctyl-acenaphthylenes, as well as

the aryl substituted 1,2-diphenyl- and 1,2-di(4-octylphenyl)-acenaphthylenes. These acenaphthylenes provide a handle to incorporate multiple solubilizing chains, as well as a means to extend the conjugation of the monomer even further. These monomers could then be used to produce TP-based materials with very low band gaps, below 1.0 eV, that are also solution processable.

#### 4.4. Experimental

**General.** Unless noted, all materials were reagent grade and used without further purification. Chromatographic separations were performed using standard column chromatography methods with silica gel (230-400 mesh). All glassware was oven-dried, assembled hot, and cooled under a dry nitrogen stream before use. Transfer of liquids was carried out using standard syringe techniques and all reactions were performed under a dry nitrogen stream. Melting points were determined using a digital thermal couple with a 0.1 °C resolution. The <sup>1</sup>H NMR and <sup>13</sup>C NMR were completed on a 400 MHz spectrometer. All NMR data was referenced to the chloroform signal and peak multiplicity was reported as follows: s = singlet, d = doublet, t = triplet, q = quartet, p = pentet, dd = doublet of doublets, td = triplet of doublets, m = multiplet and br = broad. HRMS was performed in house.

**Materials.** 5-octylacenaphthylene-1,2-dione was prepared by Jon Nietfeld according to a previously published procedure.<sup>23</sup> 3',4'-diamino-2,2':5',2''-terthiophene was prepared according to previously published procedure.<sup>24</sup> Dry THF and toluene were obtained via distillation over sodium/benzophenone. CH<sub>2</sub>Cl<sub>2</sub> and CH<sub>3</sub>CN were dried over

CaH<sub>2</sub> and distilled prior to use. All other materials were reagent grade and used without further purification.

**1,2-Dibromoacenaphthylene (16).** The following is a modification of previously reported methods.<sup>25</sup> Acenaphthene (3.08 g, 20.0 mmol) and NBS (14.24 g, 80 mmol) were added to a flask under nitrogen atmosphere, which was then charged with CCl<sub>4</sub> (50 mL) and AIBN (0.328 g, 2 mmol). The reaction mixture was heated to reflux for 3 hours and then cooled to room temperature. Once cool, the succinimide was removed via filtration and the organic phase was quenched with aq. sodium thiosulfate (100 mL). The organic phase was then dried with MgSO<sub>4</sub>, filtered and concentrated. The crude product was recrystallized in ethanol to give 3.58-4.34 g of yellow-orange crystals (58-70%). <sup>1</sup>H NMR:  $\delta$  7.82 (d, *J* = 8.5 Hz, 2H), 7.63 (d, *J* = 8.5 Hz, 2H), 7.59 (t, *J* = 8.5 Hz, 2H); <sup>13</sup>C NMR:  $\delta$  137.3, 128.4, 128.1, 127.6, 126.9, 123.4, 121.2. <sup>1</sup>H NMR values agree with previously reported values.<sup>25</sup>

**1,2-Dihydroxy-1,2-dioctylacenaphthene (20a).** Magnesium metal shavings (2.17 g, 90 mmol) were oven dried and polished via mortar and pestle immediately prior to use. The magnesium and a flake of iodine were added to a flask fitted with an addition funnel under nitrogen atmosphere, which was then evacuated and backfilled with nitrogen 3 times and charged with THF (400 mL). To the addition funnel was added 1-bromooctane (17.38 g, 15.6 mL, 90 mmol) and THF (60 mL). A small portion of the octyl bromide/THF solution was added to the reaction mixture and allowed to stir at room temperature until activated (yellow color from iodine disappears). Once activated, the reaction mixture was cooled in a cool water bath, while the octyl bromide solution was added dropwise over a 2 hour period and then allowed to stir overnight. The acenaphthene quinone (5.47 g, 30

mmol) was added in 3 equal portions in 30 minute intervals and allowed to stir at room temperature overnight. The reaction was quenched with water (300 mL) and the THF was removed via rotary evaporation. The solid was filtered and washed with hexanes until the rinses were colorless. The solid was then dissolved in hot ethanol and filtered to remove unreacted quinone. The filtrate was then concentrated via rotary evaporation giving 3.80-4.15 g of an off white powder (30-33%).  $^1\text{H}$  NMR:  $\delta$  7.69 (d,  $J = 8.3, 6.8$  Hz, 2H), 7.53 (dd,  $J = 6.8$  Hz, 2H), 7.39 (d,  $J = 8$  Hz, 2H), 2.16 (s, 2H), 1.98 (td,  $J = 12.0, 4.8$  Hz, 2H), 1.61 (td,  $J = 12.0, 4.8$  Hz, 2H), 1.30 (m, 24H), 0.84 (t,  $J = 7.1$  Hz, 6H);  $^{13}\text{C}$  NMR:  $\delta$  145.1, 134.3, 130.8, 128.0, 124.4, 119.5, 87.8, 39.0, 32.0, 30.3, 29.7, 29.5, 23.9, 22.8, 14.3; HRMS  $m/z$  433.3088  $[\text{M} + \text{Na}]^+$  (calcd for  $\text{C}_{28}\text{H}_{42}\text{O}_2\text{Na}$  433.3077).

**1,2-Dihydroxy-1,2-diphenylacenaphthene (20c).** Bromobenzene (9.89 g, 63 mmol) was added to a flask under nitrogen atmosphere, which was then evacuated and backfilled with nitrogen 3 times and charged with THF (500 mL). The solution was then cooled to  $-78$  °C in a dry ice/acetone bath and the butyllithium (25.2 mL, 2.5 M in hexanes, 63 mmol) was added dropwise over a period of an hour. Once the addition of butyllithium was complete the reaction was allowed to stir at  $-78$  °C for 1 hour. The acenaphthene quinone (5.47 g, 30 mmol) was added in 3 equal portions in 30 minute intervals and allowed to slowly warm to room temperature and stir overnight. The reaction was quenched with water (300 mL) and the THF was removed via rotary evaporation. The solid was filtered and washed with hexanes until the rinses were colorless. The solid was then dissolved in hot ethanol and filtered to remove unreacted quinone. The filtrate was then concentrated via rotary evaporation giving 8.09 g of an off white powder (80%).  $^1\text{H}$  NMR:  $\delta$  7.90 (dd,  $J = 8.5, 0.8$  Hz, 2H), 7.65 (dd,  $J = 8.5, 7.0$  Hz, 2H), 7.36 (m, 8H), 7.24

(m, 4H), 2.14 (s, 2H);  $^{13}\text{C}$  NMR:  $\delta$  145.8, 141.0, 137.5, 131.3, 129.2, 128.3, 128.2, 127.9, 125.5, 122.0, 90.3.

**1,2-Dihydroxy-1,2-bis(4-octylphenyl)acenaphthene (20d).** The 1-bromo-4-octylbenzene (5.87 g, 21.8 mmol) was added to a flask fitted with an addition funnel under nitrogen atmosphere, which was then evacuated and backfilled with nitrogen 3 times and charged with THF (110 mL). The solution was then cooled to  $-78\text{ }^{\circ}\text{C}$  in a dry ice/acetone bath and the t-butyllithium (26.9 mL, 1.7 M in pentane, 45.8 mmol) was added to the addition funnel. The t-butyllithium was then added dropwise over a period of 1.5 hours and allowed to stir at  $-78\text{ }^{\circ}\text{C}$  for an additional 30 minutes. The acenaphthenequinone (1.89 g, 10.4 mmol) was added in 3 equal portions in 30 minute intervals and allowed to slowly warm to room temperature and stir overnight. The reaction was quenched with water (10 mL) and the THF was removed via rotary evaporation. The solid was filtered and washed with hexanes until the rinses were colorless. The product was an oil, so it was dissolved in DCM (100 mL) and washed with sat. aq.  $\text{NaHCO}_3$  (2 x 50 mL), brine (2 x 50 mL), dried with  $\text{MgSO}_4$ , filtered, and concentrated via rotary evaporation. The crude yellow oil was purified via column chromatography (gradient of 100% hexanes to 100% DCM). The purified product gave 5.47 g of a light yellow, very thick oil that solidifies into a white, hard waxy solid (93%).  $^1\text{H}$  NMR:  $\delta$  7.90 (dd,  $J = 8.5, 0.8\text{ Hz}$ , 2H), 7.64 (dd,  $J = 8.5, 7.0\text{ Hz}$ , 2H), 7.37 (dd,  $J = 8.5, 0.8\text{ Hz}$ , 2H), 7.14 (m, 8H), 2.61 (t,  $J = 8.0\text{ Hz}$ , 4H), 2.18 (s, 2H), 1.62 (p,  $J = 8.0\text{ Hz}$ , 4H), 1.31 (m, 20H), 0.89 (t,  $J = 8.0\text{ Hz}$ , 6H);  $^{13}\text{C}$  NMR:  $\delta$  146.0, 143.1, 138.3, 137.4, 131.2, 129.1, 128.3, 127.8, 127.3, 126.9, 125.3, 121.9, 90.3, 35.9, 32.1, 31.6, 29.7, 29.6, 29.5, 22.9, 14.3.

**General procedure for the reductive dehydration.** The diol (**20a-d**, 3 mmol) was added to a flask fitted with a condenser, charged with glacial acetic acid (40 mL), and heated to near reflux. Once warm, Zn granules (15 mmol, 3 x 5 mmol) were added and immediately followed by the addition of concentrated HCl (7.2 mmol, 3 x 2.4 mmol) and heated to reflux. The Zn/HCl combination was done in 3 equal portions done 0.5-1.0 hours apart and then allowed to stir at reflux for 24 hours. The reaction was then cooled to room temperature and poured into water (50 mL) and extracted with DCM (3 x 50 mL). The combined organics were washed with sat. aq. NaHCO<sub>3</sub> (3 x 50 mL), brine (3 x 50 mL), dried with MgSO<sub>4</sub>, filtered, and concentrated via rotary evaporation. Crude products were purified by column chromatography with hexanes as the eluent giving an orange oil.

**1,2-Dioctylacenaphthylene (17a).** Reaction produced 0.904 g (2.4 mmol) of an orange oil (80%). <sup>1</sup>H NMR:  $\delta$  7.67 (dd,  $J = 8.0, 0.9$  Hz, 2H), 7.50 (m, 4H), 2.72 (t,  $J = 7.8$  Hz, 4H), 1.68 (p,  $J = 7.6$  Hz, 4H), 1.43 (m, 4H), 1.31 (m, 16H), 0.89 (t,  $J = 7.6$  Hz, 6H); <sup>13</sup>C NMR:  $\delta$  141.4, 138.6, 128.8, 128.0, 127.6, 126.1, 121.0, 32.2, 31.2, 30.2, 29.8, 29.5, 26.1, 22.9, 14.3.

**1,2-Bis(2-ethylhexyl)acenaphthylene (17b).** Reaction produced 0.565 g (1.5 mmol) of an orange oil (50%). <sup>1</sup>H NMR:  $\delta$  7.68 (dd,  $J = 8.5, 1.2$  Hz, 2H), 7.52 (dd,  $J = 8.5, 1.2$  Hz, 2H), 7.48 (dd  $J = 8.5, 7.1$  Hz, 2H), 2.65 (m, 4H), 1.78 (m, 2H), 1.35 (m, 16H), 0.92 (m, 12H).

**1,2-Diphenylacenaphthylene (17c).** Reaction produced 0.639 g (2.1 mmol) of an orange-yellow powder (70%). <sup>1</sup>H NMR:  $\delta$  7.88 (dd,  $J = 8.5, 0.8$  Hz, 2H), 7.76 (dd,  $J = 8.5, 0.8$  Hz, 2H), 7.61 (dd  $J = 8.5, 7.1$  Hz, 2H), 7.46 (m, 4H), 7.38 (m, 4H), 7.32 (m, 2H); <sup>13</sup>C NMR:  $\delta$  140.2, 138.3, 135.5, 130.3, 128.7, 128.6, 128.4, 128.0, 127.5, 127.3, 124.2.

**1,2-Bis(4-octylphenyl)acenaphthylene (17d).** Reaction produced 0.465 g (0.880 mmol) of an orange oil (30%).  $^1\text{H}$  NMR:  $\delta$  7.85 (d,  $J$  = 8.5 Hz, 2H), 7.75 (d,  $J$  = 8.5 Hz, 2H), 7.59 (dd,  $J$  = 8.5, 7.1 Hz, 2H), 7.38 (d,  $J$  = 8.5 Hz, 4H), 7.18 (d,  $J$  = 8.5 Hz, 4H), 2.65 (t,  $J$  = 8.0 Hz, 4H), 1.67 (p,  $J$  = 7.2 Hz, 4H), 1.33 (m, 24H), 0.91 (t,  $J$  = 6.8 Hz, 6H);  $^{13}\text{C}$  NMR:  $\delta$  142.0, 140.5, 137.9, 132.8, 130.1, 128.6, 128.5, 128.3, 128.0, 127.2, 124.0, 36.0, 32.1, 31.6, 29.7, 29.6, 29.5, 22.9, 14.4

**Dibenzo[*j,l*]fluoranthene (23).** To a flask under a nitrogen atmosphere, **20c** (2.03 g, 6 mmol) and dry toluene (10 mL) was added. The suspension was cooled to 0 C in an ice bath and trifluoromethanesulfonic acid (13.57 g, 8 mL, 90.4 mmol) was added in one portion. The ice bath was removed and the mixture was stirred at room temperature for 24 hours. The resulting mixture was poured over 100 g of ice and extracted with toluene (3 x 50 mL). The combined organic layers were washed with water (3 x 100 mL), brine (3 x 100 mL), dried with  $\text{MgSO}_4$ , filtered, and concentrated via rotary evaporation. The solid was suspended in hexane and filtered, followed by washing with  $\text{Et}_2\text{O}$  until washes were colorless. The solid was dried on the filter giving 0.150 g (0.5 mmol) of fine, needle-like yellow crystals (8%).  $^1\text{H}$  NMR:  $\delta$  8.91 (dd,  $J$  = 8.0, 1.2 Hz, 2H), 8.79 (dd,  $J$  = 8.0, 1.2 Hz, 2H), 8.55 (d,  $J$  = 8.0 Hz, 2H), 7.89 (d,  $J$  = 8.0, 2H), 7.71 (m, 6H).

**1-Bromo-4-octylbenzene.** The 1,4-dibromobenzene (3.54 g, 15 mmol) was added to a flask fitted with an addition funnel under nitrogen atmosphere, which was then evacuated and backfilled with nitrogen 3 times and charged with THF (110 mL). The solution was then cooled to -78 °C in a dry ice/acetone bath and the *t*-butyllithium (18.5 mL, 1.7 M in pentane, 31.5 mmol) was added to the addition funnel. The *t*-butyllithium was then added dropwise over a period of 1 hour and allowed to stir at -78 °C for an

additional 30 minutes. The 1-bromooctane (3.19 g, 2.86 mL, 16.5 mmol) was added dropwise and allowed to stir at -78 °C for 2 hours. It was then quenched with water (50 mL) and the THF was removed via rotary evaporation. The oil residue was then dissolved in Et<sub>2</sub>O (150 mL), washed with brine (3 x 50 mL), dried with MgSO<sub>4</sub>, filtered and concentrated via rotary evaporation. The crude product was filtered through silica gel and washed with hexanes to give a clear oil that is a mixture of 1-bromooctane and product. The product ratio was determined by GC-MS (typically 65% product) and used without further purification. Purified 1-bromo-4-octylbenzene can be obtained via vacuum distillation. <sup>1</sup>H NMR: δ 7.39 (d, *J* = 8.5 Hz, 2H), 7.05 (d, *J* = 8.5 Hz, 2H), 2.55 (t, *J* = 8 Hz, 2H), 1.58 (p, *J* = 7.4 Hz, 2H), 1.29 (m, 10H), 0.89 (t, *J* = 7.2 Hz, 3H); <sup>13</sup>C NMR: δ 142.1, 131.4, 130.4, 119.4, 35.6, 32.1, 31.5, 29.6, 29.5, 29.4, 22.9, 14.3.

**3-Octyl-8,10-bis(2-thienyl)acenaphtho[1,2-*b*]thieno[3,4-*e*]pyrazine (24).** The 5-octylacenaphthylene-1,2-dione (0.120 g, 0.41 mmol) and 3',4'-diamino-2,2':5',2''-terthiophene (0.114 g, 0.41 mmol) were added to a flask fitted with a condenser under nitrogen atmosphere and charged with absolute ethanol (25 mL). The reaction mixture was then heated to reflux for 24 hours. It was then allowed to cool to room temperature and brought to dryness via rotary evaporation. The purple solid was then suspended in hexanes, filtered, and washed with hexanes until washing were colorless. It was purified by silica gel column chromatography (75:25, hexanes:chloroform) giving 0.135 g (0.32 mmol) of a purple solid (78%). <sup>1</sup>H NMR: δ 8.34 (d, *J* = 8.0 Hz, 1H), 8.26 (d, *J* = 8.0 Hz, 1H), 8.19 (d, *J* = 8.0 Hz, 1H), 7.81 (t, *J* = 8.0, 1H), 7.75 (d, *J* = 4.8 Hz, 2H), 7.61 (d, *J* = 8.0 Hz, 1H), 7.43 (d, *J* = 4.8 Hz, 2H), 7.16 (t, *J* = 4.8 Hz, 2H), 3.19 (t, *J* = 7.2 Hz, 2H),



1.83 (p,  $J = 7.2$  Hz, 2H), 1.47 (p,  $J = 7.2$  Hz, 2H), 1.34 (m, 8H), 0.89 (t,  $J = 7.2$  Hz, 3H); HRMS  $m/z$  1095.2727  $[M + Na]^+$  (calcd for  $C_{64}H_{56}N_4S_6Na$  1095.2721).

#### 4.5. Instrumentation

**UV-vis Spectroscopy.** UV-visible spectra were measured on a dual beam scanning spectrophotometer using samples prepared as dilute  $CH_3CN$  solutions in 1 cm quartz cuvettes.

**Electrochemistry.** Cyclic Voltammetry (CV) experiments were performed on a Bioanalytical Systems BAS 100B/W electrochemical analyzer. All measurements were completed using a step rate of 100 mV/s. The CVs were performed using a three-electrode cell consisting of platinum disc working electrode, pt wire counter-electrode, and a  $Ag/Ag^+$  reference electrode (0.1 M  $AgNO_3$ /0.1 M  $TBAPF_6$  in MeCN; 0.320 V vs. SCE) and internally standardized to ferrocene (51 mV vs  $Ag/Ag^+$ ).<sup>18</sup> Dilute solutions were prepared from dissolution in MeCN dried via distillation over  $CaH_2$ . The supporting electrolyte was 0.10 M tetrabutylammonium hexafluorophosphate ( $TBAPF_6$ ). Prior to each scan the solutions were sparged for 20 min with argon and blanketed with argon during the experiment.

#### 4.6. References

1. Roncali, J. *Chem. Rev.* **1997**, 97, 173.
2. Rasmussen, S. C.; Pomerantz, M. In *Handbook of Conducting Polymers*, 3rd ed.; Skotheim, T. A., Reynolds, J. R., Eds.; CRC Press: Boca Raton, FL, 2007; Vol. 1, Chapter 12.

3. Rasmussen, S. C.; Ogawa, K.; Rothstein, S. D. In *Handbook of Organic Electronics and Photonics*; Nalwa, H. S., Ed.; American Scientific: Stevenson Ranch, CA, 2008; Vol. 1, Chapter 1.
4. Roland, M. M.; Anderson, R. C. *J. Heterocyclic Chem.* **1977**, *14*, 541.
5. Pohmer, J.; Lakshmikantham, M. V.; Cava, M. P. *J. Org. Chem.* **1995**, *60*, 8283.
6. S. Tanaka and Y. Yamashita, *Synth. Met.* **1997**, *84*, 229.
7. Nietfeld, J. P.; Schwiderski, R.; Gonnella, T. P.; Rasmussen, S. C. *J. Org. Chem.* **2011**, *76*, 6383.
8. Mondal, R.; Miyaki, N.; Becerril, H. A.; Norton, J. E.; Parmer, J.; Mayer, A. C.; Tang, M. L.; Bredas, J.; McGehee, M. D.; Bao, Z. *Chem. Mater.* **2009**, *21*, 3618.
9. Čík, G.; Krajčovič, J.; Veis, P.; Végh, D.; Šeršen, F. *Synth. Met.* **2001**, *118*, 111.
10. Rasmussen, S. C.; Mulholland, M. E.; Schwiderski, R. L.; Larsen, C. A. *J. Heterocyclic Chem.* **2012**, *49*, 479.
11. Rasmussen, S. C.; Schwiderski, R. L.; Mulholland, M. E. *Chem. Commun.* **2011**, *47*, 11394.
12. Karsten, B. P.; Viani, L.; Gierschner, J.; Cornil, J.; Janssen, R. A. J. *J. Phys. Chem. A*, **2009**, *113*, 10343.
13. Wen, L.; Heth, C. L.; Rasmussen, S. C. *Phys. Chem. Chem. Phys.* **2014**, *16*, 7231.
14. Marvel, C. S.; Hager, F. D.; Coffman, D. D. *J. Am. Chem. Soc.* **1927**, *49*, 2323.
15. Siegel, D. *Lithium-Halogen Exchange*, **2008**, Harvard University, class presentation.
16. Miao, S.; Smith, M. D.; Bunz, U. H. F. *Org. Lett.* **2006**, *8*, 757.

17. Miao, S.; Appleton, A. L.; Berger, N.; Barlow, S.; Marder, S. R.; Hardcastle, K. I.; Bunz, U. H. F. *Chem. Eur. J.* **2009**, *15*, 4990.
18. He, B.; Tian, H.; Geng, Y.; Wang, F.; Müllen, K. *Org. Lett.* **2008**, *10*, 773.
19. Olah, G. A.; Klumpp, D. A.; Baek, D. N.; Neyer, G.; Wang, Q. *Org. Synth.* **2004**, *10*, 359.
20. Olah, G. A.; Klumpp, D. A.; Baek, D. N.; Neyer, G.; Wang, Q. *Org. Synth.* **1999**, *76*, 294.
21. Kürti, L.; Czakó, B. *Strategic Applications of Named Reactions in Organic Synthesis*; Elsevier Academic Press: Burlington, MA, 2005; pp 176-177.
22. Saito, S.; Saito, S.; Ohwada, T.; Shudo, K. *Chem. Pharm. Bull.* **1991**, *39*, 2718.
23. Rasmussen, S.C.; Nietfeld, J.P. Low band gap semiconducting polymers, their preparation and use in electronic devices. U.S. Patent 0065059, March 12, 2009.
24. Schwiderski, R. L.; Rasmussen, S. C. *J. Org. Chem.* **2013**, *78*, 5453-5462.
25. Brittelli, D. R.; Trost, B. M. *J. Org. Chem.* **1967**, *32*, 2620.

## CHAPTER 5. SUMMARY

### 5.1. Conclusion

The work presented in this thesis describes the synthesis and characterization of new classes of TP-based terthienyls containing various electron-donating and electron-withdrawing groups that have been prepared from terthienyls containing central 2,3-ditriflato- and 2,3-bis(bromomethyl)thieno[3,4-*b*]pyrazines. As was previously demonstrated for the thieno[3,4-*b*]pyrazine monomers, the ability to vary the functional groups allowed for a significant degree of tuning of the electronic and optical properties of these popular conjugated building blocks. The addition of the external thiophenes of the TP-based terthienyls reduced the effect of the functional groups on the modulation of the HOMO energies by approximately one-third when compared to that of the TP monomers. However, it was also demonstrated that the effect on the modulation of the corresponding LUMO energies was analogous to that found with the TP monomers. The tunability of these TP-based terthienyls is complementary to that of the TP monomers, with variations of the HOMO-LUMO gap energies of these materials of almost a full 1.0 eV. As such, the robust nature of TP-based materials, the tunability of these systems, and the degree to which they have been studied provides reason to believe that these materials are indeed a promising class of building blocks for the production of new low band gap materials.

As a means to showcase the versatility of these new TP-based terthienyls, beyond the simple dialkyl or diaryl analogs, the corresponding polymers were electrochemically produced to demonstrate the tunability of the optical and electronic properties of these polymeric materials, while also minimizing the loss of starting materials through unwanted

reactivity. Contrary to the trends commonly observed with polythiophene materials, the addition of electron-donating groups results in higher HOMO-LUMO energies in the monomers, as well as higher  $E_g$  values in the resulting polymers. Correspondingly, the use of electron withdrawing groups provides reduced HOMO-LUMO energies, as well as lower  $E_g$  values. The application of these tunable TP-based terthienyl building blocks towards the productions of conjugated materials appears to be a promising approach for controlling the corresponding frontier orbitals and band gaps of the final copolymeric materials.

The effect of the side chains on the HOMO is diminished in the application of TP-based terthienyls into copolymeric systems with fluorine. Even though the effect on the HOMO is weakened, the TP unit is still responsible for determining the HOMO energy level and is essentially the factor that determines the LUMO energy of the resultant material and as a result the material's band gap as well. The ability to modulate the optical and electronic properties of materials via TP functionalization would allow for the production of systems that are much more structurally and synthetically simple. Also, this would provide a means to accomplish the desired electronic and optical property modifications for various device applications, while holding the backbone structure constant. This would result in a reduction of the issues that arise from morphological changes of structurally different materials.

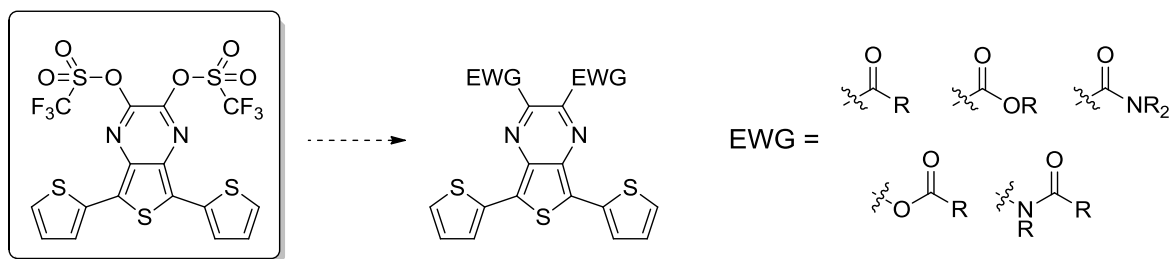
Also, the synthesis and characterization of a new extended fused-ring TP-based terthienyl, 3-octyl-8,10-bis(2-thienyl)acenaphtho[1,2-*b*]thieno[3,4-*e*]pyrazine, was accomplished. Contrary to most extended fused-ring TP analogs in the literature, this new TP-based terthienyl contains a solubilizing chain attached to the central TP unit. In TP-

based terthienyls, the introduction of solubilizing chains on the external thiophenes introduces complicating factors, such as steric interactions, that cause decreased conjugation along the backbone because of torsional rotation about the interannular bonds. Torsional rotation along the polymer backbone would lead to undesirable consequences in materials prepared from these species, most notably increased band gaps. It was shown that the addition of solubilizing chains on the central TP unit would increase the solubility of these monomers while also still maintaining the desirable characteristics of their unfunctionalized counterparts. Therefore, the incorporation of alkyl chains on the central TP unit as a means to increase the solubility of these oligomers while maintaining their desirable optical and electronic properties is a promising approach to developing TP-based low band gap materials with enhanced solubility.

Methods have been developed towards the production of extended fused-ring diones via 1,2-dialkyl- and 1,2-diaryl-acenaphthylenes that can be used to develop TPs with even greater solubility in common organic solvents. Progress was made towards the production of four 1,2-disubstituted-acenaphthylene analogs with the successful synthesis of the alkyl substituted 1,2-bis(2-ethylhexyl)- and 1,2-dioctyl-acenaphthylenes, as well as the aryl substituted 1,2-diphenyl- and 1,2-bis(4-octylphenyl)-acenaphthylenes. These acenaphthylenes provide a handle to incorporate multiple solubilizing chains, as well as a means to extend the conjugation of the monomer even further. These monomers could then be used to produce TP-based materials with very low band gaps, below 1.0 eV, that would have the realistic potential to also be solution processable.

## 5.2. Future Directions

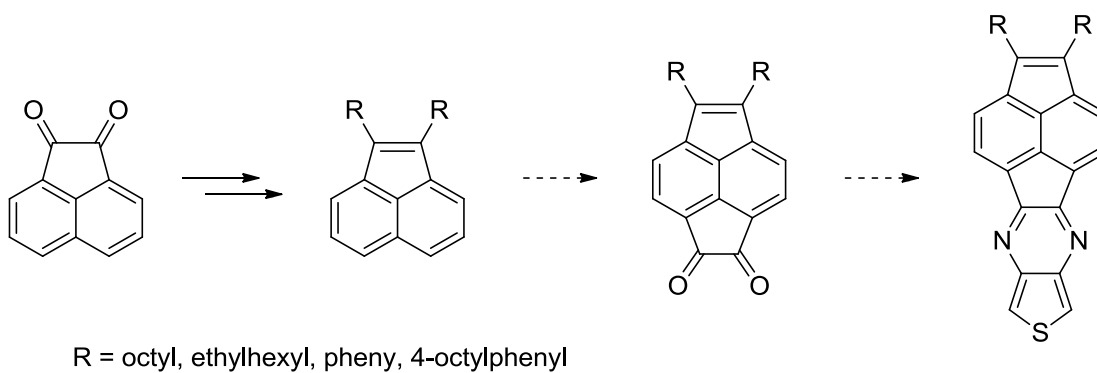
Although a variety of TP-based terthienyls incorporating both electron-donating and electron-withdrawing functionalities have been produced, there is still a desire to synthesize TP-based terthienyls with electron-withdrawing groups that also include solubilizing chains, with representative examples shown below in Scheme 5.1. This would allow for the production of polymers with desirable optical and electronic properties, such as a low band gap, while also imparting enough solubility to become solution processable. Oxidative electrochemical polymerizations of TP-based terthienyls would allow for the further study of the structure-function relationships that give rise to their desirable optical and electronic properties. Polymers of these materials could also be produced via traditional Suzuki or Stille cross-coupling reactions with various comonomers so their behavior in multicomponent copolymers could be understood.



Scheme 5.1. Example of TP-based terthienyls that incorporate electron-withdrawing groups with solubilizing chains.

Progress was also made towards the production of fused-ring acenes with solubilizing chains, but their corresponding diones and subsequent extended fused-ring TPs were not achieved (Scheme 5.2). Extended fused-ring TPs of this nature would allow

for the production of materials with very low band gaps, while still maintaining a high degree of solubility. Continuing the generation of solution processable, low band gap extended fused-ring TPs would expand the scope of TP-based materials and allow for their use in a wider range of device applications.



Scheme 5.2. Extended fused-ring TPs with solubilizing multiple chains.



## APPENDIX. CRYSTALLOGRAPHIC INFORMATION

### A.1. 5,7-Bis(2-thienyl)thieno[3,4-*b*]pyrazine-2,3-(1*H*,4*H*)-dione (Chapter 2, 10).

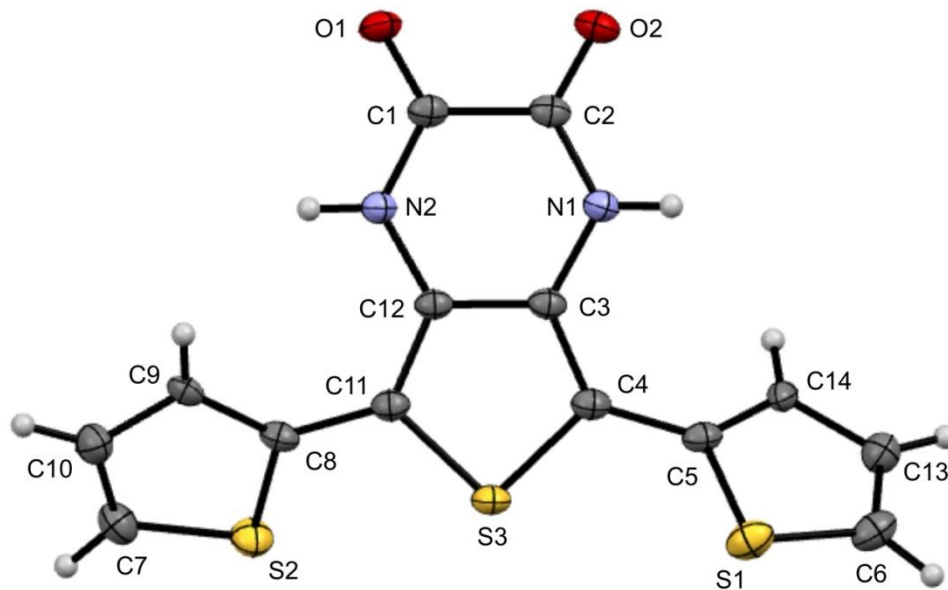


Figure A.1. Thermal ellipsoid plot of diamide **10** at the 50% probability level.

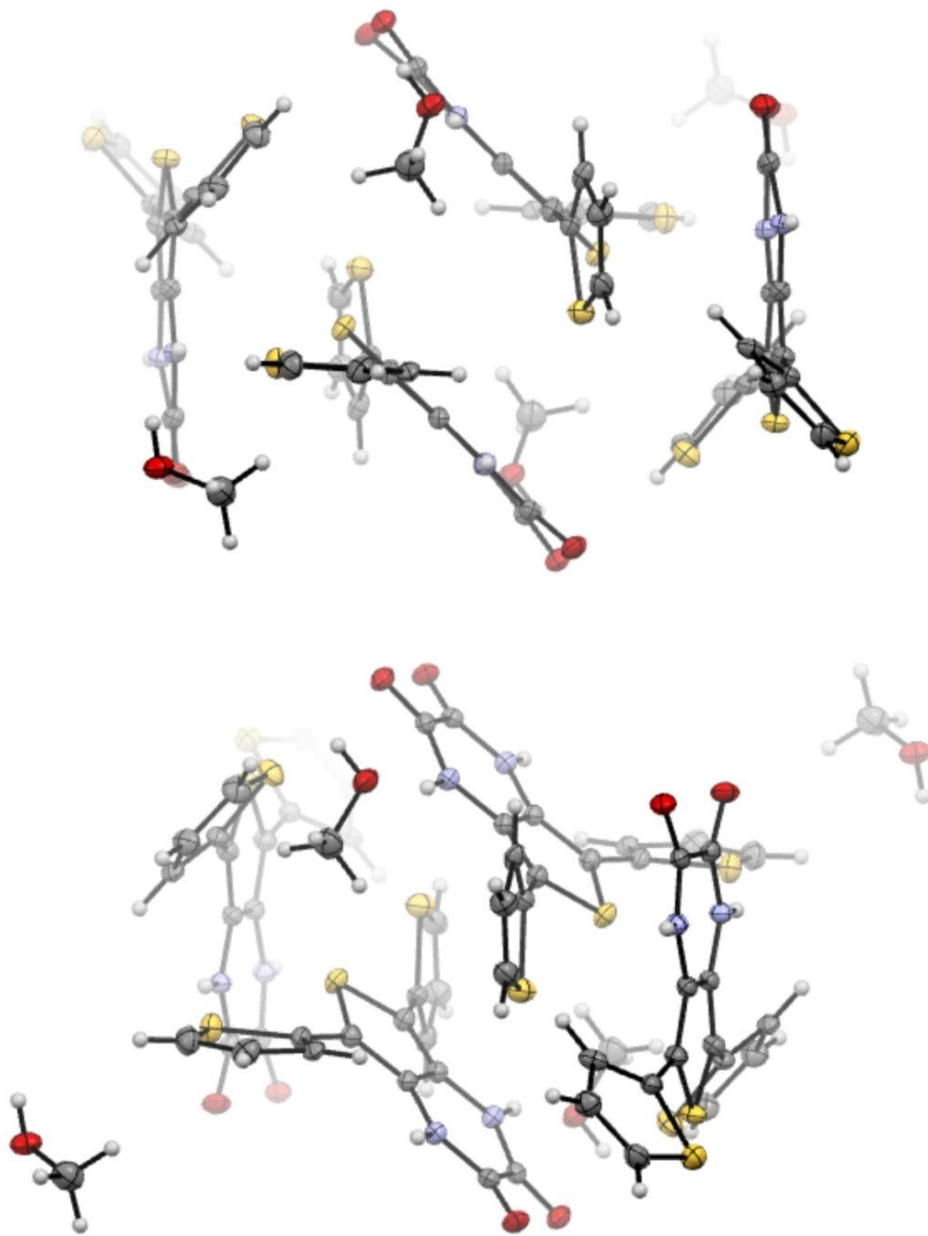


Figure A.2. Crystal packing of diamine **10** with depth cue for clarity.

Table A.1. Crystal data for diamide **10**.

---

Empirical formula	C <sub>14</sub> H <sub>8</sub> N <sub>2</sub> O <sub>2</sub> S <sub>3</sub> ,CH <sub>4</sub> O	
Formula weight	364.45	
Temperature	100(2) K	
Wavelength	0.71073 Å	
Crystal system	Monoclinic	
Space group	P2(1)/c	
Unit cell dimensions	a = 11.9818(3) Å b = 13.2018(3) Å c = 10.9061(3) Å	α = 90.00° β = 115.4920(10)° γ = 90.00°
Volume	1557.19(7) Å <sup>3</sup>	
Z	4	
Density (calculated)	1.555 g/cm <sup>-3</sup>	
Absorption coefficient	0.491 mm <sup>-1</sup>	
F(000)	752	
Crystal size	0.14 x 0.25 x 0.36 mm <sup>3</sup>	
Theta range for data collection	2.58 to 27.87°	
Reflections collected	20415	
Independent reflections [I>2σ]	3733 [R(int) = 0.0480]	
Reflections (I>2σ)	3316	
Goodness of fit on F <sup>2</sup>	1.056	
Final R indices [I>2σ]	R <sub>1</sub> = 0.0427, wR <sub>2</sub> = 0.1209	
R indices (all data)	R <sub>1</sub> = 0.0480, wR <sub>2</sub> = 0.1256	

---

Table A.2. Atomic coordinates and equivalent isotropic displacement parameters ( $\text{\AA}^2 \times 10^3$ ) for diamide **10**.

Atom	X	Y	Z
S3	0.56441(5)	0.18918(4)	1.01300(5)
S2	0.76292(5)	0.30937(4)	0.93112(6)
S1	0.39093(6)	0.12114(4)	1.17783(6)
O3	-0.05076(15)	-0.03571(13)	0.25820(16)
O2	0.14326(14)	0.03351(12)	0.49764(16)
O1	0.34511(15)	0.01830(12)	0.43930(15)
N2	0.46731(16)	0.08638(13)	0.64418(17)
N1	0.26966(16)	0.07608(13)	0.71436(17)
C9	0.76738(17)	0.14670(16)	0.7977(2)
C8	0.70159(19)	0.19335(15)	0.8634(2)
C7	0.8758(2)	0.29994(18)	0.8768(3)
C6	0.2578(2)	0.15532(17)	1.1864(2)
C5	0.33517(19)	0.15755(15)	1.0098(2)
C4	0.41235(19)	0.14808(15)	0.9375(2)
C3	0.38390(19)	0.11240(15)	0.8092(2)
C2	0.24685(19)	0.05434(15)	0.5847(2)
C15	-0.0493(3)	0.0283(2)	0.1535(3)
C14	0.21343(19)	0.19709(16)	0.9605(2)
C13	0.1728(2)	0.19280(17)	1.0674(2)
C12	0.48402(19)	0.11874(15)	0.7726(2)
C11	0.58908(19)	0.16077(15)	0.8720(2)
C10	0.8674(2)	0.21229(18)	0.8079(2)
C1	0.35776(19)	0.05163(15)	0.5491(2)

Table A.3. Bond lengths [ $\text{\AA}$ ] for diamide **10**.

<b>Bonds</b>	<b>Length</b>	<b>Bonds</b>	<b>Length</b>
S1 – C5	1.727(2)	C6 – H6	0.951
S1 – C6	1.699(3)	C6 – C13	1.352(3)
S2 – C7	1.699(3)	C7 – H7	0.950
S2 – C8	1.722(2)	C7 – C10	1.360(4)
S3 – C4	1.732(2)	C8 – C9	1.414(4)
S3 – C11	1.727(3)	C8 – C11	1.456(3)
O1 – C1	1.222(3)	C9 – H9	0.950
O2 – C2	1.226(2)	C9 – C10	1.443(3)
N1 – H1	0.880	C10 – H10	0.949
N1 – C2	1.351(3)	C11 – C12	1.376(2)
N1 – C3	1.398(2)	C13 – H13	0.950
N2 – H12	0.879	C13 – C14	1.445(4)
N2 – C1	1.355(2)	C14 – H14	0.950
N2 – C12	1.394(3)	O3 – H3	0.840
C1 – C2	1.537(4)	O3 – C15	1.427(4)
C3 – C4	1.373(3)	C15 – H15A	0.980
C3 – C12	1.420(4)	C15 – H15B	0.981
C4 – C5	1.456(4)	C15 – H15C	0.980
C5 – C14	1.419(3)		

Table A.4. Bond angles[°] for diamide **10**.

<b>Bonds</b>	<b>Angle</b>	<b>Bonds</b>	<b>Angle</b>
S3 – C4 – C3	109.9(2)	H15B – C15 – H15C	109.5
S3 – C4 – C5	119.9(2)	H15A – C15 – H15B	109.5
S3 – C11 – C8	120.7(2)	H15A – C15 – H15C	109.5
S3 – C11 – C12	109.9(2)	H13 – C13 – C14	122.9
S2 – C7 – H7	124	H12 – N2 – C1	118.5
S2 – C7 – C10	112.0(2)	H12 – N2 – C12	118.5
S2 – C8 – C9	112.1(2)	H1 – N1 – C2	118.7
S2 – C8 – C11	118.1(2)	H1 – N1 – C3	118.7
S1 – C5 – C4	120.3(2)	C9 – C8 – C11	129.6(2)
S1 – C5 – C14	111.7(2)	C9 – C10 – H10	122.8
S1 – C6 – H6	123.8	C8 – C9 – H9	125.6
S1 – C6 – C13	112.4(2)	C8 – C9 – C10	109.0(2)
O3 – C15 – H15A	109.5	C8 – C11 – C12	128.8(2)
O3 – C15 – H15B	109.4	C7 – S2 – C8	92.4(1)
O3 – C15 – H15C	109.5	C7 – C10 – C9	114.5(2)
O2 – C2 – N1	122.7(2)	C7 – C10 – H10	122.7
O2 – C2 – C1	119.8(2)	C6 – C13 – H13	122.8
O1 – C1 – N2	122.8(2)	C6 – C13 – C14	114.4(2)
O1 – C1 – C2	120.0(2)	C5 – S1 – C6	92.3(1)
N2 – C1 – C2	117.2(2)	C5 – C14 – C13	109.2(2)
N2 – C12 – C3	119.4(2)	C5 – C14 – H14	125.5
N2 – C12 – C11	127.0(2)	C4 – S3 – C11	93.3(1)
N1 – C2 – C1	117.5(2)	C4 – C3 – C12	113.4(2)
N1 – C3 – C4	127.3(2)	C4 – C5 – C14	128.0(2)
N1 – C3 – C12	119.3(2)	C3 – C4 – C5	130.1(2)
H9 – C9 – C10	125.5	C3 – C12 – C11	113.5(2)
H7 – C7 – C10	124	C2 – N1 – C3	122.7(2)
H6 – C6 – C13	123.8	C13 – C14 – H14	125.4
H3 – O3 – C15	109.4	C1 – N2 – C12	123.1(2)

A.2. 2,3-Bis(bromomethyl)-5,7-bis(2-thienyl)thieno[3,4-*b*]pyrazine (Chapter 2, 7).

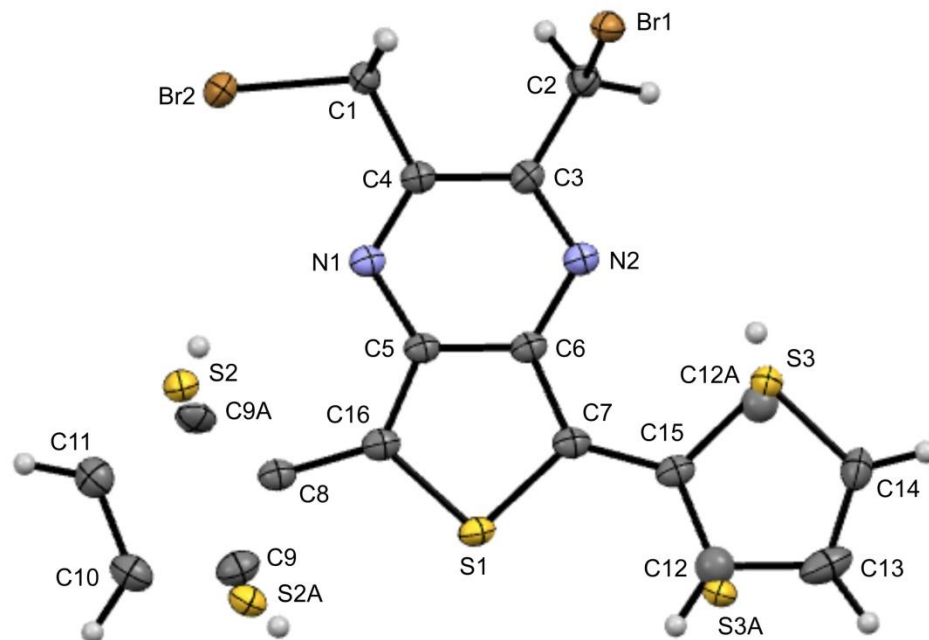


Figure A.3. Thermal ellipsoid plot of bromomethyl **7** at the 50% probability level.

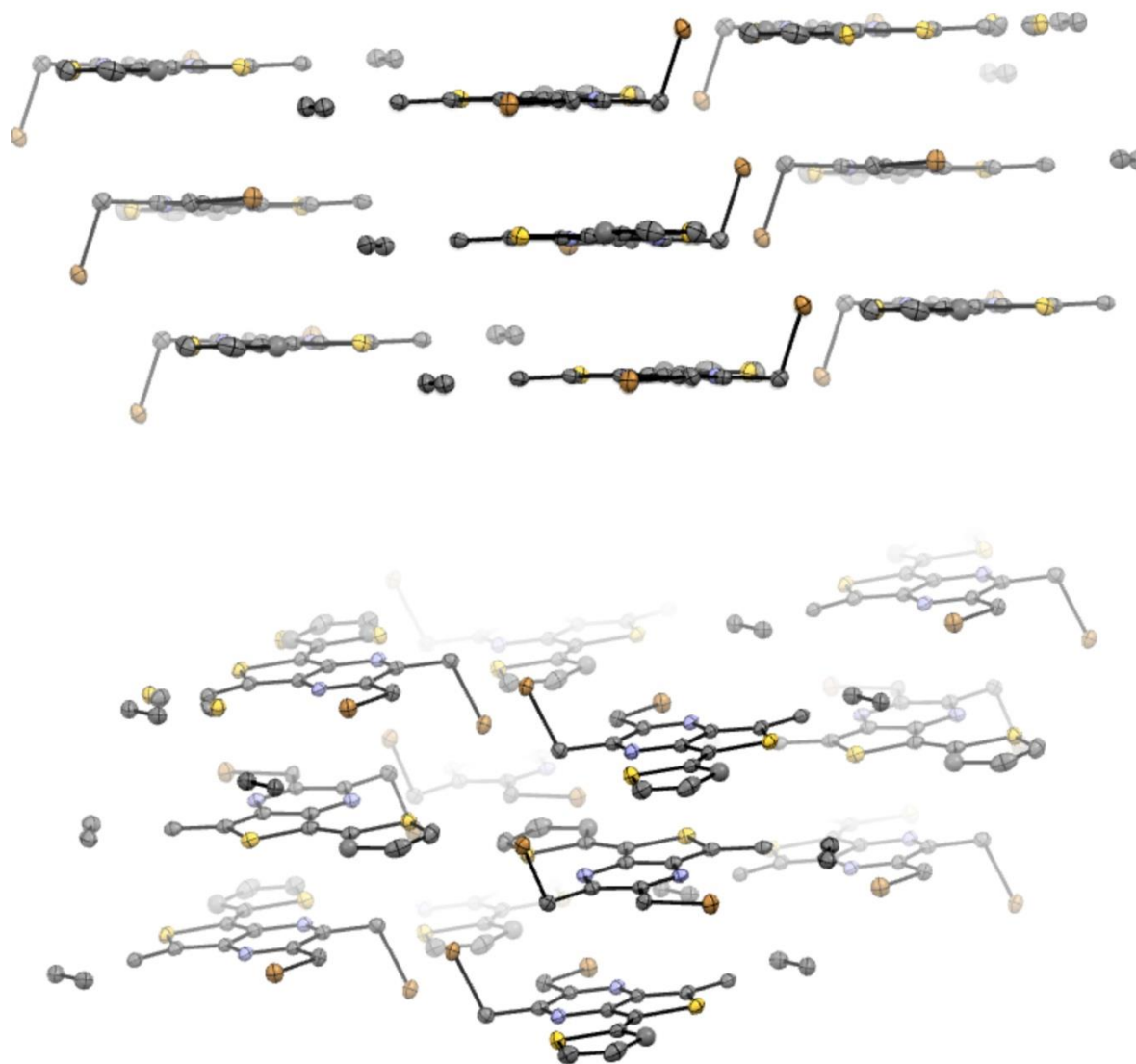


Figure A.4. Crystal packing of bromomethyl **7** with depth cue for clarity.



Table A.5. Crystal data for bromomethyl 7.

Empirical formula	$C_{16} H_{10} Br_2 N_2 S_3$	
Formula weight	486.26	
Temperature	100(2) K	
Wavelength	1.54178 Å	
Crystal system	Monoclinic	
Space group	P2(1)/c	
Unit cell dimensions	a = 16.1751 (4) Å b = 13.4330 (3) Å c = 7.5616 (2) Å	$\alpha = 90.00^\circ$ $\beta = 95.5760 (10)^\circ$ $\gamma = 90.00^\circ$
Volume	1635.21 (7) Å <sup>3</sup>	
Z	4	
Density (calculated)	1.975 g/cm <sup>-3</sup>	
Absorption coefficient	9.858 cm <sup>-1</sup>	
F(000)	952	
Crystal size	0.03 x 0.068 x 0.11 mm <sup>3</sup>	
Theta range for data collection	2.74 to 67.42°	
Reflections collected	13535	
Independent reflections [I>2s]	2841 [R(int) = 0.0201]	
Reflections (I>2s)	2785	
Goodness of fit onF2	1.240	
Final R indices [I>2s]	R <sub>1</sub> = 0.0191, wR <sub>2</sub> = 0.0535	
R indices (all data)	R <sub>1</sub> = 0.0201, wR <sub>2</sub> = 0.0666	

Table A.6. Atomic coordinates and equivalent isotropic displacement parameters ( $\text{\AA}^2 \times 10^3$ ) for bromomethyl **7**.

<b>Atom</b>	<b>X</b>	<b>Y</b>	<b>Z</b>
S3A	0.76035(18)	1.1288(3)	0.8329(4)
S3	0.88957(13)	1.00164(14)	0.9878(2)
S2A	0.4762(5)	0.8306(6)	0.5539(12)
S2	0.54285(7)	0.62590(8)	0.6331(2)
S1	0.64654(3)	0.92621(4)	0.72370(7)
N2	0.84050(11)	0.78871(14)	0.9489(2)
N1	0.71517(11)	0.65212(14)	0.8091(2)
C9A	0.5371(16)	0.6594(18)	0.615(4)
C9	0.4872(5)	0.7997(5)	0.5618(11)
C8	0.55653(14)	0.75489(17)	0.6364(3)
C7	0.74536(14)	0.92082(16)	0.8345(3)
C6	0.76703(14)	0.82122(16)	0.8628(3)
C5	0.70445(13)	0.75288(16)	0.7943(3)
C4	0.78572(14)	0.62199(16)	0.8903(3)
C3	0.84907(13)	0.69189(16)	0.9632(3)
C2	0.92864(14)	0.65654(17)	1.0580(3)
C16	0.63303(14)	0.79894(16)	0.7143(3)
C15	0.79263(14)	1.00920(16)	0.8813(3)
C14	0.89941(16)	1.12512(18)	0.9980(3)
C13	0.83472(18)	1.17736(19)	0.9216(4)
C12A	0.8736(11)	1.0129(15)	0.980(3)
C12	0.7694(5)	1.1062(5)	0.8496(10)
C11	0.44625(15)	0.63905(19)	0.5314(3)
C10	0.42145(15)	0.73459(19)	0.5000(3)
C1	0.80358(14)	0.51262(16)	0.9110(3)
Br2	0.711757(15)	0.428511(17)	0.82362(3)
Br1	1.007719(13)	0.625576(16)	0.88227(3)

Table A.7. Bond lengths [ $\text{\AA}$ ] for bromomethyl 7.

<b>Bonds</b>	<b>Length</b>	<b>Bonds</b>	<b>Length</b>
S3 – C15	1.695(3)	C2 – H2A	0.990
S3 – C14	1.667(3)	C2 – H2B	0.990
S3 – H12A	0.695	C15 – C12A	1.44(2)
S2 – H9A	0.582	C15 – S3A	1.718(4)
S1 – C7	1.733(2)	C14 – H14	0.949
S1 – C16	1.724(2)	C14 – C13	1.343(4)
N2 – C3	1.311(3)	C14 – C12A	1.57(2)
N2 – C6	1.370(3)	C13 – H13	0.950
N1 – C5	1.368(3)	C13 – S3A	1.472(4)
N1 – C4	1.306(3)	C12A – H12A	0.950
H12 – S3A	0.736	C12 – H12	0.949
C9A – H9A	0.950	C12 – C15	1.371(7)
C9 – H9	0.950	C12 – C13	1.488(8)
C8 – C16	1.445(3)	C11 – C10	1.359(4)
C8 – S2	1.747(3)	C11 – S2	1.682(3)
C8 – C9	1.347(8)	C11 – C9A	1.57(3)
C8 – C9A	1.33(2)	C11 – H11	0.950
C8 – S2A	1.719(8)	C10 – C9	1.420(8)
C7 – C15	1.438(3)	C10 – S2A	1.595(8)
C7 – C6	1.394(3)	C10 – H10	0.949
C5 – C6	1.426(3)	C1 – H1A	0.990
C5 – C16	1.396(3)	C1 – H1B	0.990
C4 – C1	1.503(3)	Br2 – C1	1.931(2)
C3 – C4	1.458(3)	Br1 – C2	1.976(2)
C3 – C2	1.489(3)		

Table A.8. Bond angles[°] for bromomethyl 7.

Bonds	Angle	Bonds	Angle
S3 – C15 – C12	111.4(3)	C7 – C15 – S3A	125.2(2)
S3 – C15 – C7	120.9(2)	C7 – C6 – C5	113.8(2)
S3 – C15 – C12A	6.0(8)	C6 – C5 – C16	113.6(2)
S3 – C15 – S3A	113.9(2)	C5 – N1 – C4	116.3(2)
S3 – C14 – H14	122.2	C5 – C16 – C8	129.4(2)
S3 – C14 – C13	115.7(2)	C4 – C3 – C2	121.3(2)
S3 – C14 – C12A	10.0(7)	C4 – C1 – H1A	108.8
S3 – H12A – C12A	11	C4 – C1 – H1B	108.8
S2A – C10 – H10	109.6	C3 – N2 – C6	115.8(2)
S2 – C8 – C9	109.8(4)	C3 – C4 – C1	118.0(2)
S2 – C8 – C9A	9(1)	C3 – C2 – H2A	109.9
S2 – C8 – S2A	119.4(3)	C3 – C2 – H2B	109.9
S2 – C11 – C9A	16(1)	C16 – C8 – S2	121.0(2)
S2 – C11 – H11	122.4	C16 – C8 – C9	129.3(4)
S2 – H9A – C9A	24	C16 – C8 – C9A	129(1)
S1 – C7 – C15	121.9(2)	C16 – C8 – S2A	119.5(3)
S1 – C7 – C6	108.7(2)	C15 – S3 – C14	92.4(1)
S1 – C16 – C5	109.0(2)	C15 – S3 – H12A	122.1
S1 – C16 – C8	121.5(2)	C15 – C12 – C13	111.9(5)
N2 – C3 – C4	122.9(2)	C15 – C7 – C6	129.4(2)
N2 – C3 – C2	115.8(2)	C15 – C12A – C14	107(1)
N2 – C6 – C7	124.9(2)	C15 – C12A – H12A	126
N2 – C6 – C5	121.3(2)	C15 – S3A – C13	95.7(2)
N1 – C5 – C6	121.8(2)	C14 – S3 – H12A	143.2
N1 – C5 – C16	124.6(2)	C14 – C13 – H13	125.8
N1 – C4 – C3	121.9(2)	C14 – C13 – S3A	122.2(3)
N1 – C4 – C1	120.1(2)	C14 – C12A – H12A	126
H2A – C2 – H2B	108.2	C13 – C14 – C12A	106.0(8)
H1A – C1 – H1B	107.7	C12A – C15 – S3A	108.6(8)
H14 – C14 – C13	122.1	C12 – H12 – S3A	19.6
H14 – C14 – C12A	131.8	C12 – C15 – C7	127.7(4)
H13 – C13 – S3A	112	C12 – C15 – C12A	106.1(9)
H12 – C12 – C15	124	C12 – C15 – S3A	2.8(3)
H12 – C12 – C13	124.1	C12 – C13 – C14	108.5(4)
H12 – S3A – C15	107	C12 – C13 – H13	125.7
H12 – S3A – C13	156.8	C12 – C13 – S3A	13.8(3)
C9A – C8 – S2A	111(1)	C11 – C10 – C9	109.0(4)
C9A – C11 – H11	139	C11 – C10 – S2A	124.9(4)

Table A.8. Bond angles[°] for bromomethyl **7** (continued).

<b>Bonds</b>	<b>Angle</b>	<b>Bonds</b>	<b>Angle</b>
C9 – C8 – C9A	102(1)	C11 – C10 – H10	125.5
C9 – C8 – S2A	9.8(4)	C11 – S2 – H9A	156.2
C9 – C10 – S2A	16.0(4)	C11 – C9A – H9A	123
C9 – C10 – H10	125.5	C10 – C11 – S2	115.1(2)
C8 – S2 – C11	90.8(1)	C10 – C11 – C9A	99(1)
C8 – S2 – H9A	108.1	C10 – C11 – H11	122.4
C8 – C9 – C10	115.4(6)	C10 – C9 – H9	122.3
C8 – C9 – H9	122.3	Br2 – C1 – C4	113.8(2)
C8 – C9A – C11	115(2)	Br2 – C1 – H1A	108.8
C8 – C9A – H9A	123	Br2 – C1 – H1B	108.8
C8 – S2A – C10	89.8(4)	Br1 – C2 – C3	109.2(2)
C7 – S1 – C16	94.9(1)	Br1 – C2 – H2A	109.8
C7 – C15 – C12A	126.1(8)	Br1 – C2 – H2B	109.8

A.3. 2,3-Dihexyloxy-5,7-bis(2-thienyl)thieno[3,4-*b*]pyrazine (Chapter 2, 14).

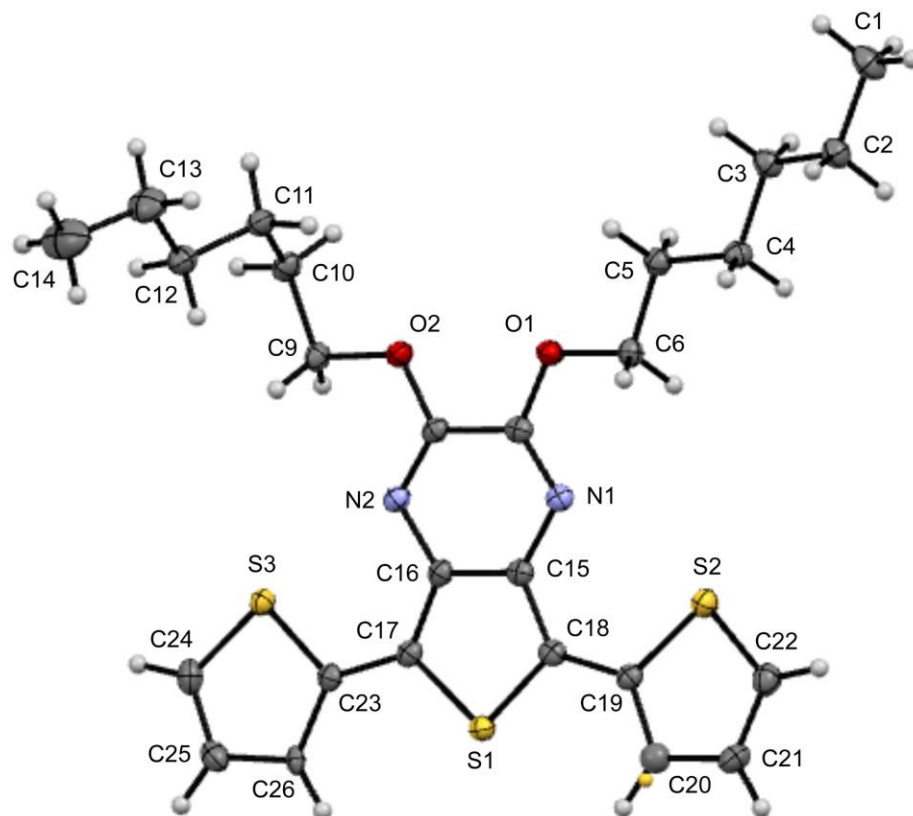


Figure A.5. Thermal ellipsoid plot of hexyloxy **14** at the 50% probability level.

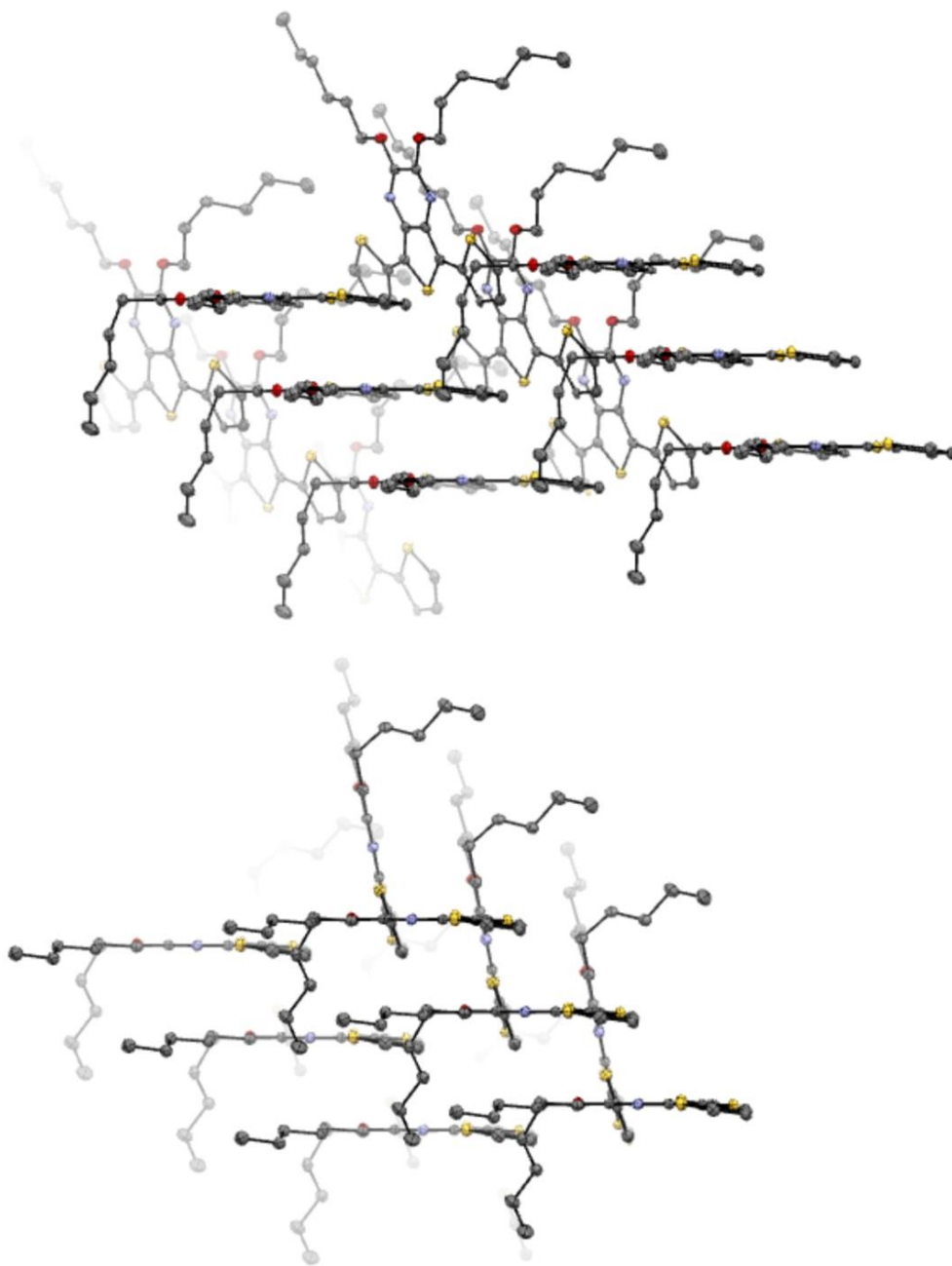


Figure A.6. Crystal packing of hexyloxy **14** with depth cue for clarity.

Table A.9. Crystal data for hexyloxy **14**.

---

Empirical formula	C <sub>26</sub> H <sub>32</sub> N <sub>2</sub> O <sub>2</sub> S <sub>3</sub>	
Formula weight	500.72	
Temperature	100(2) K	
Wavelength	1.54178 Å	
Crystal system	Monoclinic	
Space group	P2(1)/c	
Unit cell dimensions	a = 13.7138(4) Å b = 5.5493(2) Å c = 33.3099(10) Å	α = 90.00° β = 94.945(2)° γ = 90.00°
Volume	2525.51(14) Å <sup>3</sup>	
Z	4	
Density (calculated)	1.317 g/cm <sup>-3</sup>	
Absorption coefficient	2.886 mm <sup>-1</sup>	
F(000)	1064	
Crystal size	0.04 x 0.05 x 0.22 mm <sup>3</sup>	
Theta range for data collection	2.66 to 66.61°	
Reflections collected	16117	
Independent reflections [I>2σ]	4348 [R(int) = 0.0404]	
Reflections (I>2σ)	3724	
Goodness-of-fit on F <sup>2</sup>	1.039	
Final R indices [I>2σ]	R <sub>1</sub> = 0.0324, wR <sub>2</sub> = 0.0840	
R indices (all data)	R <sub>1</sub> = 0.0404, wR <sub>2</sub> = 0.0892	

---



Table A.10. Atomic coordinates and equivalent isotropic displacement parameters ( $\text{\AA}^2 \times 10^3$ ) for hexyloxy **14**.

Atom	X	Y	Z
S3	0.13825(3)	0.36568(8)	0.259190(14)
S2	0.67268(3)	0.36643(8)	0.363638(14)
S1	0.43629(3)	0.07722(7)	0.279777(12)
O2	0.24387(9)	0.9026(2)	0.36249(4)
O1	0.42431(9)	0.9143(2)	0.39635(4)
N2	0.27633(10)	0.5846(2)	0.32162(4)
N1	0.47222(10)	0.5914(2)	0.35973(4)
C9	0.14527(12)	0.8939(3)	0.34267(5)
C8	0.30528(12)	0.7386(3)	0.34916(5)
C7	0.40574(13)	0.7433(3)	0.36842(5)
C6	0.52229(13)	0.9098(3)	0.41688(5)
C5	0.53095(13)	1.1236(3)	0.44484(5)
C4	0.62829(13)	1.1209(3)	0.47088(5)
C3	0.64026(13)	1.3346(3)	0.49960(5)
C26	0.22195(12)	-0.0198(3)	0.23326(5)
C25	0.12335(14)	-0.0131(3)	0.21561(5)
C24	0.07144(13)	0.1810(3)	0.22667(5)
C23	0.24032(13)	0.1838(3)	0.25873(5)
C22	0.76944(14)	0.1761(3)	0.36331(6)
C21	0.75219(13)	-0.0169(3)	0.33882(5)
C20	0.65616(17)	-0.0124(5)	0.31926(8)
C2	0.72670(13)	1.3090(3)	0.53128(5)
C19	0.60231(12)	0.1876(3)	0.32975(5)
C18	0.50219(13)	0.2460(3)	0.31658(5)
C17	0.32989(12)	0.2429(3)	0.28278(5)
C16	0.34658(12)	0.4235(3)	0.31104(5)
C15	0.44316(13)	0.4256(3)	0.33010(5)
C14	-0.1183(2)	0.6226(4)	0.45434(9)
C13	-0.04478(17)	0.8235(4)	0.45014(6)
C12	-0.00634(14)	0.8344(3)	0.40878(6)
C11	0.06256(13)	1.0457(3)	0.40387(5)
C10	0.08649(13)	1.0908(3)	0.36057(5)
C1	0.74087(15)	1.5302(4)	0.55817(6)

Table A.11. Bond lengths [ $\text{\AA}$ ] for hexyloxy **14**.

<b>Bonds</b>	<b>Length</b>	<b>Bonds</b>	<b>Length</b>
S1 – C17	1.735(2)	C6 – H6B	0.991
S1 – C18	1.734(2)	C7 – C8	1.469(2)
S2 – C19	1.733(2)	C9 – H9A	0.99
S2 – C22	1.697(2)	C9 – H9B	0.991
C20 – H20	0.951	C9 – C10	1.511(2)
C20 – C19	1.394(3)	C10 – H10A	0.989
C20 – C21	1.418(3)	C10 – H10B	0.99
S3 – C23	1.727(2)	C10 – C11	1.527(2)
S3 – C24	1.701(2)	C11 – H11A	0.989
O1 – C6	1.454(2)	C11 – H11B	0.989
O1 – C7	1.338(2)	C11 – C12	1.524(2)
O2 – C8	1.341(2)	C12 – H12A	0.99
O2 – C9	1.454(2)	C12 – H12B	0.989
N1 – C7	1.293(2)	C12 – C13	1.518(3)
N1 – C15	1.383(2)	C13 – H13A	0.991
N2 – C8	1.291(2)	C13 – H13B	0.99
N2 – C16	1.382(2)	C13 – C14	1.518(3)
C1 – H1A	0.98	C14 – H14A	0.98
C1 – H1B	0.981	C14 – H14B	0.981
C1 – H1C	0.98	C14 – H14C	0.98
C1 – C2	1.522(3)	C15 – C16	1.419(2)
C2 – H2A	0.99	C15 – C18	1.384(2)
C2 – H2B	0.99	C16 – C17	1.380(2)
C2 – C3	1.524(2)	C17 – C23	1.445(2)
C3 – H3A	0.99	C18 – C19	1.442(2)
C3 – H3B	0.989	C21 – H21	0.95
C3 – C4	1.524(2)	C21 – C22	1.355(2)
C4 – H4A	0.989	C22 – H22	0.949
C4 – H4B	0.99	C23 – C26	1.422(2)
C4 – C5	1.528(2)	C24 – H24	0.95
C5 – H5A	0.989	C24 – C25	1.359(2)
C5 – H5B	0.99	C25 – H25	0.95
C5 – C6	1.507(2)	C25 – C26	1.428(2)
C6 – H6A	0.989	C26 – H26	0.95

Table A.12. Bond angles [°] for hexyloxy **14**.

<b>Bonds</b>	<b>Angle</b>	<b>Bonds</b>	<b>Angle</b>
S3 – C23 – C17	120.9(1)	H12B – C12 – C13	108.8
S3 – C23 – C26	111.6(1)	H12A – C12 – H12B	107.8
S3 – C24 – H24	123.7	H12A – C12 – C13	108.9
S3 – C24 – C25	112.6(1)	H11B – C11 – C12	108.7
S2 – C19 – C20	110.0(1)	H11A – C11 – H11B	107.7
S2 – C19 – C18	122.1(1)	H11A – C11 – C12	108.6
S2 – C22 – C21	113.6(1)	H10B – C10 – C11	108.5
S2 – C22 – H22	123.2	H10A – C10 – H10B	107.6
S1 – C17 – C16	109.5(1)	H10A – C10 – C11	108.5
S1 – C17 – C23	121.8(1)	C9 – C10 – H10A	108.6
S1 – C18 – C15	109.6(1)	C9 – C10 – H10B	108.6
S1 – C18 – C19	121.2(1)	C9 – C10 – C11	114.8(1)
O2 – C8 – N2	121.4(1)	C8 – N2 – C16	115.5(1)
O2 – C8 – C7	115.8(1)	C8 – O2 – C9	114.4(1)
O2 – C9 – H9A	110.2	C7 – N1 – C15	115.4(1)
O2 – C9 – H9B	110.2	C6 – O1 – C7	115.3(1)
O2 – C9 – C10	107.7(1)	C5 – C6 – H6A	110.3
O1 – C6 – C5	107.3(1)	C5 – C6 – H6B	110.2
O1 – C6 – H6A	110.3	C4 – C5 – H5A	109.4
O1 – C6 – H6B	110.2	C4 – C5 – H5B	109.4
O1 – C7 – N1	121.5(2)	C4 – C5 – C6	111.2(1)
O1 – C7 – C8	115.6(1)	C3 – C4 – H4A	109.1
N2 – C16 – C15	121.7(1)	C3 – C4 – H4B	109
N2 – C16 – C17	124.4(1)	C3 – C4 – C5	113.0(1)
N2 – C8 – C7	122.8(1)	C25 – C26 – H26	125.2
N1 – C15 – C16	121.7(1)	C24 – C25 – H25	123
N1 – C15 – C18	124.8(2)	C24 – C25 – C26	114.1(2)
N1 – C7 – C8	122.9(2)	C23 – C26 – C25	109.7(1)
H9B – C9 – C10	110.2	C23 – C26 – H26	125.1
H9A – C9 – H9B	108.4	C23 – S3 – C24	91.99(8)
H9A – C9 – C10	110.2	C21 – C22 – H22	123.2
H6A – C6 – H6B	108.6	C20 – C19 – C18	127.9(2)
H5B – C5 – C6	109.4	C20 – C21 – H21	124.2
H5A – C5 – H5B	108	C20 – C21 – C22	111.7(2)
H5A – C5 – C6	109.4	C2 – C3 – H3A	108.8
H4B – C4 – C5	109	C2 – C3 – H3B	108.9
H4A – C4 – H4B	107.8	C2 – C3 – C4	113.4(1)
H4A – C4 – C5	108.9	C19 – C20 – C21	112.9(2)

Table A.12. Bond angles [°] for hexyloxy **14** (continued).

<b>Bonds</b>	<b>Angle</b>	<b>Bonds</b>	<b>Angle</b>
H3B – C3 – C4	108.9	C19 – S2 – C22	91.79(9)
H3A – C3 – H3B	107.8	C17 – C23 – C26	127.5(2)
H3A – C3 – C4	108.9	C17 – S1 – C18	93.59(8)
H2B – C2 – C3	109.1	C16 – C15 – C18	113.5(2)
H2A – C2 – H2B	107.8	C16 – C17 – C23	128.7(2)
H2A – C2 – C3	109	C15 – C16 – C17	113.9(1)
H25 – C25 – C26	122.9	C15 – C18 – C19	129.2(2)
H24 – C24 – C25	123.8	C13 – C14 – H14A	109.4
H21 – C21 – C22	124.1	C13 – C14 – H14B	109.5
H20 – C20 – C19	123.5	C13 – C14 – H14C	109.4
H20 – C20 – C21	123.6	C12 – C13 – H13A	108.9
H1C – C1 – C2	109.5	C12 – C13 – H13B	108.9
H1B – C1 – H1C	109.4	C12 – C13 – C14	113.5(2)
H1B – C1 – C2	109.5	C11 – C12 – H12A	108.9
H1A – C1 – H1B	109.5	C11 – C12 – H12B	109
H1A – C1 – H1C	109.4	C11 – C12 – C13	113.3(2)
H1A – C1 – C2	109.5	C10 – C11 – H11A	108.6
H14B – C14 – H14C	109.5	C10 – C11 – H11B	108.6
H14A – C14 – H14B	109.6	C10 – C11 – C12	114.4(1)
H14A – C14 – H14C	109.4	C1 – C2 – H2A	109.1
H13B – C13 – C14	108.9	C1 – C2 – H2B	109.1
H13A – C13 – H13B	107.6	C1 – C2 – C3	112.6(1)
H13A – C13 – C14	108.9		

A.4. Acenaphtho[1,2-*b*]thieno[3,4-*e*]pyrazine (Chapter 4, 3a).

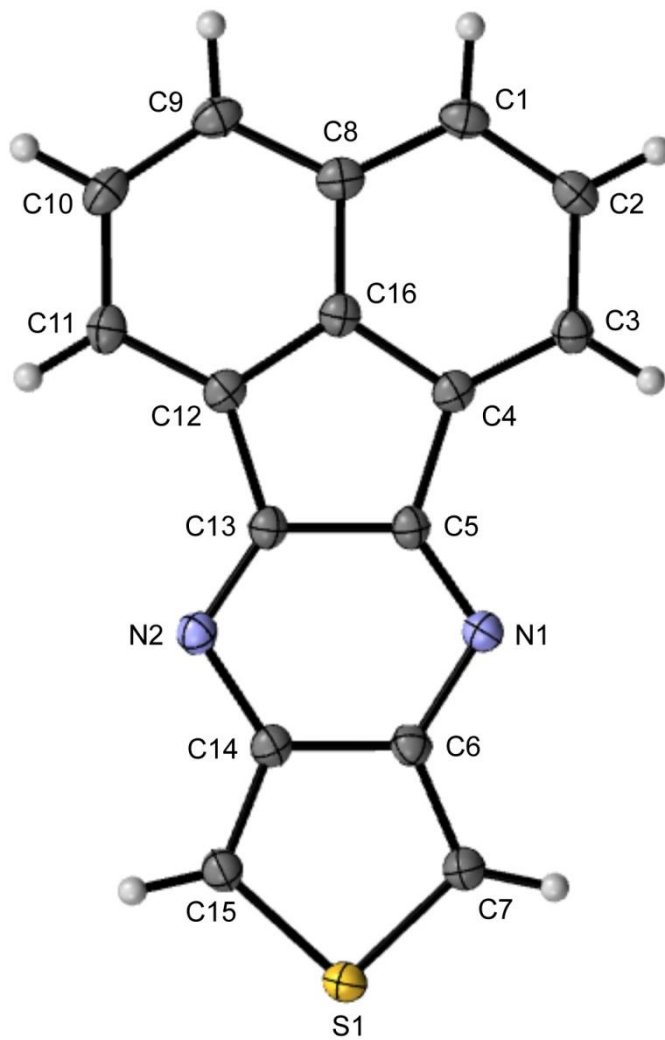


Figure A.7. Thermal ellipsoid plot of TP **3a** at the 50% probability level.

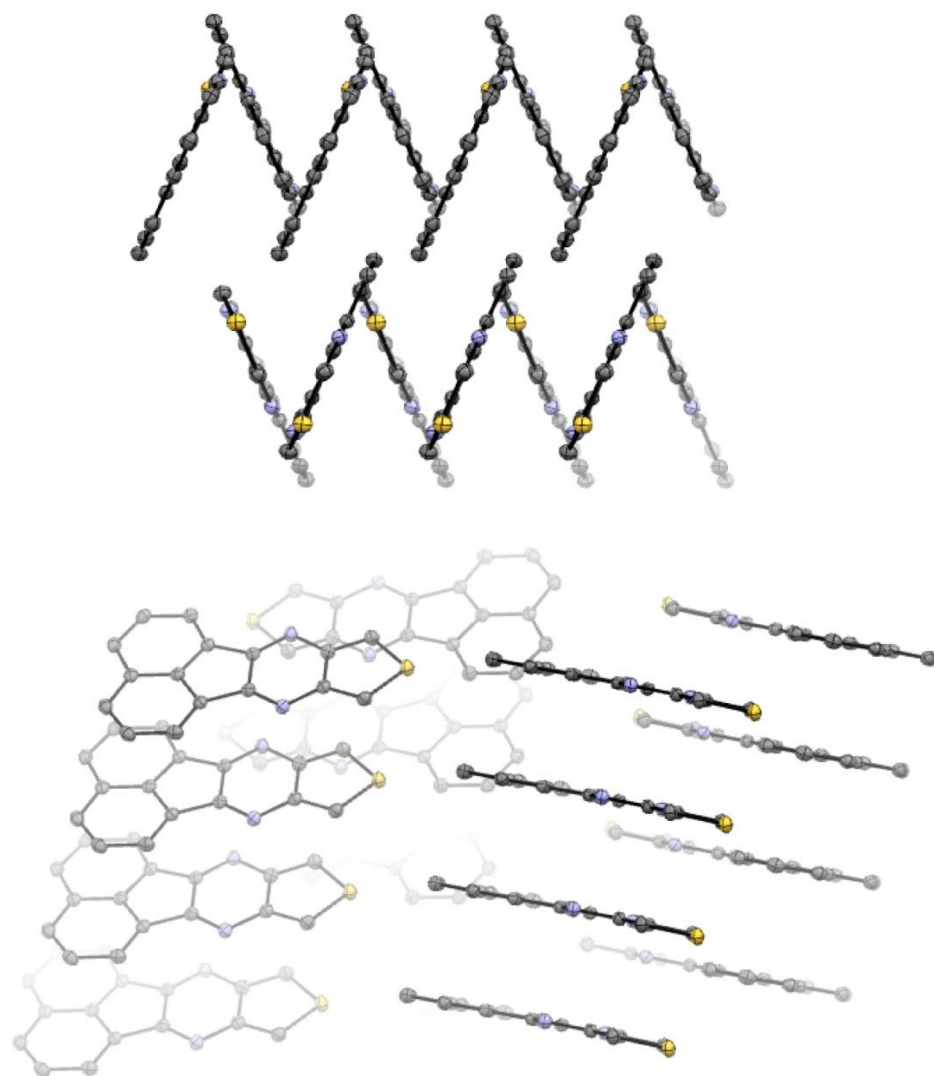


Figure A.8. Crystal packing of TP **3a** with depth cue for clarity.

Table A.13. Crystal data for TP **3a**.

Empirical formula	C <sub>16</sub> H <sub>8</sub> N <sub>2</sub> S	
Formula weight	260.30	
Temperature	100(2) K	
Wavelength	1.54178 Å	
Crystal system	Monoclinic	
Space group	P2(1)/c	
Unit cell dimensions	a = 3.8298(2) Å b = 12.6432(7) Å c = 23.0950(14) Å	α = 90.00° β = 92.939(3)° γ = 90.00°
Volume	1116.81(11) Å <sup>3</sup>	
Z	4	
Density (calculated)	1.548 g/cm <sup>-3</sup>	
Absorption coefficient	2.421 mm <sup>-1</sup>	
F(000)	536	
Crystal size	0.03 x 0.12 x 0.30 mm <sup>3</sup>	
Theta range for data collection	3.83 to 66.99°	
Reflections collected	8480	
Independent reflections [I>2σ]	1937 [R(int) = 0.0337]	
Reflections (I>2σ)	1879	
Goodness of fit on F <sup>2</sup>	1.168	
Final R indices [I>2σ]	R <sub>1</sub> = 0.0337, wR <sub>2</sub> = 0.0986	
R indices (all data)	R <sub>1</sub> = 0.0361, wR <sub>2</sub> = 0.1112	

Table A.14. Atomic coordinates and equivalent isotropic displacement parameters ( $\text{\AA}^2 \times 10^3$ ) for TP 3a.

<b>Atom</b>	<b>X</b>	<b>Y</b>	<b>Z</b>
S1	0.20815(11)	0.64895(3)	1.133351(17)
N2	0.3114(4)	0.62765(12)	0.96744(6)
N1	0.5798(4)	0.83022(12)	1.01490(6)
C9	0.7089(4)	0.74892(14)	0.76239(8)
C8	0.7782(4)	0.82454(15)	0.80699(8)
C7	0.3912(5)	0.76130(14)	1.10746(8)
C6	0.4304(4)	0.75328(14)	1.04870(7)
C5	0.5916(4)	0.80207(13)	0.96050(7)
C4	0.7318(4)	0.86161(14)	0.91205(8)
C3	0.8838(4)	0.95915(14)	0.90611(8)
C2	0.9818(5)	0.98931(14)	0.85018(8)
C16	0.6812(4)	0.79590(14)	0.86246(7)
C15	0.1688(5)	0.58923(14)	1.06732(7)
C14	0.2996(5)	0.65403(14)	1.02560(8)
C13	0.4582(4)	0.70059(13)	0.93709(7)
C12	0.5193(4)	0.69870(14)	0.87493(7)
C11	0.4545(5)	0.62674(15)	0.83103(7)
C10	0.5516(5)	0.65395(14)	0.77454(8)
C1	0.9346(4)	0.92574(15)	0.80202(8)



Table A.15. Bond lengths [ $\text{\AA}$ ] for TP 3a.

<b>Bonds</b>	<b>Length</b>	<b>Bonds</b>	<b>Length</b>
S1 – C7	1.706(2)	C3 – H3	0.951
S1 – C15	1.701(2)	C3 – C4	1.374(2)
N2 – C13	1.303(2)	C2 – H2	0.950
N2 – C14	1.387(2)	C2 – C3	1.416(3)
N1 – C5	1.309(2)	C15 – H15	0.951
N1 – C6	1.389(2)	C14 – C15	1.378(3)
C9 – H9	0.949	C12 – C13	1.467(2)
C9 – H10	1.379(3)	C12 – C16	1.413(2)
C8 – C9	1.420(3)	C11 – H11	0.950
C8 – C16	1.400(2)	C11 – C12	1.375(2)
C7 – H7	0.950	C10 – H10	0.950
C6 – C7	1.377(2)	C10 – C11	1.417(3)
C6 – C14	1.443(2)	C1 – H1	0.950
C5 – C13	1.473(2)	C1 – C2	1.377(3)
C4 – C5	1.473(2)	C1 – C8	1.420(3)
C4 – C16	1.420(2)		

Table A.16. Bond angles[°] for TP 3a.

<b>Bonds</b>	<b>Angle</b>	<b>Bonds</b>	<b>Angle</b>
S1 – C7 – C6	110.6(1)	C7 – C6 – C14	112.0(2)
S1 – C7 – H7	124.7	C6 – C7 – H7	124.7
S1 – C15 – C14	110.1(1)	C6 – C14 – C15	113.0(2)
S1 – C15 – H15	125	C5 – N1 – C6	112.6(1)
N2 – C13 – C5	124.7(1)	C5 – N1 – C6	105.9(1)
N2 – C13 – C12	127.6(2)	C5 – C13 – C12	107.7(1)
N2 – C14 – C6	122.6(2)	C4 – C5 – C13	107.4(1)
N2 – C14 – C15	124.4(2)	C4 – C16 – C8	123.7(2)
N1 – C5 – C4	128.5(2)	C4 – C16 – C12	112.8(1)
N1 – C5 – C13	124.1(1)	C3 – C4 – C5	135.1(2)
N1 – C6 – C7	124.8(2)	C3 – C4 – C16	119.1(2)
N1 – C6 – C14	123.1(2)	C2 – C3 – H3	121.1
H9 – C9 – C10	119.8	C2 – C3 – C4	117.8(2)
H3 – C3 – C4	121.1	C2 – C1 – C8	120.0(2)
H2 – C2 – C3	118.4	C14 – C15 – H15	124.9
H11 – C11 – C12	120.9	C13 – N2 – C14	112.8(1)
H10 – C10 – C11	118.8	C13 – C12 – C16	106.2(1)
H1 – C1 – C8	120	C11 – C12 – C13	134.5(2)
H1 – C1 – C2	120	C11 – C12 – C16	119.3(2)
C9 – C8 – C16	116.2(2)	C10 – C11 – H11	121
C9 – C10 – H10	118.8	C10 – C11 – C12	118.2(2)
C9 – C10 – C11	122.5(2)	C1 – C2 – H2	118.3
C8 – C9 – H9	119.8	C1 – C2 – C3	123.4(2)
C8 – C9 – C10	120.4(2)	C1 – C8 – C9	127.7(2)
C8 – C16 – C12	123.5(2)	C1 – C8 – C16	116.1(2)
C7 – S1 – C15	94.27(9)		

A.5. 1,2-Dibromoacenaphthylene (Chapter 4, 16).

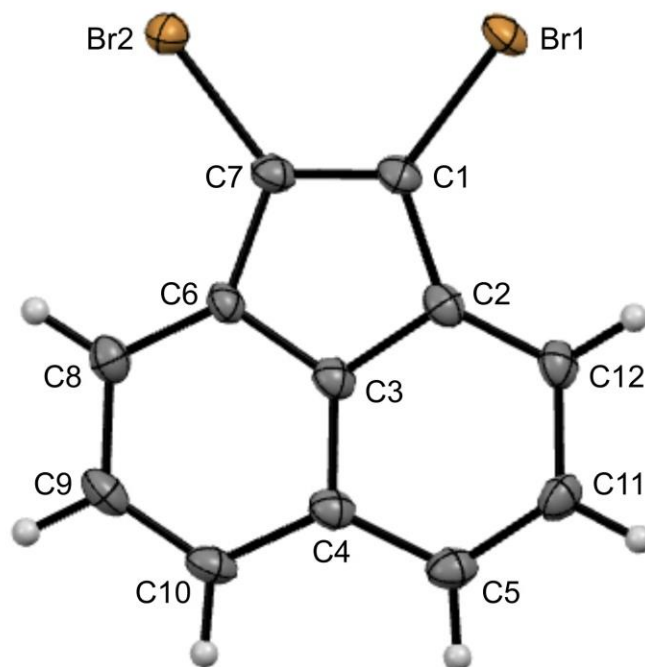


Figure A.9. Thermal ellipsoid plot of **16** at the 50% probability level.

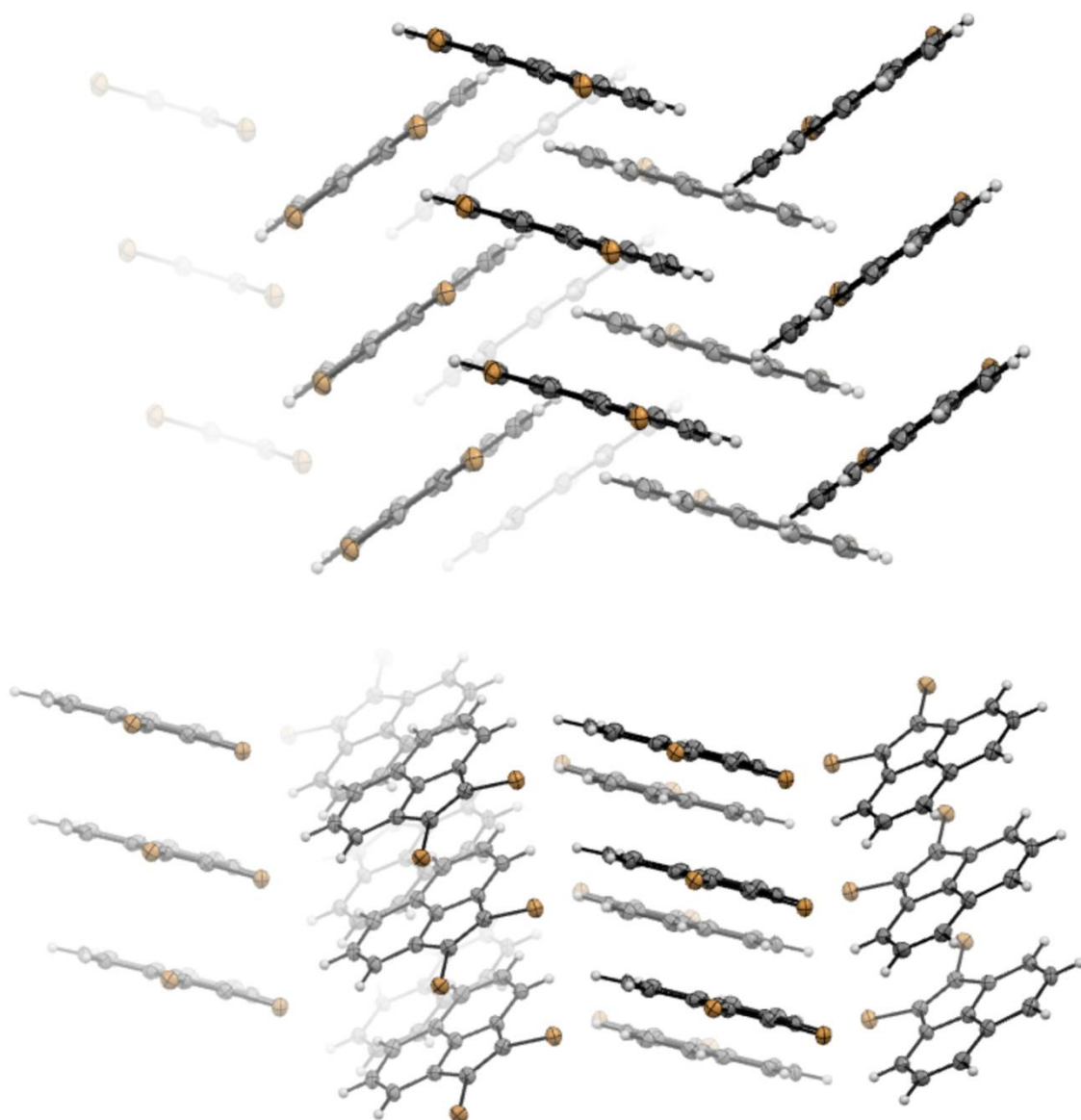


Figure A.10. Crystal packing of **16** with depth cue for clarity.

Table A.17. Crystal data for **16**.

---

Empirical formula	C <sub>12</sub> H <sub>6</sub> Br <sub>2</sub>	
Formula weight	309.99	
Temperature	100(2) K	
Wavelength	1.54178Å	
Crystal system	Monoclinic	
Space group	P2(1)/n	
Unit cell dimensions	a = 14.5267(15) Å	α = 90.00°
	b = 3.9001(4) Å	β = 110.259(2)°
	c = 18.3204(16) Å	γ = 90.00°
Volume	973.742 Å <sup>3</sup>	
Z	4	
Density (calculated)	2.115 g/cm <sup>-3</sup>	
Absorption coefficient	10.139 mm <sup>-1</sup>	
F(000)	592	
Crystal size	0.03 x 0.04 x 0.20 mm <sup>3</sup>	
Theta range for data collection	3.37 to 65.37°	
Reflections collected	4739	
Independent reflections [I>2σ]	1603 [R(int) = 0.0344]	
Reflections (I>2σ)	1497	
Goodness of fit on F <sup>2</sup>	1.055	
Final R indices [I>2σ]	R <sub>1</sub> = 0.0326, wR <sub>2</sub> = 0.0863	
R indices (all data)	R <sub>1</sub> = 0.0344, wR <sub>2</sub> = 0.0879	

---

Table A.18. Atomic coordinates and equivalent isotropic displacement parameters ( $\text{\AA}^2 \times 10^3$ ) for **16**.

<b>Atom</b>	<b>X</b>	<b>Y</b>	<b>Z</b>
C9	0.6204(3)	0.3470(9)	0.6515(2)
C8	0.6403(3)	0.3197(9)	0.7329(2)
C7	0.5607(3)	0.0890(9)	0.83281(19)
C6	0.5704(3)	0.1682(9)	0.7574(2)
C5	0.3667(3)	-0.0461(10)	0.57447(19)
C4	0.4605(3)	0.0819(10)	0.62143(19)
C3	0.4824(3)	0.0534(9)	0.70145(19)
C2	0.4193(3)	-0.0882(9)	0.73707(19)
C12	0.3290(3)	-0.2086(9)	0.6906(2)
C11	0.3039(3)	-0.1826(10)	0.6088(2)
C10	0.5342(3)	0.2337(9)	0.5975(2)
C1	0.4736(3)	-0.0630(9)	0.82109(19)
Br2	0.65824(3)	0.19188(10)	0.92804(2)
Br1	0.42579(3)	-0.21790(10)	0.89783(2)

Table A.19. Bond lengths [ $\text{\AA}$ ] for **16**.

<b>Bonds</b>	<b>Length</b>	<b>Bonds</b>	<b>Length</b>
C9 – H9	0.948	C3 – C6	1.406(5)
C9 – C10	1.373(5)	C2 – C3	1.409(6)
C8 – H8	0.950	C2 – C12	1.376(5)
C8 – C9	1.421(5)	C12 – H12	0.950
C6 – C7	1.469(6)	C11 – H11	0.950
C6 – C8	1.377(6)	C11 – C12	1.418(5)
C5 – H5	0.950	C10 – H10	0.949
C5 – C11	1.382(6)	C1 – C2	1.470(4)
C4 – C5	1.426(5)	C1 – C7	1.345(6)
C4 – C10	1.419(6)	Br2 – C7	1.871(3)
C3 – C4	1.393(5)	Br1 – C1	1.871(4)

Table A.20. Bond angles[°] for **16**.

<b>Bonds</b>	<b>Angle</b>	<b>Bonds</b>	<b>Angle</b>
H9 – C9 – C10	118.9	C3 – C2 – C12	118.8(3)
H8 – C8 – C9	121.0	C3 – C4 – C5	115.4(3)
H5 – C5 – C11	119.8	C3 – C4 – C10	115.9(3)
H11 – C11 – C12	118.6	C3 – C6 – C7	105.0(3)
C9 – C10 – H10	119.6	C3 – C6 – C8	119.1(4)
C8 – C9 – H9	118.8	C2 – C1 – C7	109.3(3)
C8 – C9 – C10	122.4(4)	C2 – C3 – C4	124.8(4)
C7 – C6 – C8	135.9(4)	C2 – C3 – C6	111.1(3)
C6 – C8 – H8	121.0	C2 – C12 – C11	118.1(4)
C6 – C8 – C9	118.0(3)	C2 – C12 – H12	121.0
C5 – C4 – C10	128.7(4)	C11 – C12 – H12	120.9
C5 – C11 – H11	118.7	C1 – C2 – C3	105.0(3)
C5 – C11 – C12	122.7(4)	C1 – C2 – C12	136.2(4)
C4 – C3 – C6	124.1(4)	C1 – C7 – C6	109.5(3)
C4 – C5 – H5	119.9	Br2 – C7 – C1	127.6(3)
C4 – C5 – C11	120.3(4)	Br2 – C7 – C6	122.9(3)
C4 – C10 – C9	120.6(4)	Br1 – C1 – C2	124.1(3)
C4 – C10 – H10	119.8	Br1 – C1 – C7	126.6(3)

A.6. Dibenzof[*j,l*]fluoranthene (Chapter 4, 23).

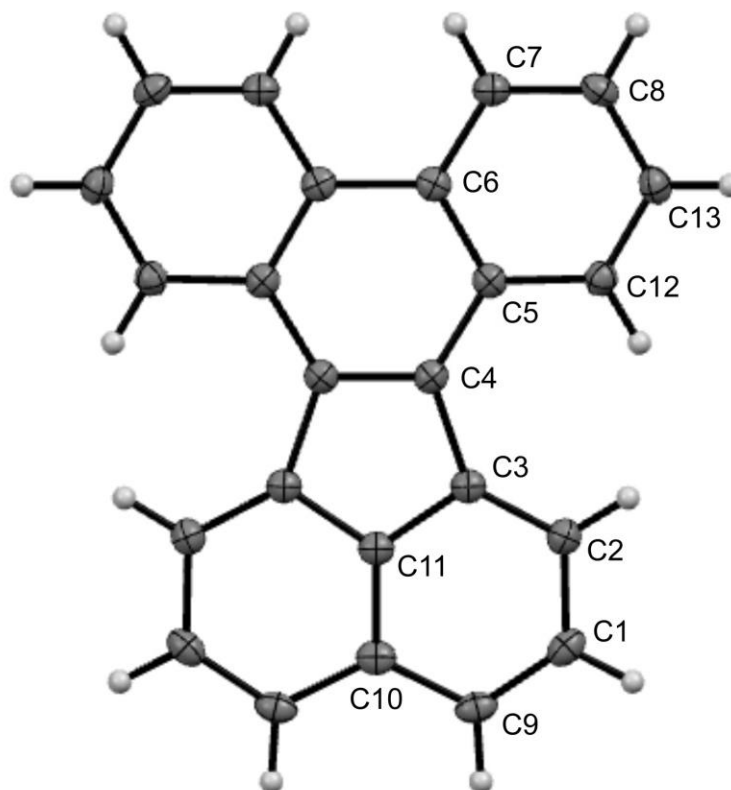


Figure A.11. Thermal ellipsoid plot of **23** at the 50% probability level.



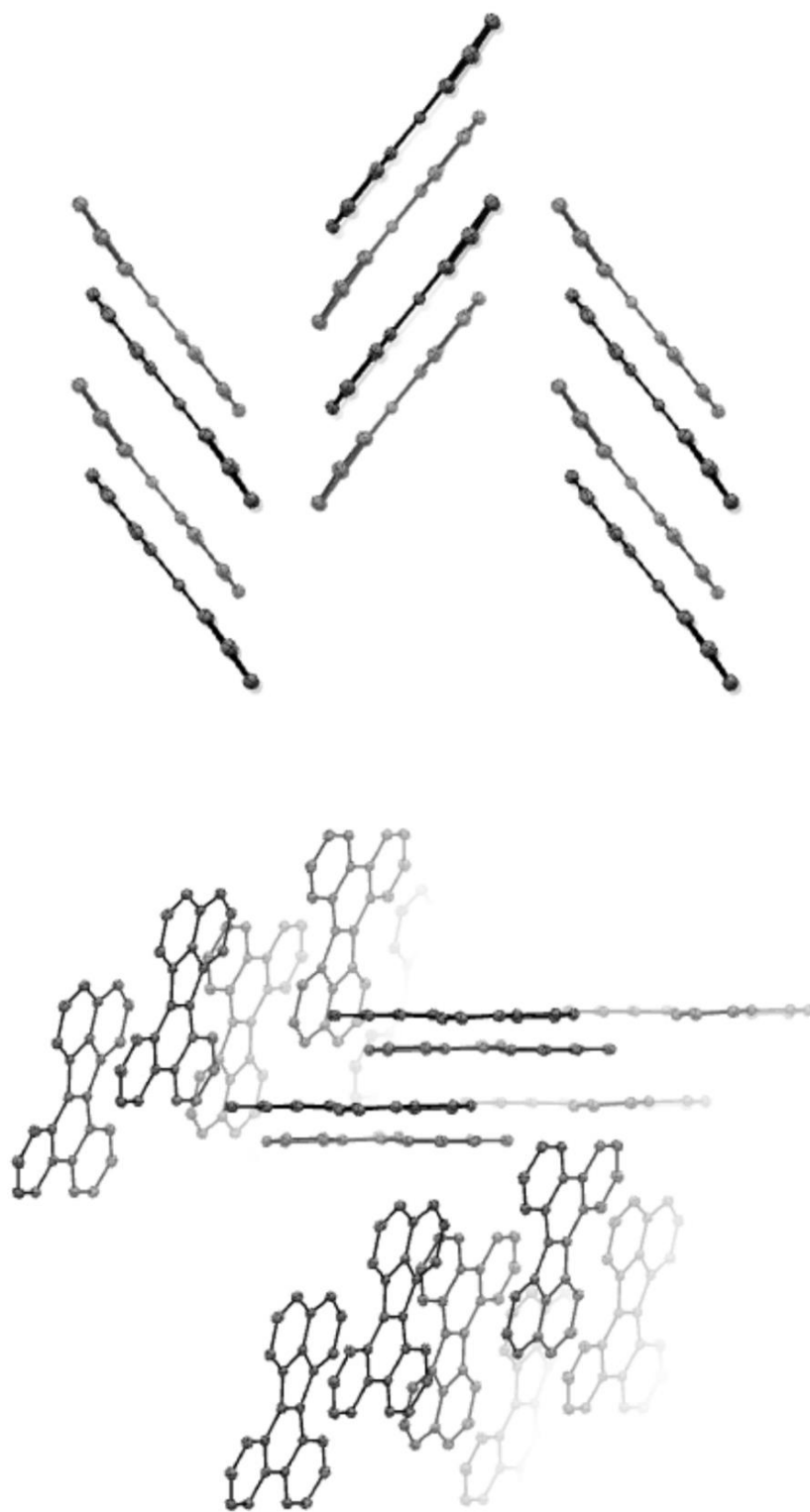


Figure A.12. Crystal packing of **23** with depth cue for clarity.

Table A.21. Crystal data for **23**.

---

Empirical formula	C <sub>12</sub> H <sub>7</sub>	
Formula weight	151.18	
Temperature	99.99 K	
Wavelength	1.54178 Å	
Crystal system	Orthorhombic	
Space group	Pbcm	
Unit cell dimensions	a = 5.5071(2) Å	α = 90.00°
	b = 14.5759(6) Å	β = 90.00°
	c = 17.7728(7) Å	γ = 90.00°
Volume	1426.64 Å <sup>3</sup>	
Z	8	
Density (calculated)	1.408 g/cm <sup>-3</sup>	
Absorption coefficient	0.608 mm <sup>-1</sup>	
F(000)	632.0	
Crystal size	0.23 x 0.126 x 0.077 mm <sup>3</sup>	
Theta range for data collection	9.954 to 136.348°	
Reflections collected	6759	
Independent reflections [I>2σ]	1344 [R(int) = 0.0192]	
Reflections (I>2σ)	1344/0/113	
Goodness of fit on F <sup>2</sup>	1.070	
Final R indices [I>2σ]	R <sub>1</sub> = 0.0329, wR <sub>2</sub> = 0.0848	
R indices (all data)	R <sub>1</sub> = 0.0350, wR <sub>2</sub> = 0.0870	

---

Table A.22. Atomic coordinates and equivalent isotropic displacement parameters ( $\text{\AA}^2 \times 10^3$ ) for **23**.

<b>Atom</b>	<b>X</b>	<b>Y</b>	<b>Z</b>
C9	1.3102(2)	0.64984(8)	0.82145(6)
C9	1.3102(2)	0.64984(8)	0.67855(6)
C8	0.1774(2)	0.31714(8)	0.90965(6)
C8	0.1774(2)	0.31714(8)	0.59035(6)
C7	0.17242(19)	0.31980(7)	0.83247(6)
C7	0.17242(19)	0.31980(7)	0.66753(6)
C6	0.34895(19)	0.36858(7)	0.79101(6)
C6	0.34895(19)	0.36858(7)	0.70899(6)
C5	0.53220(19)	0.41682(7)	0.83104(6)
C5	0.53220(19)	0.41682(7)	0.66896(6)
C4	0.70760(19)	0.46884(7)	0.78920(6)
C4	0.70760(19)	0.46884(7)	0.71080(6)
C3	0.90594(19)	0.52956(7)	0.81576(6)
C3	0.90594(19)	0.52956(7)	0.68424(6)
C2	0.9974(2)	0.55763(7)	0.88420(6)
C2	0.9974(2)	0.55763(7)	0.61580(6)
C13	0.3606(2)	0.36278(8)	0.94909(6)
C13	0.3606(2)	0.36278(8)	0.55091(6)
C12	0.5337(2)	0.41174(8)	0.91057(6)
C12	0.5337(2)	0.41174(8)	0.58943(6)
C11	1.0189(3)	0.56394(10)	0.7500
C10	1.2194(3)	0.62276(10)	0.7500
C1	1.1995(2)	0.61802(8)	0.88563(6)
C1	1.1995(2)	0.61802(8)	0.61437(6)

Table A.23. Bond lengths [ $\text{\AA}$ ] for **23**.

Bonds	Length	Bonds	Length
C9 – H9	0.950	C3 – C11	1.416
C9 – C10	1.421	C3 – C4	1.483(1)
C9 – H9	0.950	C2 – H2	0.950
C8 – H8	0.950	C2 – C3	1.379(2)
C8 – C13	1.397(2)	C2 – H2	0.950
C8 – H8	0.950	C2 – C3	1.379(2)
C8 – C13	1.397(2)	C13 – H13	0.950
C7 – H7	0.950	C13 – H13	0.950
C7 – C8	1.373(2)	C12 – H12	0.950
C7 – H7	0.950	C12 – C13	1.374(2)
C7 – C8	1.373(2)	C12 – H12	0.950
C6 – C7	1.412(1)	C12 – C13	1.374(2)
C6 – C6	1.458(2)	C11 – C3	1.416
C6 – C7	1.412(1)	C10 – C11	1.398
C5 – C6	1.421(1)	C10 – C9	1.421
C5 – C12	1.415(2)	C1 – H1	0.950
C5 – C6	1.421(1)	C1 – C2	1.419(2)
C5 – C12	1.415(2)	C1 – C9	1.374(2)
C4 – C5	1.436(1)	C1 – H1	0.950
C4 – C4	1.393(2)	C1 – C2	1.419(2)
C4 – C5	1.436(1)	C1 – C9	1.374(2)
C3 – C4	1.483(1)		

Table A.24. Bond angles [°] for **23**.

<b>Bonds</b>	<b>Angle</b>	<b>Bonds</b>	<b>Angle</b>
H9 – C9 – C10	120.2	C5 – C12 – C13	121.4(1)
H8 – C8 – C13	119.9	C5 – C6 – C7	118.48(9)
H8 – C8 – C13	119.9	C5 – C12 – H12	119.3
H7 – C7 – C8	119.2	C5 – C12 – C13	121.4(1)
H7 – C7 – C8	119.2	C4 – C3 – C11	105.8
H2 – C2 – C3	120.4	C4 – C5 – C6	118.68(9)
H2 – C2 – C3	120.4	C4 – C5 – C12	122.7(1)
H12 – C12 – C13	119.3	C4 – C4 – C3	108.56(9)
H12 – C12 – C13	119.3	C4 – C4 – C5	121.20(9)
H1 – C1 – C2	118.6	C4 – C5 – C6	118.68(9)
H1 – C1 – C9	118.6	C4 – C5 – C12	122.7(1)
H1 – C1 – C2	118.6	C3 – C4 – C5	130.23(9)
H1 – C1 – C9	118.6	C3 – C4 – C4	108.56(9)
C9 – C10 – C11	116.6	C3 – C11 – C10	124.3
C9 – C10 – C9	126.7	C3 – C11 – C3	111.3
C8 – C13 – C12	119.9(1)	C3 – C4 – C5	130.23(9)
C8 – C13 – H13	120.1	C2 – C1 – C9	122.9(1)
C8 – C13 – C12	119.9(1)	C2 – C3 – C4	136.6(1)
C8 – C13 – H13	120.1	C2 – C3 – C11	117.6
C7 – C6 – C6	121.46(9)	C2 – C1 – C9	122.9(1)
C7 – C8 – H8	119.9	C2 – C3 – C4	136.6(1)
C7 – C8 – C13	120.2(1)	C12 – C13 – H13	120
C7 – C8 – H8	119.9	C12 – C13 – H13	120
C7 – C8 – C13	120.2(1)	C11 – C10 – C9	116.6
C6 – C5 – C12	118.6(1)	C11 – C3 – C2	117.6
C6 – C7 – H7	119.3	C11 – C3 – C4	105.8
C6 – C7 – C8	121.5(1)	C10 – C11 – C3	124.3
C6 – C5 – C12	118.6(1)	C10 – C9 – C1	119.5
C6 – C6 – C5	120.05(9)	C10 – C9 – H9	120.2
C6 – C6 – C7	121.46(9)	C1 – C2 – H2	120.5
C6 – C7 – H7	119.3	C1 – C2 – C3	119.1(1)
C6 – C7 – C8	121.5(1)	C1 – C9 – H9	120.3
C5 – C4 – C4	121.20(9)	C1 – C9 – C10	119.5
C5 – C6 – C7	118.48(9)	C1 – C2 – H2	120.5
C5 – C6 – C6	120.05(9)	C1 – C2 – C3	119.1(1)
C5 – C12 – H12	119.3	C1 – C9 – H9	120.3